NASA CR-174923

LIGHTWEIGHT TWO-STROKE CYCLE AIRCRAFT DIESEL ENGINE TECHNOLOGY ENABLEMENT PROGRAM

VOLUME I
FINAL REPORT

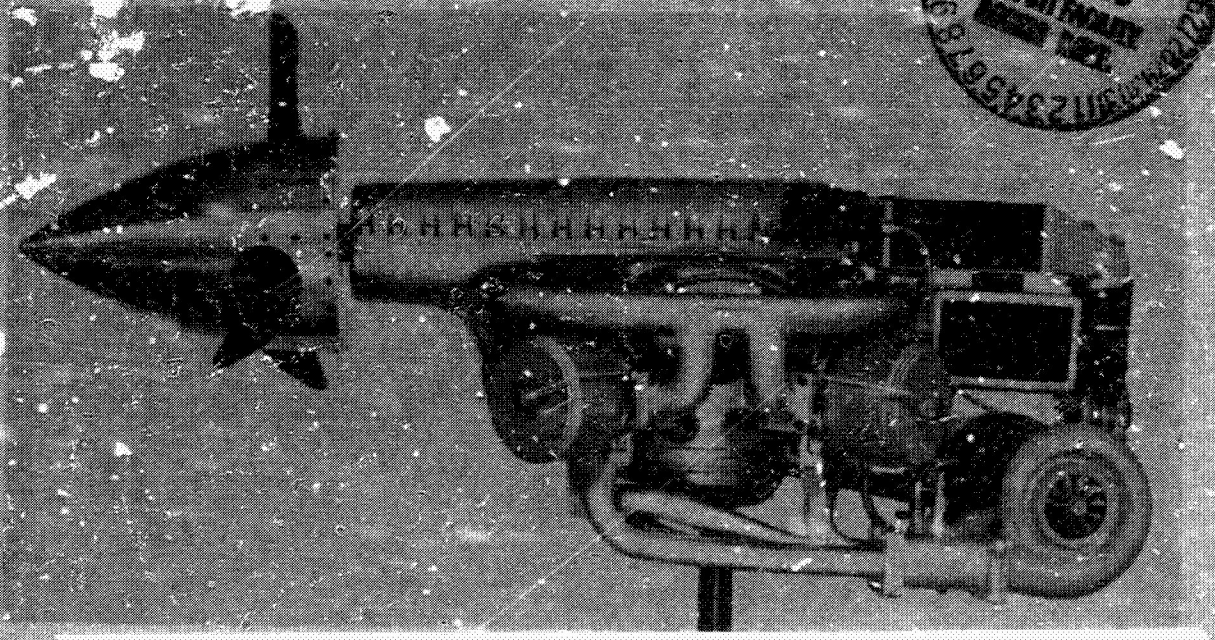

(NASA-CR-174923-Vol-1) LIGHTWEIGHT TWO-STROKE CYCLE AIRCRAFT DIESEL ENGINE TECHNOLOGY ENABLEMENT PROGRAM, VOLUME 1 Final Report, Dec. 1979 - Aug. 1985 (Teledyne Continental Motors, Muskegon,

N86-13328

Unclas

G3/07 04751

TELEDYNE CONTINENTAL MOTORS
General Products Division

P.D. FREEN, S.Q. SERENYI, A.P. BROUWERS
M.E. MOYNIHAN

PREPARED FOR
NATIONAL AERONAUTICS AND SPACE ADMINISTRATION
NASA LEWIS RESEARCH CENTER

CONTRACT NAS3-22218

NASA

NASA CR-174923

VOLUME I

LIGHTWEIGHT TWO-STROKE CYCLE AIRCRAFT DIESEL ENGINE TECHNOLOGY ENABLEMENT PROGRAM

FINAL REPORT

TELEDYNE CONTINENTAL MOTORS
General Products Division

P.D. FREEN, S.G. BEREBVI, A.P. BROUWERS
M.E. MOYNIHAN

PREPARED FOR

NATIONAL AERONAUTICS AND SPACE ADMINISTRATION
NASA LEWIS RESEARCH CENTER

CONTRACT NAS3-22218

NASA
National Aeronautics
and Space Administration

Scientific and Technical
Information Office

1. Report No.	2. Government Accession No.	3. Recipient's Catalog No.
NASA CR-174923		

4. Title and Subtitle	5. Report Date
LIGHTWEIGHT TWO-STROKE CYCLE AIRCRAFT DIESEL ENGINE TECHNOLOGY ENABLEMENT PROGRAM	August, 1985
	6. Performing Organization Code: 505-40-62

7. Author(s)	8. Performing Organization Report No.
P. D. FREEN, S. G. BERENYI, and A. P. BROUWERS, M. E. MOYNIHAN	
	10. Work Unit No.

9. Performing Organization Name and Address	11. Contract or Grant No.
TELEDYNE CONTINENTAL MOTORS 76 GETTY STREET MUSKEGON, MICHIGAN 49442	NAS3-22218
	13. Type of Report and Period Covered: Contract Report 12/79 - 8/85

12. Sponsoring Agency Name and Address	14. Sponsoring Agency Code
NATIONAL AERONAUTICS AND SPACE ADMINISTRATION WASHINGTON D.C. 20546	NASA LEWIS RESEACH CENTER

15. Supplementary Notes

FINAL REPORT. PROJECT MANAGER, JOHN J. MCFADDEN, SMALL ENGINE PROPULSION BRANCH, NASA-LEWIS RESEARCH CENTER, CLEVELAND, OHIO

16. Abstract

An experimental Single Cylinder Test Engine Program was conducted to confirm the analytically projected performance of a two-stroke cycle diesel engine for aircraft applications. The test engine delivered 78kW indicated power from 1007cc displacement, operating at 3500 RPM on Schnuerle loop scavenged two-stroke cycle. Testing confirmed the ability of a proposed 4-cylinder version of such an engine to reach the target power at altitude, in a highly turbocharged configuration. The experimental program defined all necessary parameters to permit a detailed design of a multicylinder engine for eventual flight applications; including injection system requirement, turbocharging, heat rejection, breathing, scavenging, and structural requirements.

The multicylinder engine concept is configured to operate with an augmented turbocharger, but with no primary scavenge blower. The test program was oriented to provide a balanced turbocharger compressor to turbine power balance without an auxiliary scavenging system. Engine cylinder heat rejection to the ambient air has been significantly reduced and the minimum overall turbocharger efficiency required is within the range of commercially available turbochargers.

Analytical studies and finite element modeling was made of insulated configurations of the engine - including both ceramic and metallic versions. A second generation test engine was designed based on current test results.

17. Key Words (Suggested by Author(s))	18. Distribution Statement
Diesel Aircraft Engine; Advanced Engines; Adiabatic Diesel Engine; Diesel with independent turbocharger loop; Two-Stroke Cycle Aircraft Diesel; Radial Diesel Engine; High Pressure Fuel Injection	UNCLASSIFIED - UNLIMITED STAR CATEGORY 07 AND GENERAL RELEASE

19. Security Classif. (of this report)	20. Security Classif. (of this page)	21. No. of pages	22. Price*
UNCLASSIFIED	UNCLASSIFIED		

*For sale by the National Technical Information Service, Springfield, Virginia 22161

VOLUME I

This final report is subdivided into three specific volumes.

Volume I contains the following material:

- Lists of Figures, Tables, and Appendicies; and Metric System Conversion Table.
- Section 1.0 Summary
- Section 2.0 Introduction
- Section 3.0 Engine Design and Cycle Analysis

Volume II of the report covers:

- Lists of Figures, Tables, and Appendicies; and Metric System Conversion Table.
- Section 4.0 Development Testing
- Section 5.0 Multicylinder Performance Projections
- Section 6.0 Conclusions
- Section 7.0 Recommendations
- Section 8.0 References

Volume III of the report covers:

- Lists of Figures, Tables, and Appendicies; and Metric System Conversion Table.
- Section 9.0 Appendicies

TABLE OF CONTENTS

PAGE NUMBER

VOLUME I (CONTINUED)

VOLUME II

PAGE NUMBER

VOLUME II (CONTINUED)

PAGE NUMBER

VOLUME II (CONTINUED)

VOLUME III

LIST OF FIGURES

LIST OF FIGURES (2)

LIST OF FIGURES (3)

LIST OF FIGURES (4)

LIST OF FIGURES (5)

PAGE NUMBER

VOLUME II (CONTINUED)

PAGE NUMBER

VOLUME II (CONTINUED)

LIST OF FIGURES (8)

LIST OF TABLES

LIST OF APPENDICES

VOLUME III

I. ENGINE CYCLE SIMULATION AND DETAILED HEAT TRANSFER ANALYSIS OF THE SINGLE CYLINDER TEST ENGINE WITH CORRELATION TO TEST MEASUREMENTS.

II. STRUCTURAL ANALYSIS OF THE SINGLE CYLINDER TEST ENGINE

III. SECOND GENERATION SINGLE CYLINDER TEST ENGINE PARTS LIST

IV. FEASIBILITY ASSESSMENT OF LOW HEAT REJECTION CONFIGURATION OF THE TELEDYNE LIGHTWEIGHT DIESEL ENGINE.

V. PROJECT SUMMARY REPORT ON ELECTRONICALLY CONTROLLED FUEL INJECTION SYSTEM FOR GENERAL AVIATION DIESEL ENGINE.

VI. EVALUATION OF K-1000F PISTON RING SET FROM TWO CYCLE AIRCRAFT ENGINE.

VII. EVALUATION OF TELEDYNE RINGS AND PISTON WITH STEEL CROWN AND ALUMINUM SKIRT

VIII. FUEL AND OIL SPECIFICATIONS

Metric Conversion Factors

FROM:	MULTIPLY BY:	TO:	FROM:	MULTIPLY BY:	TO:
km	0.6214	mi	bar	100	kPa
km	3281	ft	bar	1.01972	kg/cm^2
m	3.281	ft	bar	14.50377	psi
m	39.37	in	MPa	1000	kPa
dm	3.937	in	MPa	10.1972	kg/cm^2
mm	0.03937	in	MPa	145.0377	psi
m^3	35.31	ft^3	kPa	0.14504	psi
m^3	61,023	in^3	kg/cm^2	9.812	N/cm^2
m^3	264.2	gallons	kg/cm^2	14.223	psi
ℓ	0.0353	ft^3	N-m	0.10197	kgm
ℓ	61.02	in^3	N-m	0.73759	ft-lb
ℓ	0.264	g	kgm	7.2333	ft-lb
m^2	10.76	ft^2	m^3/kW	26.331	ft^3/HP
metric ton	2.205	lb	m^3/kg	16.0165	ft^3/lb
kg	2.2046	lb	kW/ℓ	0.02198	HP/in^3
MN	224,810	lb	kg/kW	1.644	lb/HP
kN	224.81	lb	kg/ℓ	0.03613	lb/in^3
N	0.102	kg	kcal	3.9683	BTU
N	0.22481	lb	kcal/kg	1.8	BTU/lb
°K	1.8	°R	kcal/kg-°C	1	BTU/lb-°F
°C	1.8°C + 32	°F	g/kWh	0.00164	lb/HP-hr
kW	1.341	HP			

1.0 SUMMARY

A Single Cylinder Test Engine (SCTE) program has been conducted to confirm the analytically projected performance characteristics of a two-stroke cycle diesel engine for aircraft application.

The engine was of a high power density configuration delivering 78kW indicated power from 1007cc displacement and operating at 3500 RPM on Schnuerle loop scavenged two-stroke cycle.

Testing confirmed the projections for a proposed 4-cylinder version of such an engine to deliver the target brake power of 268kW at 6,100m and 186kW at 7800m altitude in a highly turbocharged configuration. Indicated specific fuel consumption data as low as 200gm/kW-hr have been demonstrated in an operational SCTE at this power level. The projected multicylinder brake specific fuel consumption is 230gm/kW-hr. A mechanical efficiency of 87% for the multicylinder engine is required to reach this goal. This is well within the current state-of-the-art.

The experimental program defined all necessary parameters to permit a detailed design of a multicylinder engine for eventual flight applications. Injection system requirements, turbocharging, heat rejection, breathing, scavenging, and structural requirements of the engine are discussed.

The multicylinder engine is configured to operate with an augmented turbocharger, but with no primary scavenge blower. However, because of the fuel consumption penalties, it is highly desirable to operate without turbocharger augmentation whenever possible. Therefore, the test program was oriented to provide a balanced turbocharger compressor/turbine power requirement without auxiliary scavenging systems.

During the test program, engine heat rejection was reduced from 23% of the input energy to 7.8% at 9 bar IMEP at 3500 RPM. These numbers are based on indicated power and do not reflect engine friction. This reduced cylinder heat rejection, has in turn, increased the temperature of the exhaust gas available to the turbocharger and, therefore, reduced the minimum overall turbocharger efficiency to 52% at this power cruise condition. This is within the range for commercially available turbochargers.

In addition to the experimental hardware testing, analytical studies and finite element modeling was made of various insulated configurations of the engine - including both ceramic and metallic versions. A second generation test engine was designed based on test results obtained with the first generation hardware.

2.0 INTRODUCTION

This final report presents the results of a multiyear analytical and experimental study sponsored by National Aeronautics and Space Administration (NASA), Lewis Research Center (NASA-LeRC). The study was conducted under contract NAS3-22218 by Teledyne Continental Motors, General Products Division (TCM/GPD) to investigate the feasibility of applying engines based on the diesel cycle to general aviation aircraft.

Design data, hardware descriptions, experimental Single Cylinder Test Engine (SCTE) results, and multicylinder engine performance projections are presented. Evaluations of current shortcomings and recommendations for future programs are also included.

The material presented in this report is divided into the following 3 volumes:

- Volume I - Design and Analysis
  Sections 1, 2, and 3
- Volume II - Development
  Sections 4, 5, 6, 7, and 8
- Volume III - Appendicies (including finite element studies). Section 9

2.1 Background

Since 1978 TCM/GPD has conducted several analytical and experimental studies for NASA-LeRC relative to aircraft applications of diesel engines. These past studies evaluated technical feasibilities and potential economic benefits in terms of fuel consumption, multifuel operation, improved performance, lower costs and extended life.

Prior to awarding of this current contract, TCM/GPD completed an engine design study (Contract No. NAS3-20830) which identified the two-stroke cycle radial diesel concept as the best alternative configuration for aircraft applications. That original study contract was initially completed for engine performance levels of 150 and 300 kW's (Report CR3260). (Reference 1). Both engines were of two-stroke, loop scavenged design. One was four, and the other a six-cylinder configuration. Concurrent to the design study, NASA, in conjunction with the general aviation industry, evaluated the impact that the proposed engine configuration and performance goals would have on existing and future aircraft performance. (Reference 2 and 3). Installation possibilities in both single and twin engine aircraft were verified. As a result of the performance evaluation, a new power level requirement of 186 net kW's was defined. Therefore, in response to NASA's request, TCM/GPD designed a third 186 net kW engine configuration

(Reference 4). That design was the technical base used in this contract for designing and testing a Single Cylinder Test Engine (SCTE) version of the 186kW engine.

2.2 Previous Aircraft Diesel Engines

Some forms of aircraft diesel engines date back in history to the 1930's. For proper perspective of this current study, a survey is included of previous aircraft diesel engines. Table I shows a listing and design data of aircraft diesel engines. No clear trends follow from this tabulation. Seven of the thirteen engines have a radial configuration, seven were air-cooled, eight were two-stroke cycle.

The tabulation becomes more meaningful if specific ratios are used. (See Table II).

Some observations can be made from the Tables I and II. Average specific weight values are:

Four-stroke cycle engines	1.408 kg/kW
Two-stroke cycle engines	1.071 kg/kW
Air-ccoled engines	1.277 kg/kW
Liquid-cooled engines	1.082 kg/kW

The numbers indicate that a two-stroke cycle engine can be expected to be lighter than a four-stroke cycle engine. A comparison of air-cooled and liquid engines would seem to favor the liquid-cooled engine. However, the engine weights of liquid-cooled engines do not include the weight of the cooling package, which accounts for approximately .160 kg/kW. The corrected values then become:

Air-cooled engines	1.277 kg/kW
Liquid-cooled engines	1.242 kg/kW

The currently proposed air-cooled engines apply modern technologies to improve on these specific numbers.

2.3 Scope of Work and Program Plan

The specific tasks that were actually performed in the execution of this contract consisted of the following:

- Single Cylinder Test Engine (SCTE) Design
  - Cycle simulation, performance projection, fuel injection and turbocharging requirements definition
  - Thermal, structural, and aerodynamic design of the cylinder, ports, pistons, and combustion chamber

TABLE I
Previous Aircraft Diesels

	Make	Model	Config.	Cycle	Cooling	No. Cyl.	Bore mm	Stroke mm	Displ. ℓ	Compr. Ratio	Power kW	RPM	Wgt. kg	Year
1	Packard	DR980	Radial	4	air	9	122	152	16.1	16:1	174	2050	231	1930
2.	Guiberson	A980	Radial	4	air	9	122	152	16.1	14 7:1	155	2050	231	1931
3	Deschamps		30° A	2	liquid	12	152	229	50.5	16:1	1000	1750	1089	1934
4	Bristol	Phoenix	Radial	4	air	9	146	190	28 75	14:1	318	2000	494	1934
5	Zbrojovka	ZOD	Radial	2	air	9	120	130	13 2	15:1	207	1600	297	1935
6	Hispano	Clerget 14F2	Radial	4	air	14	140	160	34 5	15:1	518	2200	600	1935
7	Salmson	SH18	Radial	2	air	18	118	150	29 5	16:1	481	1700	567	1935
8	Mercedes	OF2	60° V	4	liquid	12	165	210	53 9	15 1	592	1790	935	1935
9	Junkers	204	Opposed	2	liquid	6	120	2 x 210	28 75	17 1	570	1800	750	1935
10	Junkers	205	Opposed	2	liquid	6	105	2 x 160	16.6	16.1	444	2200	510	1936
11	Junkers (1)*	207 Turbo	Opposed	2	liquid	6	105	2 x 160	16.6	16.1	740	3000	649	1938
12	Napier (2)*	Nomad	Flat	2	liquid	12	152.4	187.33	41 0	16.1	1984	2050	1624	1953
13	McCulloch (3)*	TRAD-4180	Radial	2	air	4	98 43	98.43	3.0	15:1	150	2850	149	1970

*Numbers in parentheses refer to list of references at the end of this report

TABLE II
Specific Data of Previous Aircraft Diesels

Make	Cycle	S/B	BMEP kPa	Piston Speed m/sec	Piston Heat Load kW/cm²	Spec. Power kW/ℓ	Spec. Power kW/kg
Packard	4	1.246	633	10.39	.165	10.81	75
Guiberson	4	1 246	564	10.39	.147	9 63	67
Deschamps	2	1 507	679	13 36	459	19 80	92
Bristol	4	1.301	664	12.67	.211	11.06	.64
Zbrojovka	2	1.083	588	6.93	.203	15.68	.70
Hispano	4	1 143	819	11.73	240	15 01	.86
Salmson	2	1 271	575	8 50	244	16 31	85
Mercedes	4	1 273	736	12 53	231	10 98	63
Junkers 204	2	1 750	661	12.60	420	19 83	76
Junkers 205	2	1 524	729	11.73	.427	26 75	87
Junkers 207	2	1.524	892	16.00	.712	44.58	1 14
Napier	2	1.229	1416	12.80	.906	48 39	1 22
McCulloch	2	1.000	1053	9.35	493	50.00	1 01

- Running Gear Detailed Design
    - Mechanical design of rod, bearings, pins, cylinder-to-base engine adaptation, injection pump drive, lubrication and cooling
- Procurement and Fabrication of Initial Set of SCTE Components
    - Three cylinders and several sets of operating components based on the original design were fabricated and procured under this task
- Assembly, Set-up, and Acceptance Tests
    - The running hardware procured above was assembled to the TCM owned LABECO single cylinder test base.
    - Initial operational tests were conducted to confirm the capability of the system to run the test program and obtain valid data.
- SCTE Baseline Test and Performance Evaluation
    - Scavenging and breathing tests of the three initial port designs were run for comparison.
    - Cylinder cooling and lubrication requirements were defined
    - Mechanical operating characteristics were defined for rings, piston wrist pin bearings, piston/cylinder clearances, etc.
    - Testing was conducted to define the power levels available from the original design
- Full Power Performance Evaluation
    - Adapted high pressure mechanically driven injection pump to allow operation up to full design indicated horsepower (IHP).
    - Conducted high power tests
    - Procured an electronically controlled, hydraulically amplified high pressure fuel injection system (HPFIS)
- HPFIS Injection/Combustion System Characterization
    - Performance testing was done with the mechanically driven, close coupled HPFIS.

The hydraulically amplified system experienced much developmental problems on the test bench and was never engine tested.

- Cycle analysis work was conducted to refine performance parameters (UMIST Program). Experimental data was obtained for correlation.

- Injection system was optimized with regard to timing, burn rate, etc. based on both cycle simulation and experimental data.

- Minimum cooling flow requirements were defined and high temperature synthetic lubricants were evaluated.

- Heat rejection was minimized with the use of insulated designs using conventional materials and air gap insulation techniques.

- Detailed thermal and structural characteristics of the engine were modeled by finite element techniques.

- Cylinder Air Utilization

  - Cylinder breathing characteristics, manifold design, port sizing, reed valve potential, etc. were evaluated by cycle simulations and compared to experimentally observed data.

  - Turbocharging requirements were defined and minimized within the thermal limitations of the metallic cylinder design.

- Insulated Component Test Engine Design

  - The goal of this task was to provide maximum heat to the exhaust for energy recovery. This engine required an insulated combustion chamber. Under this task two versions of the test engine were designed: 1) an insulated configuration utilizing monolithic ceramics, and 2) a cooled metallic version using design techniques to minimize heat rejection.

  - Finite element modeling was conducted to define the of thermal and structural characteristics using ceramic insulating materials, and also using state-of-the-art materials with air gap insulations.

  - Mechanical design of major components

- Insulated SCTE Procurement
  - The metallic (minimum cooled) configuration of this second generation engine design was procured.
  - Ceramic hardware was not procured; and assembly and testing of the second generation engine was deleted from the program due to funding limitations.
- Multicylinder System Performance Projections
  - Projected friction characteristics
  - Propeller load power curve definition
  - Projected higher speed operation
  - Turbocharger power balance for the multicylinder engine
- Final Report
  - A detailed final report was prepared describing the program results obtained, conclusions reached and recommendations made regarding future work.

This entire experimental program was conducted by TCM/GPD at its facilities in Muskegon, Michigan. The finite element thermal and structural modeling for the program was done under subcontract to TCM/GPD by Analysis and Design Applications Company, Ltd. (ADAPCO) of Melville, New York. The Appendicies of this report include complete final reports prepared by ADAPCO describing their finite element studies.

Bendix, Engine Products Division of Sidney, New York designed and fabricated the electronic HPFIS under subcontract, and their final report is also included in the Appendix. In addition, AVL, Inc. of Graz, Austria conducted some of the preliminary design work under subcontract to TCM/GPD. Their work is integrated into the report.

2.4 Significance of This Project

It is evident from the list of past aircraft diesel engines in 2.2, and the results of the previously cited studies, that diesel engines for aircraft propulsion can be successfully applied.

However, the introduction of such engines into commercial applications will require significantly more than

demonstration of technical feasibility. Other studies (Reference 5) have found significant objections to the application of diesel engines to aircraft. In the interest of presenting an unbiased picture of both sides, the following direct quotations are included from Reference 5 which presents some of the negative aspects of such a propulsion system.

> "Technology and concepts for simple cycle engines are well established in the aviation community, and any new concept will have to overcome a natural resistance to change unless it is shown that the new concept is very clearly superior."
>
> "If the weight and mechanical reliability of advanced diesel's are shown to be as projected for weight; and comparable to turbines for reliability; the favorable fuel efficiency and other beneficial characteristics available from diesel engines are significant enough to warrant serious considerations for aircraft application."
>
> "Mechanical reliability is a special concern because, historically, reciprocating engines have not demonstrated either the life or the inflight reliability that turbines are now experiencing."
>
> "If aircraft diesel engines are fundamentally limited to service lives of several hundred hours, as compared to a few thousand hours for turbines, this would be a severe obstacle to overcome."

The design and test program undertaken in this contract is the first step in an attempt to address whether the projected performance parameters can be demonstrated in actual operating hardware. Once demonstrated, the questions of weight, reliability, and durability may begin to be explored and evaluated.

As will be shown in this report, the performance parameters initially projected were indeed reached in an experimental single cylinder test engine (SCTE)

3.0 ENGINE DESIGN AND CYCLE ANALYSIS

This current program is a follow-on to the design and analysis of a previous contract NAS3-20830, reported in NASA CR3261 (Reference 4). Using that four-cylinder engine as the base, additional computer generated studies were made of the multicylinder engine to confirm those preliminary results. In addition, detailed mechanical designs were made of actual SCTE hardware which was ultimately tested. AVL of Graz, Austria - a consulting and design firm with acknowledged expertise in two-stroke cycle engines - conducted these initial design studies under subcontract to TCM.

Subsequently, further detailed computer analyses was made by TCM to expand upon the AVL studies. The following elements of this Section 3 describe first, the AVL projections and second, the extended TCM analysis of performance beyond the original AVL design.

These computer generated parametric studies were the basis for guiding the subsequent experimental programs.

3.1 Preliminary Design and Cycle Analysis

The multicylinder engine was designed to meet the following criteria:

- Represent the projected technology level of the mid 1980's. The most important performance parameters that determine engine size and technology level are BMEP and piston speed. The chosen values were:

  BMEP = 11 to 12 bar
  Piston speed = 12 to 13 m/sec

  These criteria resulted in the following engine data:

Bore	108	mm
Stroke	110	mm
Number of cylinders	4	
Displacement	4.031	liters
RPM	3500	
Gross take-off power	268	kW
BMEP	11.70	bar
Piston speed v_p	12.83	m/sec
BMEP x v_p	147	kg/cm^2 x m/sec

- Have a configuration that meets conditions that are critical for an aircraft engine:

  Low Weight
  Low Drag
  Small Volume

- Meet or exceed performance targets:
  - Be fuel efficient, better than any existing aircraft powerplant.
  - Have multifuel capability
- Designed to integrate with existing aircraft with a minimum of modifications
- Contribute to longer time between overhaul (TBO), i. e. must have reliability and low maintenance and repair time and cost.

The Figures 3.1.1 and 3.1.2 show the multicylinder engine concept design which incorporated these basic requirements. It features:

- Radial cylinder configuration. This configuration results in a short crankcase, and contributes greatly to reduced engine weight. Also, there are no free inertia forces due to the cylinder arrangement, therefore, the engine should be relatively vibration free.
- Two-stroke cycle operation. Two-stroke cycle engines have a high power/displacement ratio. For a given power level, this means a smaller and lighter engine.
- Loop scavenge systems: The Curtis loop system was initially chosen (later changed to a Schnuerle System because of its higher scavenge efficiency) because loop scavenging does not utilize valves. As a result, the cylinder height is lower, which reduced frontal drag and high engine speeds are possible, uninhibited by valve train inertia. Figure 3.1.3 shows the principle of both the Schnuerle and Curtis loop systems.
- Four cylinders were chosen because this is the maximum number that can be located in one plane on a single crankpin for the bearing loads anticipated.
- Limited cylinder cooling, the extent of which was to be determined in the course of the developmental program.

  Reduction of the cylinder cooling puts more energy into the exhaust gas, and therefore, improves the turbocharger energy balance. Also, it results in less cooling drag. Finally, higher gas temperatures make the engine less sensitive to the quality of the fuel.

- Capability to run turbomachinery independent of the engine. A two-way valve in the intake manifold, a combustor, and a separate starter allow the turbocharger to run in an APU mode. This mode is applied at starting and low load operation of the main engine.

- High pressure injection system which provides a highly atomized fuel into the cylinder. This results in intensive mixing of fuel and therefore:

  - efficient combustion of the fuel

  - short ignition delay and multifuel capability

  - short combustion period and low BSFC

3.2 Multi-cylinder Cycle Simulation and Single Cylinder Test Engine Design

The design and preliminary performance calculations reported in NASA CR3261 (Reference 4) were used for a computer generated performance analysis of the multicylinder engine. The results of that analysis were then applied to the design of the single cylinder test engine.

In designing the Single Cylinder Test Engine (SCTE) TCM utilized the services of AVL, Graz, Austria. This section (3.2) described their input into the inital hardware design - both in terms of thermodynamic analysis and mechanical design. This design became the initial starting point for the subsequent hardware oriented experimental program.

3.2.1 Multicylinder Cycle Simulation. Cycle calculations were carried out for these engine operating conditions:

Full power takeoff (sea level)	268.3 kW/3500 RPM
Full power cruise (7620m altitude	194.0 kW/3500 RPM
Reduced power cruise (7620m altitude)	129.0 kW/2650 RPM

The engine power for the two cruise modes included the power required for the blower to pressurize the cabin air. The new shaft powers (input into a propeller) are correspondingly lower by 7.47 kW.

The alternator consuming 3.73 kW, was assumed to be driven by the turbine. Therefore, the turbine has to supply a correspondingly surplus power at every operating condition.

Assumptions made were:

Turbocharger efficiencies:

Compressor (adiabatic)	η_{ac}	= 79 to 80%
Turbine (adiabatic)	η_{at}	= 78 to 79%
Mechanical	η_m	= 98 to 99%

Overall turbocharger efficiency $\eta_{tc} = \eta_{ac} \times \eta_{at} \times \eta_m$ was therefore between 60.5% and 62.5%

Maximum compressor pressure ratio: 7.25:1 at cruise condition

A variable turbine nozzle area was assumed.

Engine friction mean effective pressures including oil pump and fuel injection were projected at:

3500 RPM	FMEP = 1.1 bar
2650 RPM	FMEP = .9 bar

These friction mean effective pressures were assumed from BMEP data found with AVL's high speed, two-stroke diesel engines and represent optimistic values.

3.2.1.1 Multicylinder Performance Analysis. Improvements were expected during the engine development. Favorable conditions and efficiency factors were therefore assumed for the analysis and calculations, especially with regard to:

- Flow properties of the ports
- Erficiency of scavenging and filling of the cylinder
- Combustion (Injection, mixture formation, rate of heat release)

3.2.1.1.1 Port Design. Specific data on the intake and exhaust ports as recommended by AVI are shown in Table III. The geometrical areas of the inlet and exhaust ports versus crank angle are shown in Figure 3.2.1. The port areas in Figure 3.2.1 are defined as the cross sections perpendicular to the mean direction of a port.

3.2.1.1.2 Multicylinder Cycle Calculations. AVL calculated operating parameters for takeoff and the cruise modes - full power and economy - are shown in Table IV. The AVL predicted BSFC at takeoff and at economy cruise is 5% higher than TCM's originally target during for the preliminary design analysis.

TABLE III. PORT DATA

	AVL DESIGN	TCM/GPD PRELIMINARY DESIGN
INLET PORTS		
HEIGHT: (mm):	29	21
% OF STROKE	26.4	19.1
TIME AREA (cm^2-degr.CA):	2180	1749
MEAN FLOW COEFFICIENT	.54	.85
INLET PORTS		
HEIGHT (mm):	41	30
% OF STROKE	37.3	27.3
TIME AREA (cm^2-degr.CA):	2655	1093
SCAVENGE RATIO:	1.0	1.3
SCAVENGE PRESSURE RATIO (AT 3500 rpm)	1.25	1.25

At full power cruise AVL confirmed the TCM target BSFC of 225 g/kWh as reasonable.

A turbocharger energy balance including 3.73 kW surplus power for the alternator was established. The required overall efficiencies of the turbocharger at takeoff and at full power cruise was within the assumed limits. A slightly higher overall efficiency of 64.1% would satisfy the economy cruise conditions.

The calculations indicted that variable injection timing may be required. A retard at takeoff should satisfy the control of peak cylinder pressure. The maximum firing pressure of 113 bar, calculated at takeoff conditions with retarded ignition timing at 3 degrees BTDC, however exceeds the design limit of 100 bar.

3.2.1.2 Discussion of Multicylinder Cycle Simulation Results. The TCM preliminary multicylinder design utilized a Curtis type loop scavenging system. It is an uncomplicated system but its poor trapping efficiency requires a large quantity of scavenge air due to short-circuiting from the intake to the exhaust ports, despite the steep inclination of the intake ports toward the cylinder head.

Since the inital computer runs indicated difficulty in obtaining a turbocharger power balance, it was then decided to apply the more air-efficient Schnuerle system of loop scavenging. The air is directed upward at the cylinder wall opposite the exhaust ports to produce a proper loop. This is shown in Figure 3.1.3.

The mean flow coefficient factor (C_m) reflects only to some degree the flow properties of the inlet ports related to the inlet time-area and to the total scavenge pressure ratio (p_i/p_{ex}). A more careful consideration shows that the value C_m may be influenced considerably by:

- The throttle effect of the exhaust ports, mainly determined by the size of the ports and their flow properties. A corresponding ratio of inlet air cylinder pressure to exhaust manifold pressure p_i/p_{ex}, is an improtant consideration and is required for a given mass flow.

- The exhaust blowdown (gases) controls the pressure in the cylinder at inlet opening; some back flow of residual gas into the inlet results is delaying the start of the scavenging event.

Because of these interrelations and based upon experience in compariable two-stroke engines, a mean flow factor, C_m of .55 was assumed. The port dimensions of Table III and Figure 3.2.1 were calculated with this assumption. Computer

calculations of the gas exchange with the port areas shown in Figure 3.2.1 and the assumed variable flow coefficients shown in Figure 3.2.2 resulted in a calculated mean flow factor C_m of .54 (Table III).

Calculations showed that a relatively low scavenge ratio of 1.0 could be allowed requiring a pressure tatio (p_i/p_{ex}) of 1.25 at 3500 rpm for this cylinder design.

3.2.1.3 Discussion of Cycle Calculations. The following definitions are required in the discussion of these cycle calculations:

R_s - Scavenge Ratio - This term is the ratio of the weight of air delivered to the cylinder divided by the weight of air of displacement volume at inlet density.

η_{tr} - Trapping Efficiency - This term is defined as the air volume retained divided by the air volume delivered.

η_{ch} - Charging Efficiency - This term is the useful fresh charge retained in the cylinder divided by the displacement volume.

η_{sc} - Scavenging Efficiency - This term is the volume of pure air retained in the cylinder divided by the sum of volume retained and the residual volume.

In each definition, volume refer to standard temperature and pressure (STP) conditions.

Preliminary calculations of takeoff and cruise modes had shown that in the economy cruise mode self-sustained operation of the turbocharger would be difficult to maintain without sacrifice in engine cycle efficiency. Analysis, therefore, concentrated on finding a combination of cycle parameters with which the targets of the economy cruise mode could also be accomplished as closely as possible.

TCM projected a high indicated thermal efficiency corresponding to the extremely low target BSFC of 207 g/kWh for the ultimate application with combinations of high air fuel ratios, fast burning rates of the fuel and with high compression ratio. However, these measures decrease the energy content of the exhaust, and consequently also the energy available to the turbine. Figure 3.2.3 shows, as an example, the influence of the air-fuel ratio on the indicated specific fuel consumption at economy cruise.

*"Scavenging of Two-stroke Cycle Diesel Engines", P. H. Schweitzer, 1949.

TABLE IV

OPERATING PARAMETERS

		TAKEOFF	POWER CRUISE	ECONOMY CRUISE
Altitude	m	0	7620	7620
Barometric Pressure	bar	1.014	.3765	.2765
Ambient Temperature	°C	15.5	-34.4	-34.4
RPM		3500	3500	2650
Power	kW	258.3	194	129
BMEP	bar	11.41	8.25	7.25
BSFC	g/kW	232.7	223.8	217.5
BSFC-Target	g/kW	219	225	207
Nominal Compression Ratio		18.35	18.35	18.35
Effective Compression Ratio		12	12	12
Indicated Power	kW	294.3	220	145
ISFC	g/kWh	212.1	197.4	193.5
Air-Fuel Ratio (related to fresh air trapped)		20.9	21.8	24.8
Start of ignition	deg. CA BTDC	3	7	7
Max. Firing Pressure	bar	113	100	99
Heat Transferred Through Cylinder Walls	% of Fuel Input	8	10.2	12
Intake Manifold Pressure	bar	3.55	2.63	2.53
Scavenge Pressure Ratio		1.25	1.25	1.115
Intake Manifold Temp.	°C	115	115	115
Scavenge Ratio		1	1	1
Trapping Efficiency	%	48	48	48
Scavenge Efficiency	%	83	83	83
Exhaust Manifold Press.	bar	2.84	2.10	2.27
Turbine Inlet Temperature	°C	530	470	410
Compressor Press. Ratio		3.6:1	7.25:1	6.93:1
Turbine Pressure Ratio		2.8:1	5.58:1	6.03:1
Compressor Air Flow	kg/s	.725	.547	.41
Adiabatic Compressor Power	kW	92.3	99.8	72.7
Adiabatic Turbine Power	kW	154.9	164.9	118
Required Turbocharger Eff. $\eta_{TC} = \eta_{ac} \times \eta_{at} \times \eta_{m}$	%	61.6	62.3	64.1

An increase of the exhaust temperature can be achieved by more economical use of scavenge air. Because of an asymptotic type of relation between scavenge ratio and scavenge efficiency, a reduction of the scavenge ratio may be permitted as long as the decrease of the scavenge efficiency remains acceptable.

Figure 3.2.4 shows an example of the scavenge efficiency characteristic typical for a loop scavenged engine. The decrease of the scavenge ratio from 1.3 to 1.0 decreases the scavenge efficiency from 82% to 73%. This means that the amount of fresh air retained in the cylinder decreases only by 11% while the charge density may be assumed to remain approximately unchanged.

The mass of air passing through the cylinder during the scavenging process is determined by the relation

- air flow = scavenge ratio X (1 - trapping efficiency)

Correspondingly Figure 3.2.4 shows the amount of scavenge air leaving the cylinder at a scavenging ratio of 1 is only 68% of the amount at a scavenge ratio 1.3.

A decrease in the overall air-fuel ratio can result with the same amount of injected fuel if the density of the cylinder charge cannot be increased. The reduced ratio results, therefore, in a hotter blowdown gas which, on the other hand, is mixed with a smaller amount of scavenge air in the exhaust. Therefore, an increase of the turbine inlet temperature results from a lower air-fuel ratio and from the smaller amount of scavenge air short-circuited into the exhaust.

Results of computer calculations comparing the scavenge ratios 1. and 1.3 are shown in Table V. The lower scavenge ratio of one (1) shown in Figure 3.2.4 is assumed for the calculations during the engine development.

TABLE V
COMPARISON OF SCAVENGE RATIOS
(ECONOMY CRUISE CONDITIONS 2650 RPM)

Scavenge Ratio		1	1.3
Intake Manifold Pressure	kPa	253	253
Intake Manifold Temperature	°C	115	115
Scavenge Pressure Ratio		1.115	1.21
Exhaust Manifold Pressure	kPa	227	209
Scavenge Efficiency	%	83	88
Trapping Efficiency	%	47.5	41.2
Air-Fuel Ratio (related to fresh air trapped)		24.8	27.9
Turbine Inlet Temperature	°C	410	350
Required Turbocharger Eff. $\eta_{TC} = \eta_{ac} \times \eta_{at} \times \eta_{m}$	%	64.1	71.4

Table V also shows that the trapped air-fuel ratio decreased from 27.9 to 24.8 with the reduction of the scavenge ratio. Consequently, the indicated specific fuel consumption increases by 5 g/kWh while the compression ratio remains the same (Figure 3.2.3).

The effective compression ratio was therefore increased from 10 (originally assumed by TCM/GPD) to 12 although the maximum firing pressure exceeds the limits of 100 bar. Conversely, BSFC at economy cruise comes closer to the target with the higher compression ratio (Table IV).

Figures 3.2.5 to 3.2.10 show calculated high and low pressure diagrams supplementing the data in Table IV. The assumed rates of heat release are shown in the high pressure diagrams. Ignition timing and combustion duration vary with the speed and with the amount of burned fuel.

In summary, the AVL analysis pointed to considerations that would be required during the SCTE development program:

- To achieve a high quality of scavenging with a minimum of scavenge air
- To obtain a 207 g/kWh (0.34 lb./HPh) BSFC for the economy cruise mode
- To obtain a turbocharger energy balance, in particular at power cruise

3.2.2 First Generation SCTE Design. The design of the single cylinder test engine was based on the four-cylinder two-stroke radial engine design detailed in the prior NASA lightweight aircraft diesel engine design study (NASA Report CR 3261). The SCTE design followed the multicylinder design as close as possible with modifications made, such as the connecting rod length, to adapt the cylinder assembly to the LABECO crankcase - Figure 3.2.11. The results of the cycle simulation discussed in Section 3.2.1 were applied to the design of the cylinder ports and the combustion chamber.

Figure 3.2.12 shows the fabricated components that were initially tested. Figure 3.2.13 is the LABECO test base.

3.2.2.1 Cylinder Assembly. The cylinder and head were machined in one piece from 2045 steel bar stock with fins machined from a cast-on aluminum block. The cylinder was first rough machined leaving 1 mm of material to be removed in critical areas. At this stage the vertical holes for oil cooling of the exhaust ports were drilled. An aluminum muff was then cast into the premachined cylinder using the ALFIN process for binding. The cooling fins were then machined in

the aluminum - Figure 3.2.14. The cylinder bore was then semi-finished and initially coated with NIKASIL, a electrochemically deposited plating of nickel, silicon, and carbide. At this time the NIKASIL plating was considered to be superior to chrome plating or nitriding due to its excellent corrosion resistance, very hard surface and good scuff resistance under marginal lubrication and high loading.

The bore was then honed to specifications. The cylinder bore was slightly enlarged in the port area to compensate for bore distortion due to temperature difference between the ports.

The exhaust port bridges are cooled by oil passages. These cooling passages help carry away localized heat build-up and thus reduce bore distortion.

All six intake and the three exhaust ports have a common lower port surface which is level with the top of the piston at bottom dead center position. The ports vary by height, width, and angle - Figure 3.2.15. The port top and bottom surfaces are formed by keeping the inclined cutter stationary and rotating the cylinder about its axis through the designated angles. This effectively guarantees that the port top and bottom surfaces are horizontal. Also it provides a slight nozzle effect which improves flow entry conditions.

The ports cover approximately a 300^{o} arc. The remaining cylinder wall is used as the piston thrust surface. Some material is removed in this same area at the outside of the cylinder in order to obtain a more uniform metal distribution in the port area and thus reduce bore distortion.

The cylinder is clamped to the engine mounting plate by means of a hold-down nut. This method was first applied by McCulloch on their aircraft engines and allows replacement of a cylinder in minimum time. The ring is torqued to 1085 N-m and is locked to prevent rotation. The cooling fins extend down to the port area which provide the maximum amount of cylinder cooling. Reduction of cooling can be accomplished by blocking off or removing the cooling fins.

3.2.2.2 Combustion Chamber Insert. The chamber is made of stainless steel for heat resistance and contact the cylinder only by a series of annual lands at the top and sealing ring at the circumference. The intent was to minimize heat transfer to the cylinder itself. A cold clearance between insert and cylinder bore of 0.5mm would allow the insert to expand to just close this clearance without stressing the cylinder - Figure 3.2.16.

The insert serves several purposes:

1. It facilitates optimization of the shape of the combustion chamber. Experimentation with different compression ratios and shapes of the combustion chamber are relatively simple.

2. The cylinder and cylinder head can be made in one piece.

3. The air gaps between the insert and the cylinder have an insulating effect and reduce the cylinder cooling loss.

3.2.2.3 Manifold Muff. Intake and exhaust connections are contained within a cast aluminum muff. This method ensures that the cylinder remains circular with no flanges or bolted connections which could cause bore distortion. The casting is held in place by a locating screw. Sealing to the outside is provided by two TEFLON "O" rings at the top and bottom of the muff. The exhaust outlet is a stainless steel assembly which is isolated from the aluminum housing by an asbestos gasket. This design would keep heat in the exhaust gas and result in a minimum leakage to the intake side.

3.2.2.4 Cylinder to Crankcase Adapter. The design used an existing adapter to mount the cylinder assembly to the LABECO base. The bore had to be enlarged to accommodate the larger cylinder. A dowel in the mounting plate indexes the cylinder relative to the crankshaft.

3.2.2.5 Fuel Injection System. The initial SCTE assembly utilized the American Bosch APF-1B injection pump supplied with the LABECO crankcases. The pump system demonstrated that it did not have the required capability nor the injection pressures required for the application. However, it was available and it enabled testing at low engine loads. Nine and ten mm plungers were provided and tested with this pump.

An AKN injection nozzle holder with ADB nozzles were tested. Eight hole nozzles with three different diameters were evaluated (0.20, 0.225, and 0.25mm diameter), each with three different spray angles (155^{o}, 160^{o}, and 165^{o}).

The pump was installed on top of an existing mounting pad on the crankcase adapter. The pump was driven by the LABECO engine camshaft modified to allow installation of different pump camprofiless. It was driven through a chain and sprocket system and runs at crankshaft speed. The camshaft included an adjustable advance unit.

The nozzle holder is secured to the cylinder with a standard Bosch clamp. Two copper gaskets are provided for sealing. The nozzle tip extension into the cylinder was varied by shims under the nozzle holder flange.

3.2.2.6 Piston and Piston Rings. The piston of the initial SCTE was made of aluminum because a timely delivery could be guaranteed. (This material would be adequate at light to medium loads, but nodular iron would be required as testing progressed and the performance requirements became more demanding.)

The aluminum piston had the following major features:

1. Cooling annulus behind the ring belt
2. Ni-resist cast insert to prevent top piston ring pounding
3. Five piston rings
4. Floating piston pin

The initial piston rings were configured as follows:

1. Top ring: 15^{o} keystone, chrome faced, barrel face, nodular iron
2. 2nd, 3rd, and 4th ring: Rectangular, no facing, taper face, gray iron.
3. Oil control ring: Double rail, chrome faced. The rings were pinned to prevent ring clipping at the upper edges of the cylinder ports. (This feature ultimately proved to be wrong. The pins sheared off after a short time of running).

3.2.2.7 Connecting Rod. The connecting rod initially used was an existing production Ford rod, modified to accept a larger piston pin compatible with the piston design. The large end had a thick-walled steel bushing to reduce the ID to the size required for the modified LABECO crankpin diameter.

3.2.2.8 Crankshaft. Crankshaft was a modified LABECO crankshaft with the crankpin diameter reduced to obtain the required 110mm stroke. The fillet radius was also slightly reduced to provide a larger bearing area.

3.2.2.9 LABECO Test Base. The LABECO engine is a conventional single cylinder test base. It contains the crankshaft counterbalanced to offset the rotating and primary reciprocating inertia forces. Counter rotating shafts are installed to offset the secondary reciprocating system.

The camshaft is driven at crankshaft speed required for two-stroke cycle operation of the injection pump. The engine has an integral lubrication system.

3.3 Cycle Simulation Computer Program

After the initial series of tests with the basic AVL sized hardware, it became apparent that further detailed analysis would be required to provide guidance and direction to the experimental program. TCM obtained an engine cycle simulation program developed by Professor Benson of the University of Manchester, Institute of Technology (UMIST) of Manchester, England. The use and application of that program is discussed in this Section 3.3.

3.3.1 UMIST Cycle Analysis Program Description. Initial testing of the original AVL hardware revealed that engine performance needed improvement. To evaluate the specific parameters affecting performance (i.e. combustion, air flow and heat loss), the UMIST MK14 cycle simulation program was used.

The UMIST MK14 program is a quasi steady state model which treats the cylinder as a steady state, thermodynamic control volume at every degree of crank angle. The cylinder contents have homogeneous mixture, as well as uniform pressure and temperature. Heat transfer across the cylinder boundaries (cylinder walls, piston crown, and combustion chamber) is determined by the Annand heat transfer model. The cylinder wall, piston crown, and combustion chamber temperatures are input to the model as boundary conditions.

The cylinder wall was divided into eight isothermal zones to establish a cylinder temperature gradient for the model. Heat transfer data across each of these isothermal zones were monitored on the engine and used as input to the model. Figure 3.3.1 shows a diagram of the modeled cylinder's heat transfer zones, and Figure 3.3.2 shows the heat release curve assumed in the initial cycle analysis.

The program creats dyanamic air flow in the intake and exhaust manifolds by using the "method of characteristics". The method accounts for pressure wave action in the inlet and exhaust manifolds by setting up and solving the equations for one dimensional compressible, unsteady flow. Pressure waves in manifolds can significantly affect engine air flow, especially in two-stroke engines.

Gas flow through the ports is determined by the pressure difference across the port, the gas's properties, the port area and the inputed port flow coefficient. The scavenging efficiency of the cylinder is an input to the program, as is the combustion heat release rate.

The UMIST MK14 Program was used to predict the following engine parameters at every degree of crank angle for the SCTE:

- Intake pressure
- Exhaust pressure
- Intake temperature
- Exhaust temperature
- Intake mass flow
- Exhaust mass flow
- Trapped mass in cylinder
- Cylinder gas temperature
- Heat loss through the ten heat transfer zones
- Cylinder gas pressure

The predicted steady state parameters are:

- Thermal efficiency
- Average exhaust temperature
- Average exhaust pressure
- Average intake pressure
- Average intake temperature
- Scavenge ratio
- Trapped air-fuel ratio
- Overall air-fuel ratio

3.3.2. Insulation Effects. It is well known that insulating a diesel engine can improve performance, such as:

1. Increased thermal efficiency
2. Increased available exhaust energy
3. Reduced cooling load requirement

However, insulating a diesel engine can also have the following detrimental effects:

1. Increased thermal loading of hot components
2. Reduced reliability
3. Piston, ring, and cylinder wall wear problems

Therefore, insulating the diesel engine is a compromise.

In order to address these tradeoffs, the UMIST MK14 program was used to analyze the various aspects of insulating the aircraft diesel SCTE. The first analysis focused on quantifying the heat loss paths and identifying the effect insulated components would have on performance. This was

done by independently setting the piston crown, the combustion chamber, and the cylinder wall heat loss to zero. Figures 3.3.3 and 3.3.4 show these data for power cruise and takeoff power, respectively. Most of the heat loss is through the combustion chamber, followed by the piston crown, and then a small percentage through the cylinder wall.

This means that the combustion chamber and piston crown would be the most productive items to insulate. The most difficult diesel engine component to insulate (for a valveless, ported, two-stroke engine) is the cylinder liner. This is so because of the size of the liner and also because of the piston ring and cylinder tribology problems at high temperature.

The UMIST MK14 program requires as inputs eight cylinder wall temperatures, one piston cap temperature, and one combustion chamber temperature. Therefore, to identify the range of these temperatures which were required to sufficiently insulate the engine, an average of the ten temperatures was used for the following study. This average is called the "average chamber wall temperature". Figure 3.3.5 shows the effect that average chamber wall temperatures has on thermal efficiency, exhaust temperature, peak cylinder gas pressure, peak cylinder gas temperature, and indicated heat loss. Indicated heat loss is defined as the actual heat loss rate divided by the heat addition rate from fuel combustion. All other input variables were kept constant. An increase in the average chamber wall temperatures from 450°K to 1000°K resulted in a ten percent increase in exhaust temperature, a five and one half percent increase in thermal efficiency, and a sixty-five percent reduction in heat loss. Peak cylinder pressure increased about six percent by increasing the average chamber temperature from 450°K to 1000°K. This increased cylinder pressure is a result of the 7.7 percent increase in cylinder gas temperatures caused by the reduced heat loss. This higher cylinder gas pressure results in more work output per cycle, i.e. improved thermal efficiency. The specific heat ratio of the gas, which decreases with increasing temperature, is a factor decreasing the thermal efficiency. The ten percent higher exhaust temperature would result in approximately a ten percent decrease in required overall turbocharger efficiency. Because of the decrease in specific heat ratio with increasing temperature the required turbocharger efficiency will be reduced to a lesser degree.

Figures 3.3.6 and 3.3.7 summarize the effect that the predicted average chamber wall temperature has on normalized heat loss rate and actual heat loss rate for four load points at 3500 RPM. Actual heat loss rate is the lowest for the twenty-five percent load line, and decreases with increasing average chamber wall temperature. However, the

normalized heat loss rate is the highest for the twenty-five percent load line, and it also increases with increasing average chamber wall temperature.

This indicates that the fuel energy added per cycle increases more with increasing load, than does the heat loss per cycle. The explanation for this is as follows.

All of the points plotted on Figures 3.3.6 and 3.3.7 were simulated at nearly equivalent air-fuel ratios. Air-fuel ratio defines the adiabatic flame temperature. The adiabatic flame temperature is only an approximate model for predicting combustion temperatures but it is accurate enough for this discussion. The point is, regardless of the mass of gas in the cylinder (i.e. load) the gas temperatures during combustion are nearly equal at a given air-fuel ratio. Since heat loss is primarily a function of temperature difference between the gas and the chamber walls, the heat loss during combustion is nearly a constant regardless of load. After combustion is complete, the lower load points, having less trapped mass of gas in the cylinder, and therefore, less internal energy, will cool off much quicker than the high load points. The cooler gas temperatures result in lower heat loss after combustion is complete. The nearly equal heat loss during combustion regardless of load is mostly responsible for heat loss not being directly proportional to fuel energy added during combustion.

Figures 3.3.8 through 3.3.11 show turbocharger power ratio of the turbine divided by the compressor versus normalized heat loss for lines of constant overall turbocharger efficiency (at four different loads). The area to the right of 1.0 represents a surplus of turbine power, and self-sustained turbocharger operation is possible. The area to the left of 1.0 indicates that the turbocharger will not operate self-sufficiently because the compressor requires more energy than the turbine can deliver.

These curves were used in conjunction with Figure 3.3.5 to quantify the degrees of insulation, and the average chamber wall temperature required for a given turbocharger efficiency.

It is evident from this study that even with significant reductions in heat loss, a fairly advanced turbocharger in terms of efficiency would be required. Improvements in air flow characteristics help reduce the required overall turbocharger efficiency.

3.3.3 Combustion Effects. A study was conducted to evaluate the effects that combustion and compression ratio have on peak cylinder pressure and thermal efficiencies. The combustion parameters that were investigated were

duration and point of ignition. Combustion duration was varied by compressing or expanding the baseline heat release curve shown in Figure 3.3.2. The start of combustion and compression ratio are inputs to the program so that modeling their effects on performance was straightforward.

Figure 3.3.12 shows combustion duration versus thermal efficiency and peak cylinder pressure. Both decrease with increasing combustion duration. The point of ignition for all of the data was fixed at the baseline of three degrees before top dead center and the effective compression ratio was twelve to one. A thirty-two percent reduction in combustion duration resulted in a nine percent increase in peak cylinder pressure and an eleven percent increase in thermal efficiency.

Figure 3.3.13 shows the start of ignition versus peak cylinder pressure,and thermal efficiency. The combustion duration was fixed at the baseline value of eighty-three degrees and the effective compression ratio at twelve to one. The thermal efficiency reached a maximum at a start of combustion of 350° ATDC. Cylinder pressure at this point was 137 bar.

Figure 3.3.14 shows effective compression ratio versus thermal efficiency and peak cylinder pressure. A seventeen percent decrease in effective compression ratio resulted in an eighteen percent decrease in peak cylinder pressure, and a three and one-half percent decrease in thermal efficiency.

The goal of this study was to optimize thermal efficiency, but not exceed the stress limits imposed on the hardware by the allowable peak cylinder pressure of 125 bar. This study revealed that the most logical course to take in reaching these goals was to start ignition at 350° ATDC and decrease the combustion duration as much as possible. These steps would optimize thermal efficiency. The peak cylinder pressure could then be limited by the compression ratio.

3.3.4 Manifold Effects. Intake and exhaust manifold geometry has a significant effect on the air flow characteristics of turbocharged engines. Due to the high air-fuel ratios used for a two-stroke, turbocharged diesel and the difficult turbocharger matches associated with such an engine, it is imperative to aid that match by reducing the required pressure ratio across the cylinder. The pressure ratio can be reduced through improvement of the manifold design which enhances airflow.

In the course of obtaining the most practical and efficient manifold design, several single parameters were varied and

their effects on performance were evaluated using the computer program. Manifold geometery variances included lengths and diameters of the pipes. Variables included air flow rate through the engine, fresh air trapped within the cylinder, and pressure ratio across the cylinder.

It became apparent that in general larger area pipes provided greater flow rates. It was also found that pipe length had less effect on "tuning" when pipe diameters were increased. Figure 3.3.15 shows a plot of intake and exhaust pipe area versus mass flow, divided by pressure ratio, shows that for the range investigated, a larger area exhaust pipe should be better for air flow. It also indicated that within that range where data was generated, there is an optimum intake pipe area. A similar plot, Figure 3.3.16 , shows the effect on mass trapped within the cylinder. Again, optimum manifold areas were found to maximize trapped mass.

This information was coupled with reasonable estimates of the range of pipe area, hence pipe diameters that would be usable on the test engine.

The chosen optimum configuration of 125 cm2 intake and 81 cm2 exhaust corresponds to two 8.9 cm diameter intake manifolds and one 10.1 cm exhaust manifold. This configuration was then simulated. Figure 3.3.17 shows air-fuel ratio versus cylinder pressure ratio for both the optimized manifold configuration and the original AVL manifold configuration as predicted by the UMIST MK14 program at the power cruise condition. Significant reductions in cylinder pressure ratio are possible while still maintaining the same air-fuel ratio.

Transient pressure fluctuations in the chosen manifold were also simulated by the computer analysis.

Required overall turbocharger efficiency is a function of inlet pressure, exhaust pressure, exhaust temperature, ambient pressures as shown in the following equation from a basic thermodynamic power balance (Reference 6).:

$$\eta_{tc} = \frac{\dot{w}_c}{\dot{w}_t} = \left\{\left[\left(\frac{p_1}{p_a}\right)^{\frac{\gamma_1-1}{\gamma_1}} - 1\right] \cdot T_1 \cdot c_{p_1}\right\} : \left\{\left[1-\left(\frac{p_a}{p_2}\right)^{\frac{\gamma_2-1}{\gamma_2}}\right] \cdot T_2 \cdot c_{p_2}\right\}$$

Where: P_a - ambient pressure

P_1 - compressor discharge pressure

P_2 - turbine inlet pressure

T_1 - compressor inlet temperature

T_2 - turbine inlet temperature

C_{p1} - specific heat at compressor inlet

C_{p2} - specific heat at turbine inlet

γ_1 - specific heat ratio at compressor inlet

γ_2 - specific heat ratio at turbine inlet

W_c - compressor work

W_t - turbine work

(It is assumed that the air flow into the compressor is equal to the air flow into the turbine).

The above equation was used to evaluate the required turbocharger efficiency for the original AVL manifold, and the optimized manifold at the power cruise condition. All variables were held constant with the exception of exhaust pressure (P_2). Cylinder pressure ratio would realistically only affect exhaust pressure because inlet pressure is strictly a function of required inlet density at a given load.

Extrapolating the optimized manifold's overall air-fuel ratio curve from Figure 3.3.17 to the AVL design point of 45 to 1 air-fuel ratio would require a cylinder pressure ratio of 1.185.

This would correspond to an exhaust pressure of 222.9 kPa for the optimized manifold as opposed to 210 KPa for the AVL manifold. The required overall turbocharger efficiency for a balanced turbocharger with the optimized manifold would be 60.4 percent and for the AVL manifold, 62.3 percent. While this reduction is significant, a further reduction would be desirable.

Manifold length effects were not investigated as thoroughly as were the manifold area effects, since manifold length is greatly constrained by the multicylinder engine layout and configuration. A comparison of flow and trapped mass was made between a 1/2 meter long exhaust pipe and a one meter

long exhaust pipe for both the AVL manifold and the optimized manifold. No significant difference was noticed in trapped mass and air flow for the four configurations evaluated.

Figure 3.3.18 shows both predicted and measured intake manifold pressure, versus crank angle. As can be seen, there is very close agreement between the two. Figure 3.3.19 shows the predicted and measured exhaust manifold pressure versus crank angle.

The measured and predicted exhaust pressures do not agree with each other as well as the intake pressure did. A possible explanation for this is that the pressure sensor is exposed to the high temperature exhaust which can significantly degrade its accuracy.

3.3.5 Port Timing Optimization. A further computer study was conducted to optimize the intake and exhaust port timing. A series of cycle simulations were run for the power cruise and takeoff power conditions which utilized the optimized intake and exhaust manifold sizes. Each series of simulations consisted of nine different combinations of timing for the intake and exhaust ports while all other input variables were fixed.

Figures 3.3.20 and 3.3.21 show that 90° ATDC for the exhaust port timing and 100° ATDC for the intake port timing would be the optimum porting configuration. This porting configuration gave the highest trapped air-fuel ratio, superior scavenge ratio, with a very slight degradation in indicated thermal efficiency for both the power cruise and takeoff power conditions. Further analysis of this porting configuration was not conducted because the existing hardware could not physically accommodate further advanced or raised exhaust port. As a compromise, further cycle simulation work concentrated on the porting configuration of 93° ATDC exhaust port and 103° ATDC intake port timing. If this porting arrangement had proved beneficial during development tests, then a means would have been provided to test a cylinder with 90° ATDC exhaust port and 100° ATDC intake port timing.

Figure 3.3.22 shows various porting arrangements as well as the optimized porting configuration. The optimized intake ports are considerably (16%) larger in area (i.e. higher by 5mm) than the original AVL designed intake ports. This is the main reason for the improved air-flow. The back flow into the intake ports during exhaust blowdown is not of sufficient quantity to offset the increased flow due to the larger port area.

Figure 3.3.23 shows predicted air-fuel ratio versus cylinder pressure ratio for the optimized porting and manifolding configuration. Data for the AVL configuration ports at the power cruise and takeoff power conditions is also shown. Significant increases in air-flow were predicted for the optimized configuration.

At the optimum overall air-fuel ratio predicted by AVL, the optimized configuration requires a pressure ratio of only 1.09 for power cruise and takeoff power. The computer predicted overall turbocharger efficiency required for the optimized configuration at take-off power was 53.7% and 58% at power cruise. The predicted overall turbocharger efficiency required for the original configuration was 61.8% at take-off power and 62.3% at power cruise. This optimized configuration represents a significant reduction in the required overall turbocharger efficiency. Up to this point in the analysis this reduction has been accomplished without reducing the heat loss. Further improvements in the required turbocharger efficiency would be possible with reduced heat loss.

3.3.6 Reed Valve Evaluation. The application of reed valves in the intake manifold ports of high speed, two cycle, crankcase scavenged spark ignition engines has proven to be very beneficial in improving engine performance. These performance gains result from improved mass flow conditions and longer effective strokes. The potential application of such a passive device was, therefore, explored for this engine by use of the simulation model. The simulation of reeds was accomplished by installing a hypothetical 100% efficient one-way check valve. This hypothetical reed valve is located on the cylinder wall, seals perfectly, responds instantaneously, and has no throttling or flow losses. Obviously, real reed valves do not behave in such a manner; but for purposes of predicting airflow and engine performance trends, this ideal condition was assumed. Approximately 26 sets of data were run. In each case, the same run was made with and without reed valves so a direct comparison was possible. The majority of runs were made at the take-off power level. This performance level requires the largest amount of exhaust blowdown lead time due to the high rotative speed and the highest cylinder gas pressures. The original intent of applying the reed valves was to allow the reeds to control port opening by sensing the pressure differential between the intake manifold and cylinder gas pressure. Since the reeds would control port opening, the intake and exhaust ports could be made the same height. This would eliminate the current loss of fresh air charge between intake and exhaust port closures (approximately 14°CA). Figure 3.3.24 illustrates such a condition whereby the intake and exhaust ports are the same heights. As shown, without reed valves, some negative airflow occurs into the intake

manifold due to the higher cylinder pressures expanding into both the intake and exhaust manifolds. Also, positive flow occurred sooner without the reeds due to the fact that the cylinder gases are expanding into both the intake and exhaust manifolds. In the reed valve case, intake air flow begins later because all of the cylinder pressure must expand into the exhaust manifold. The net result is less time available for air flow. Also, from Figure 3.3.24 it may be construed is that the reverse flow and pressure wave set up in the intake manifold can produce a positive tuning effect during the open period, thereby increasing total cylinder air flow.

Numerous porting sizes were evaluated to show some performance improvement with reed valves. In all cases, reviewed, reed valves did not change, or adversely effect airflow and engine performance. The conclusion drawn from this investigation was that with crankcase scavenged engines, the reed valves prevent discharging the pressurized intake charge back through the intake manifold. Since the aircraft diesel engine is not a crankcase scavenged engine, this loss of charge is not applicable. The only potential improvements that may ultimately warrant the use of reeds might be:

1. If, in the multicylinder engine, the reverse flow into the intake manifold would adversely affect adjacent cylinders, reeds might eliminate this reverse flow.

2. Expanding all of the cylinder blowdown gases into the exhaust manifold (in the reed case) may improve the exhaust energy available to the turbine, particularily if the turbine is designed as a pulse recovery type rather than as a constant pressure system.

3.3.7 Conclusions of Cycle Analysis Studies. Figure 3.3.25 shows the predicted engine performance for four load points at 3500 RPM. The engine configuration has a 125cm^2 area manifold, an 81cm^2 area exhaust manifold, 103° ATDC intake timing, 93° ATDC exhaust port timing, and increased chamber wall temperatures which simulated insulation. Also plotted on this figure is the predicted engine performance for the original AVL baseline engine configuration.

Significant reductions in heat loss and cylinder pressure ratio were predicted for the optimized configuration, which resulted in reduced required overall turbocharger efficiency for a balanced system. Indicated specific fuel consumption is slightly higher with the optimized configuration compared

to the original AVL configuration. This was probably due to the degradation in thermal efficiency caused by the advanced port timing offsetting the increase in thermal efficiency caused by the reduced heat loss.

Figure 3.3.26 shows for take-off power, the ten heat loss zone temperature inputs to the model, as well as, the percent of total heat loss and heat flux through each zone.

These data were useful in making projections of the cylinder liner, and cylinder head temperatures of the second generation SCTE design. The accuracy of these performance projections are determined by the accuracy of the input parameters:

1. Combustion burn rate
2. Annand heat transfer coefficients
3. 10 chamber wall temperatures
4. Port flow coefficients
5. Scavenge efficiency model

The goal of the cycle analysis was to optimize the AVL baseline engine configurations. Agreement between the actual SCTE test cell data and these projections was not the primary intent.

3.4 Fuel Injection

Fuel injection characteristics play an important role in optimizing the engine performance. Several possibilities were examined for this application within the constraints of hardware availability, speed capability, cost and time. This Section 3.4 describes the systems that were considered, evaluated, and tested in this program.

3.4.1 Injection Requirements. A fuel injection system for a direct injected diesel engine has to distribute a finely atomized charge of fuel uniformly throughout the combustion chamber in a short duration of time, and with exact timing during the engine cycle. These characteristics must be repeatable from one cycle to the next. An injection system that does not meet these criteria results in poor combustion, causing excessive cylinder pressure, exhaust smoke and fuel consumption.

Combustion is also effected by air-fuel ratio, the combustion chamber temperatures, the combustion chamber geometry, and air motion. Typically, inlet port induced air motion (swirl) is used to help fuel-to-air mixing, and hence, combustion.

Combustion chamber squish is another useful method for inducing combustion chamber air motion, but its effects on combustion are less prominent than swirl motion.

The high speed, two-stroke cycle, quiescent combustion chamber characteristics of this engine do not provide adequate air motion for good mixing and therefore, places severe demands on the injection system in order to obtain efficient combustion.

Table VI shows the desired injection system requirements for this engine.

TABLE VI
SCTE FUEL INJECTION SYSTEM REQUIREMENTS

Flow range	5 - 100mm^3/injection
Injection rate	8 - 60 injections/second
Injection duration	less than 1.2 ms
Injection pressure	up to 1400 bar
Injection timing	Variable
Fuel compatability	DF1, DF2, JET "A"

Three injection systems aimed at meeting these criteria were evaluated during this program. Their design is discussed in the subsequent sections.

3.4.2 Bosch APF Injection System The first fuel injection system evaluated on the SCTE consisted of an American Bosch APF1B injection pump, and a AKN 17mm nozzle holder and an ADB type injection nozzle.

The APF type pump is a constant stroke, helix controlled, plunger and barrel type unit which is actuated by an engine mounted camshaft driven at engine speed. Figure 3.4.1 shows a diagram of the camshaft profile. The lift duration is a slow 100°. This pump was designed for medium to slow speed diesel engines, and could be fitted with either a nine or ten millimeter diameter plunger.

The AKN type nozzle holder is a standard holder which allows valve opening pressure adjustment up to 303 bar by shimming the adjusting spring accordingly. A spring cavity leak-off is provided. Its maximum rated injection line pressure is 1035 bar.

This injection system was not designed, nor was it expected to meet the injection requirements of the SCTE. It was intended to be used only for initial SCTE testing.

3.4.3 CAE-X Injection System. The heart of the CAE-X Injection System was the single cylinder version of the CAE-X pump originally developed for the AVCR-1360 engine in the mid-1960's. Figure 3.4.2 shows a diagram of the pump. The pump is a constant stroke, helix controlled, plunger and barrel type unit which is actuated by a ball bearing supported camshaft. The plunger is fourteen millimeters in diameter. The plunger, barrel, camshaft, and bearings are lubricated by pressurized engine oil. In order to keep the stresses as low as possible for its adaptation to the SCTE, the pump was adapted to a double lobe camshaft which was run at half engine speed or 1750 RPM at 3500 RPM engine speed.

Stress calculations on the pump's components revealed that the chance of the pump's mechanical survival was good. Figure 3.4.3 shows the cam profile, velocity, and acceleration. The cam's high acceleration gives very high injection pressures. The cam follower is a rolling element type. This pump can provide over 1400 bar injection pressure.

The single cylinder version of the CAE-X pump was designed to be coupled to a variable timing unit. This unit is shown in Figure 3.4.4.

An American Bosch AKN type injection nozzle holder used with this pump with an ADB type nozzle. A stainless steel cooler adapter shown in Figure 3.4.5 was used to cool the nozzles. Pressurized oil was forced through the transfer passages to the annulus. This annulus was in close thermal contact with the injector nozzle by means of a light press fit. The oil then flows out of the annulus through the exit transfer passage and into the engine sump.

3.4.4 Bendix Injection System. The Bendix Corporation was contracted by TCM to design, build, test, and deliver five injection systems to meet the injection characteristics listed in Table 3.4-1. The Bendix DCX-3-28 is an electronically controlled diesel injection system. Its operation is best defined as that of an electronically actuated hydraulic relay switch. The injector has two

operating modes; fuel metering and fuel injection. Fuel injection occurs at the instant fuel metering ends. Thus, fuel injection advance is controlled by the beginning of metering. The injector can give very high injection pressures (1350 bar) by hydraulically amplifying a moderate (350 bar) fuel supply pressure. This high pressure fuel is delivered to the combustion chamber through a nozzle similar to the Bosch ADB type.

Figure 3.4.6 shows the positions of the injector components during metering. To begin metering, an electric impulse is sent to the coil. The signal is a 70 volt spike leading a 12 volt pulse.

The armature of the pilot valve (Item 1) is attracted to the coil causing the hole in the end of the needle to be sealed off by the piston. Simultaneously, the needle is lifted off its seat allowing the pressure at the right end of the spool valve (Item 2) to be dumped to atmosphere. The spool is then moved to the right by the force of the supply pressure. The spool valve, in this position blocks supply pressure from reaching the primary piston (Item 3) and vents the top of the primary piston to atmosphere. The fuel, at supply pressure, moves through the ball check valve in the bottom intensifier body (Item 4) and fills the intensifier piston cavity as the piston is forced upward. When the desired metering time has been reached, the coil is de-energized and injection begins. Figure 3.4.7 shows the main fuel injection events.

When the coil (Item 5) is de-energized, supply pressure forces the needle and piston apart. The needle hole is uncovered and the needle seats, closing off the atmosphere dump to the end of the spool valve (Item 2). Supply pressure is now allowed to push the spool valve to the left which closes off the atmosphere dump passages to the top of the primary piston (Item 3), and also applies supply pressure to the top of the primary piston causing the intensifier to move and subsequently injection to start after nozzle opening pressure is reached. The ball check valve is closed, preventing fuel from dumping back to supply.

After the primary piston reaches the bottom of its stroke, the system's moving parts remain stationary until the start of metering on the next cycle or event.

The ideal static intensification ratio (no leaks or losses), for the DCX-3028 injector is nominally 5.0:1 which of course is the ratio of the areas of the primary and intensifier pistons.

There are two fuel pump ports, one in the valve body and one in the coil. The dump port in the valve body dumps fuel

from the top of the primary piston during metering and from the bottom of the primary piston during injection. This flow of fuel through the coil serves to cool the coil.

The fuel injection controller uses digital feedback techniques for precise fuel control. A block diagram of the controller is shown in Figure 3.4.8.

3.5 Finite Element Thermal and Structural Analysis.

As part of the overall design and analysis of this engine concept, detailed finite element thermal and structural analyses were made of the single cylinder test engine power components. This analysis was made under subcontract for TCM by Analysis and Design Application Company (ADAPCO) Melville, New York. The analysis utilizes the well known ANSYS finite element program, and integrates it with the same UMISA cycle analysis program as was used by TCM in conducting the work of Section 3.3 (also known as the "Benson Code"). These programs were operated in a closed loop fashion.

For the cycle simulation program it was necessary to specify combustion chamber wall temperatures. These included the combustion bowl inner surface, piston cap top surface, and cylinder inner surface. Next, using the cycle simulation temperatures of the combustion gas as a function of crank angle, a cycle average thermal analysis of the overall engine is carried out. The resulting combustion surface temperatures are compared with those which were used in the cycle simulation analysis. If there is a significant difference, the new surface temperatures are input into the cycle simulation and the coupled analysis is repeated using this technique, Configuration 12 of the test engine (described in 4.2.6) was modeled. One of the same data points that were modeled was also run as an actual test point. Annand heat transfer constants were then adjusted to bring the modeled and measured data into agreement. Using the modified constants, a second data point was simulated and the results compared to actual data.

Using this approach the correlation of the cycle simulation results with experimental data is considered to be very good with respect to indicated power and airflow. The correlations for exhaust temperature and peak cylinder pressure are reasonable but need improvement in the analytical model.

The correlation of calculated surface temperatures to experimental data is considered to be generally within the range of experimental error.

The heat loss was matched with the experimental value on one run by adjusting the heat transfer coefficient, but the program then did not predict the measured heat loss for the second run adequately.

Additional iterations and refinements are required to resolve this discrepancy. This activity was conducted close to the end of the program and funding and time constraints prevented additional work to resolve the issue.

Because of the significance of this analysis, separate reports were generated. These are included as Appendix I Cycle Simulation and Heat Transfer Analysis and Appendix II Structural Analysis.

3.6 Second Generation Single Cylinder Test Engine

The testing and analysis program conducted on the first generation hardware demonstrated the feasibility of reaching the major goals in terms of power density, specific fuel consumption and air flow requirements. Based on the knowledge acquired in that series of tests, a second generation configuration of the SCTE was designed. It incorporated the desirable features made evident in testing, and also included in the design, the ability to insulate the cylinder to varying degrees. This second generation hardware is discussed in this Section 3.6.

3.6.1 Design Goals. The second generation engine has been designed to accommodate both a cooled and an uncooled version. Figure 3.6.1 illustrates the cooled version and Figure 3.6.2 shows the insulated configuration.

1. Cooled Version. Oil cooling is provided around the cylinder head and upper portion of the cylinder liner. Materials used are:

- Cylinder head: Stainless steel AISI 302
- Cylinder liner: Nitralloy 135 Mod
- Piston cap: Stainless steel AISI 302
- Piston: Nodular iron

2. Insulated Version. This design incorporated all the features derived from the finite element studies as detailed in Appendix IV. Materials used are:

- Cylinder head: Stainless steel AISI 302
- Cylinder liner: Sintered silicon nitride
- Cylinder barrel: Stainless steel AISI 302
- Piston cap: Sintered silicon nitride
- Piston 4: Nodular iron

As much versatility as possible has been built into the engine. All major components are readily replaceable.

- Cylinder head and cylinder barrel are separate components
- Removable cylinder liners
- Replaceable piston cap

A complete set of drawings and parts list of the second generation engine has been submitted along with this report. The parts list is included as Appendix III.

The engines serve several purposes:

1. Investigate the effect of various degrees of cooling on engine performance.

2. Determine the durability of critical components.

3. Gain more knowledge on the overall behavior of ceramic components.

4. Provide knowledge on the tribology requirement of insulated engines.

However, because of funding limitations, hardware was procurred only for the cooled configuration of the second generation engine, and they were never assembled or tested. Ceramic components were not procured under this contract.

3.6.2 Finite Element Thermal and Structural Analysis of Second Generation Engine. As with the first generation engine, detailed finite element thermal and structural analysis were made of the second generation engine. Like the studies described in 3.5 and Appendix I and II, this analysis was also made by ADAPCO. It utilized the same programs, techniques and procedures as described above. The analysis for the insulated configuration was made for three different sets of monolithic ceramic components - partially stabilized Zirconia (PSZ), Alumina, and Silicon Nitride. A final report from ADAPCO on the analysis of this insulated engine is included as Appendix IV giving the details and specific values of constants used.

From the thermal and stress analysis results presented in Appendix IV, plus ADAPCO's experience on other low heat rejection concepts involving monolithic ceramics, it is ADAPCO's and TCM's opinion that the insulation of this lightweight diesel has a high probability of success. To date, the major problems in insulating low heat rejection engines has been the piston. In the case of this engine, the elimination of the combustion bowl from the piston and giving it a spherical domed shape provides a configuration which has a high probability of not failing. In addition, the entire piston surface is covered with ceramics. This is important from both a heat loss standpoint and being able to keep the rings cool.

One problem identified in the thermal analysis is the high temperature (above 955^{o}C) at which the Zirconia insulated

engine configuration is operating. This problem is important, since Zirconia should be used as the insulator due to its high thermal expansion. However, Zirconia should not be used at temperatures above 850°. To provide some minimum cooling while at the same time reducing cost, it may be possible to use a metal liner long with ceramics for the remaining components.

3.6.3 Summary of Ceramic Insulated Designs. Table VII compares peak component temperatures and tensile stresses for various insulated configurations of the engine as predicted by the UMIST cycle simulation and the ADAPCO finite element analysis. The PSZ configuration gave very low heat loss due to PSZ's low conductivity.

This configuration may not be viable, however, for several reasons. First, the temperatures and applied tensile stresses for the piston cap and combustion chamber are far in excess of PSZ's ultimate tensile strength. Secondly, PSZ's strength deteriorates at these high temperatures due to a tetragonal to monolithic transformation in Zirconia's microstructure. Thirdly, the temperatures and stresses applied to the cast iron piston are too high.

The alumina configuration also suffers from the same stress and temperature problems that the PSZ configuration did. Aluminia also has much lower fracture toughness and thermal shock resistance than PSZ.

The silicon nitride configuration has a very good chance of success due to the relatively low applied stresses and temperatures to the insulating components. However, the cast iron piston would have to be cooled due to its very high temperature in the current configuration.

The stainless steel with air gap configuration which was modeled at 3/4 load and 3000 RPM gave a higher piston cap and combustion chamber temperature than the silicon nitride configuration did which was modeled at full load and 3500 RPM. This indicates that the metallic with air gap components are better insulators than the monolithic silicon nitrides components. The cylinder liner for the stainless steel configuration was fully cooled. The high stresses in the piston cap and combustion chamber did not cause a failure because the components plastically deformed before reaching these predicted stresses. If the piston cap and combustion chamber had been made of a brittle ceramic, they would have failed.

The air gap insulated configuation for ultimate application would require a nickel based superalloy as a structural material instead of stainless steel because the peak temperatures (1100°) are beyond the temperature limit for

TABLE VII
COMPARISON OF ALTERNATE INSULATIVE CONCEPTS

	*PSZ	*ALUMINA	* Si_3N_4	**STAINLESS STEEL
Maximum Piston Cap Temperature (^{O}C)	1140^{O}C	1092	1014	1072
Maximum Piston Cap Tensile Stress (MPa)	590.6	508.6	142.8	976.2
Maximum Piston Temperatures (^{O}C)	649	704	815	399
Maximum Piston Tensile Stress (MPa)	256.3	521.3	1154.7	344.5
Maximum Combustion Chamber Temperature (^{O}C)	1126	1026	874	927
Maximum Combustion Chamber Tensile Stress (MPa)	1154.6	861.1	226.8	134.9
Maximum Liner Temperature (^{O}C)	1018	855	740	447
Maximum Liner Tensile Stress (MPa)	181.8	44.0	161.9	---
Top Ring Reversal Liner Temperature (^{O}C)	871	693	693	343
Indicated Heat Loss (% of Fuel Energy(	2.32	3.82	4.64	11.9
Heat Transfer Through:				
Piston %	13.2	15.7	19.8	19.9
Liner %	41.4	34.1	24	39.38
Combustion Chamber %	45.4	50.2	56.2	40.7

* - Full Load, 3500 RPM
** - 3/4 Load, 3500 RPM

stainless steel to survive for any appreciable length of time. The use of nickel based supralloys, however, increases the cost of the components and may ultimately make the development of ceramic components more attractive.

Presently the metallic air gap insulation scheme is the safest technology for insulating the diesel engine. In the future, if ceramic materials become both stronger and fracture resistant, they may surpass the metallic air gap insulation scheme in terms of insulation effectiveness, weight, and cost.

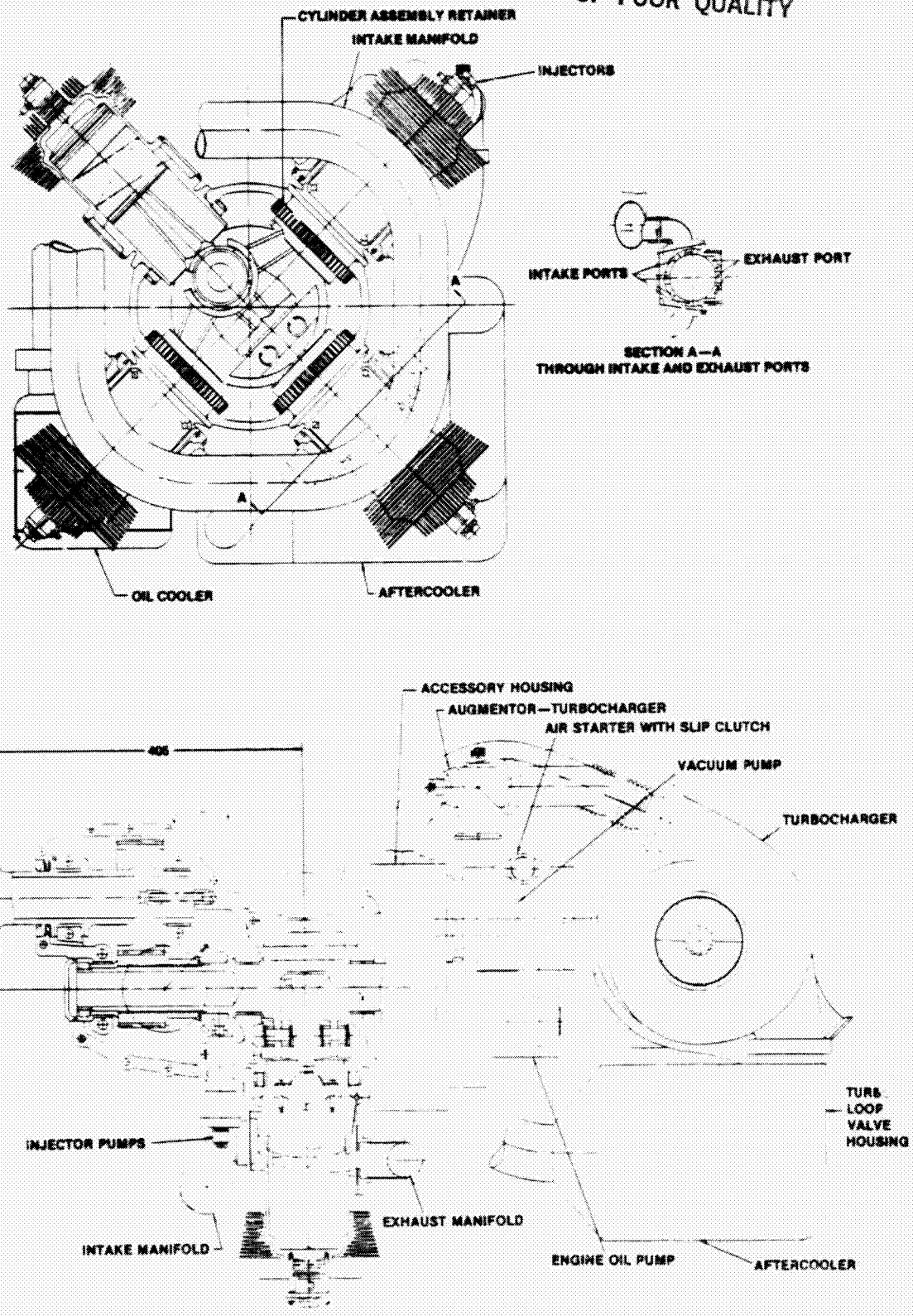

Figure 3.1-1. 186 kW Aircraft Diesel

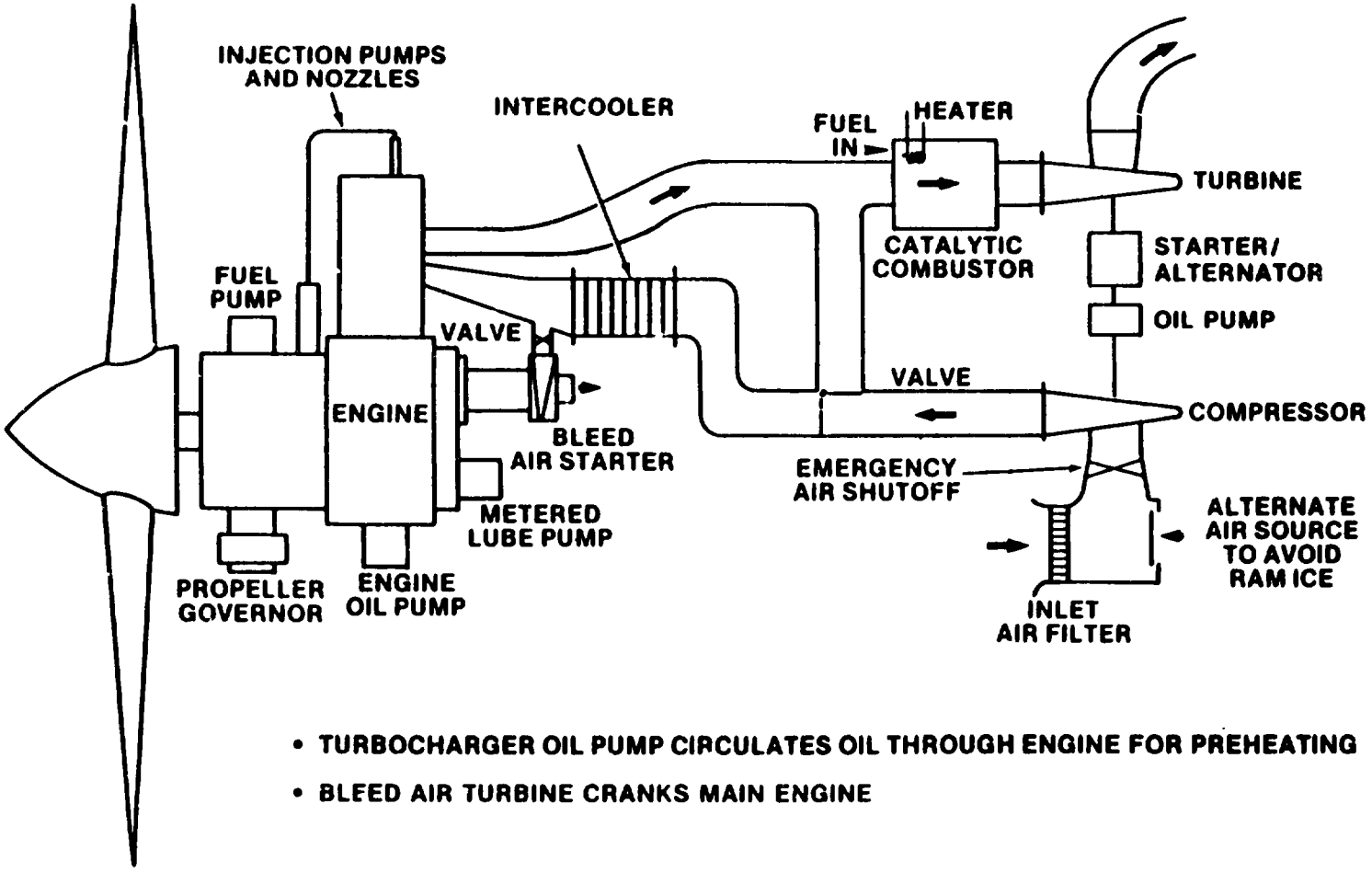

Figure 3.1-2. Schematic 2-stroke engine with independent turbo loop

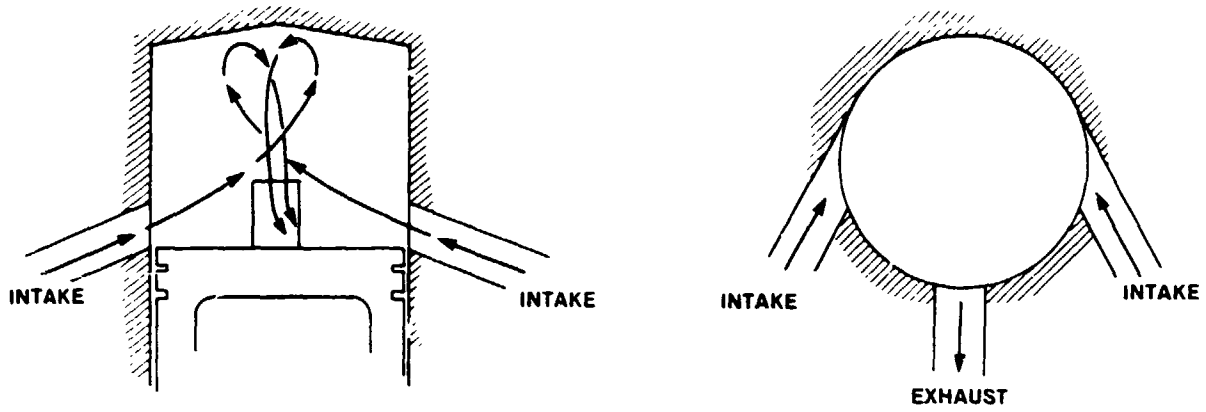

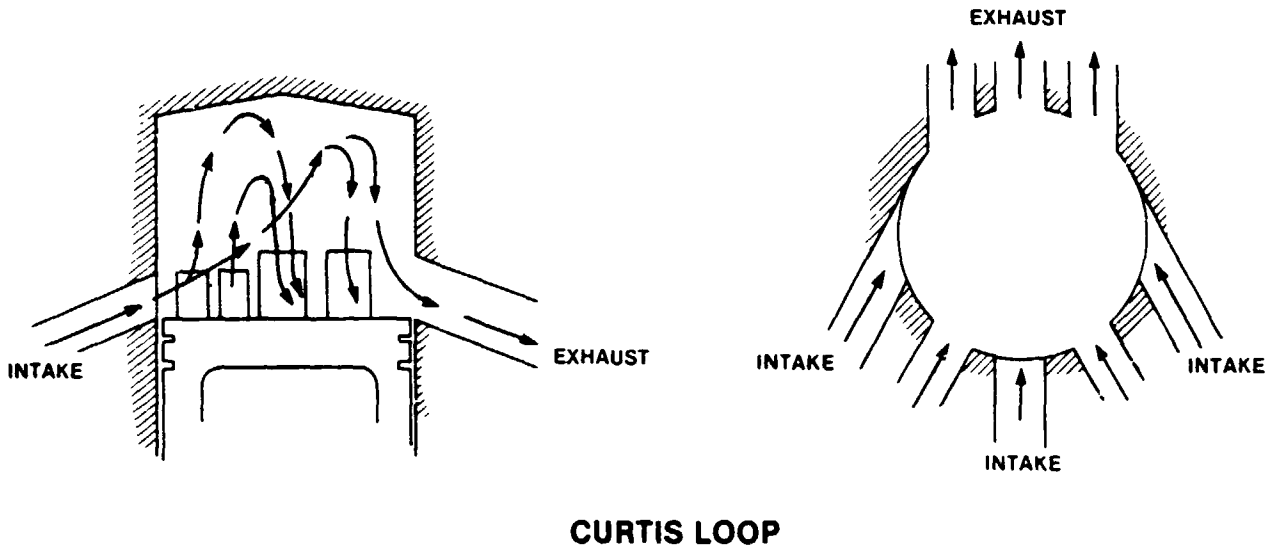

Figure 3.1-3. Comparison of Schnuerle and Curtis Loop Scavenge Systems

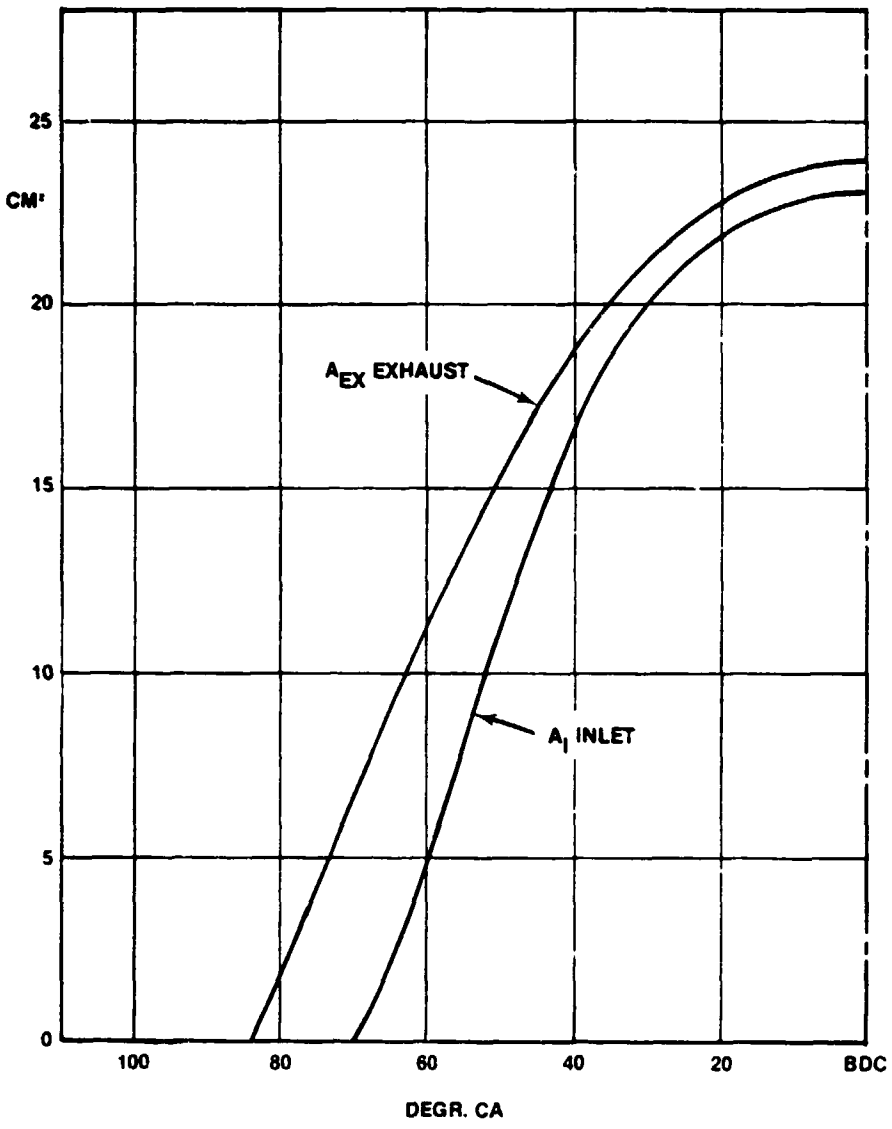

Figure 3.2-1. Geometrical Port Areas Versus Crank Angle

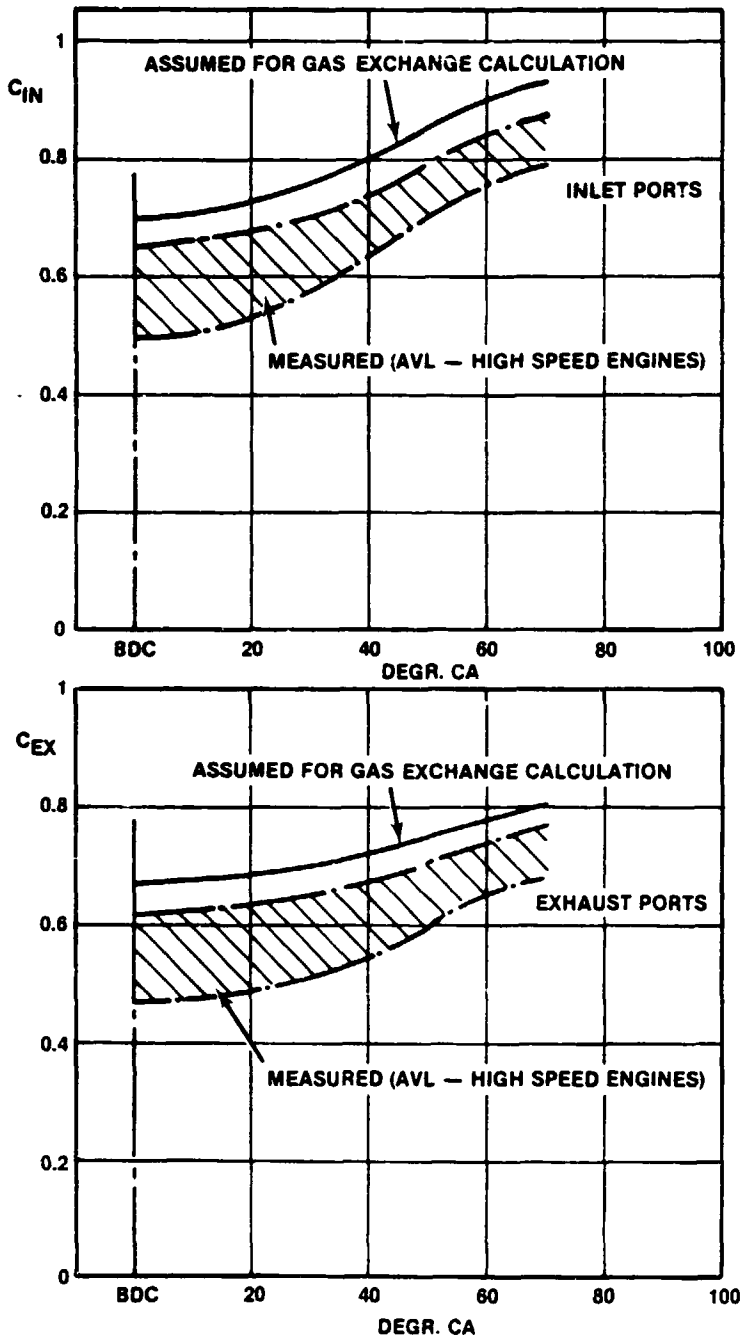

Figure 3.2-2. Flow Coefficients Versus Crank Angle

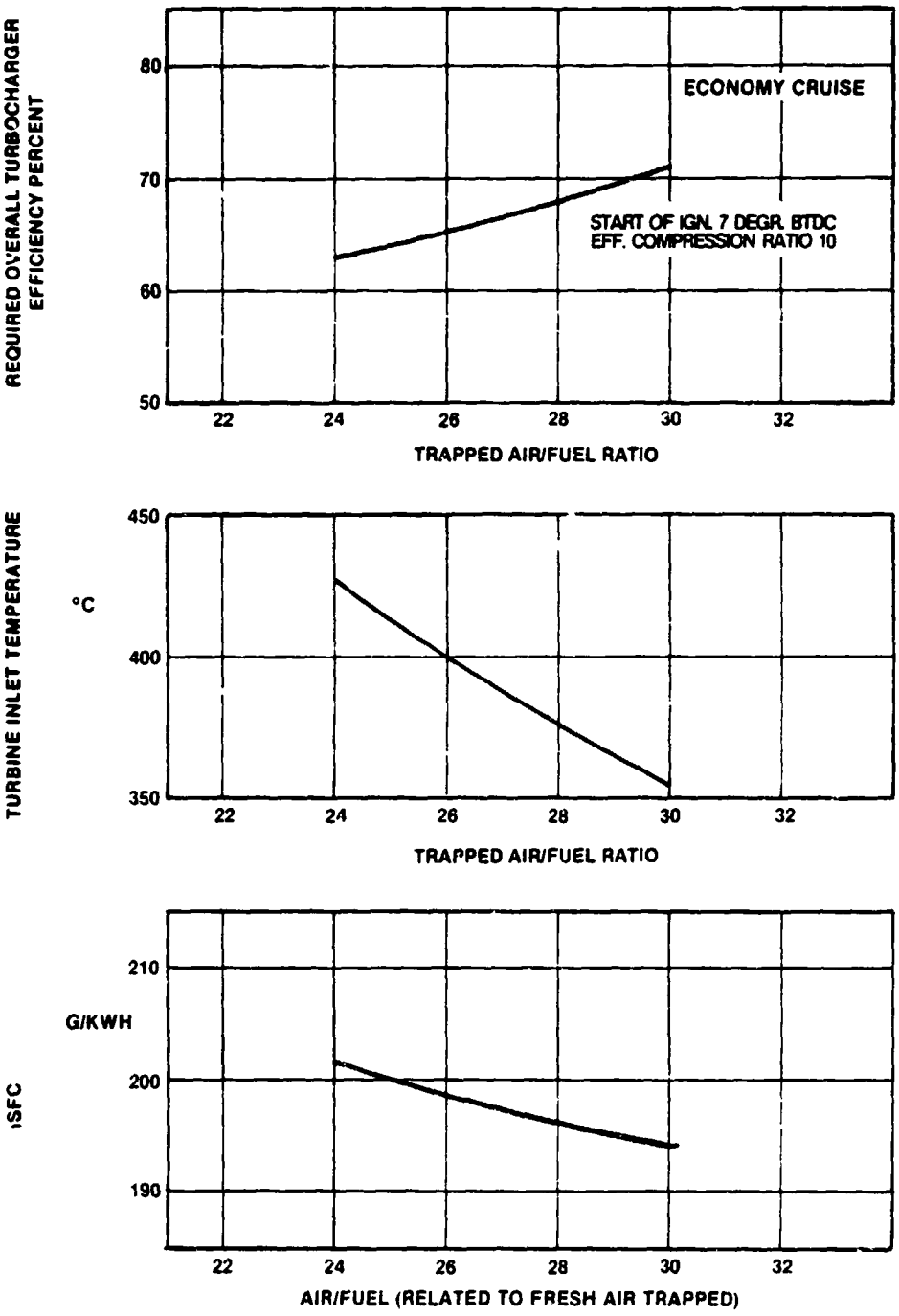

Figure 3.2-3. Effect of A/F on η_{TC}, Turb. Inlet Temp. and ISFC

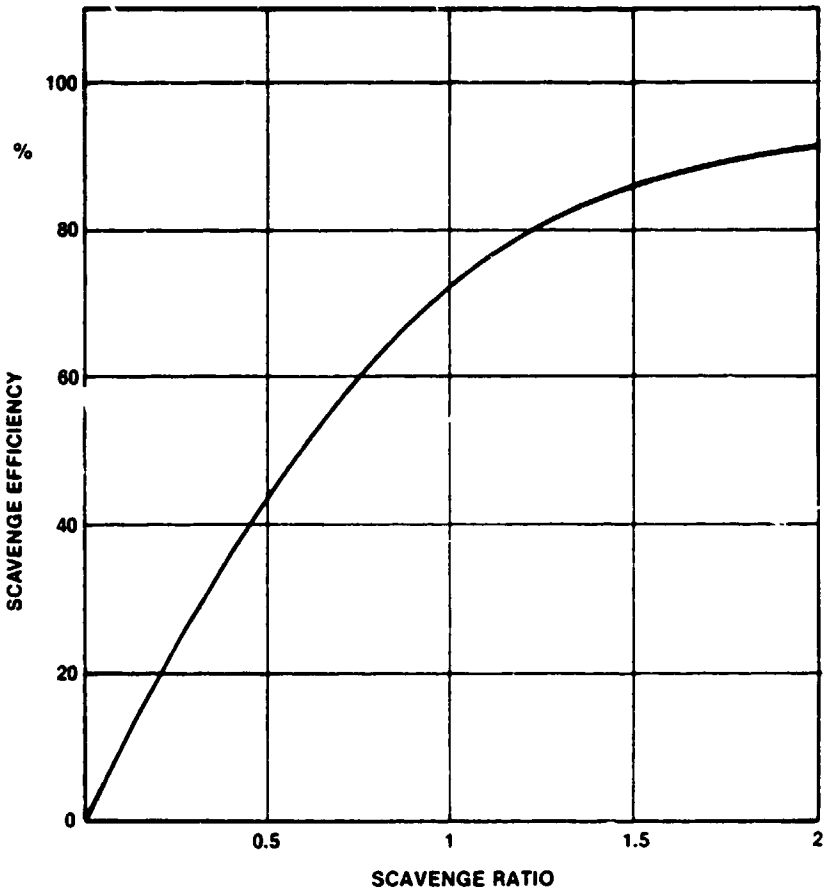

Figure 3.2-4. Effect of Scavenge Ratio on Scavenge Efficiency for Loop Scavenged Engine

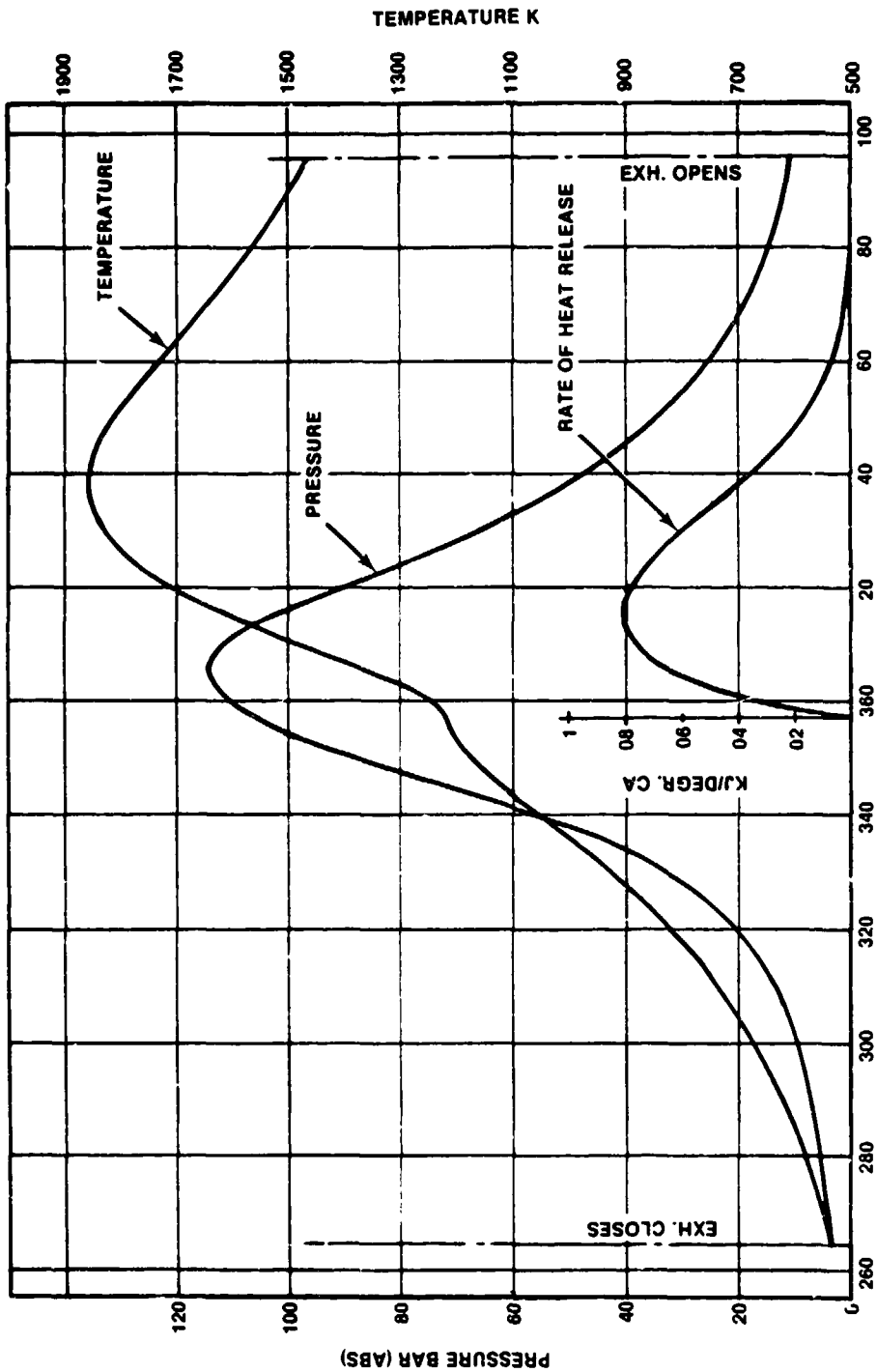

Figure 3.2-5. High Pressure Diagram for Takeoff Power

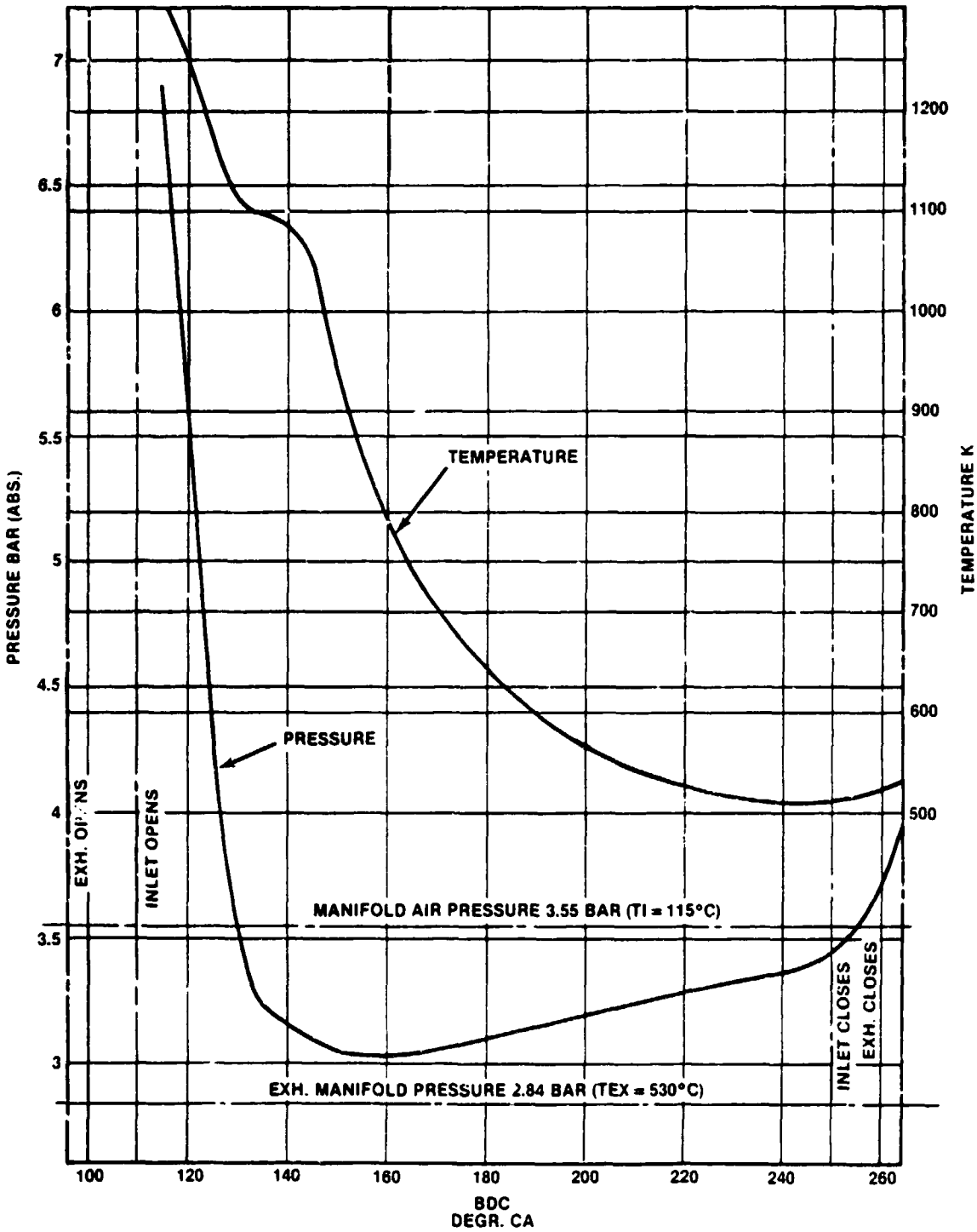

Figure 3.2-6. Low Pressure Diagram for Takeoff Power

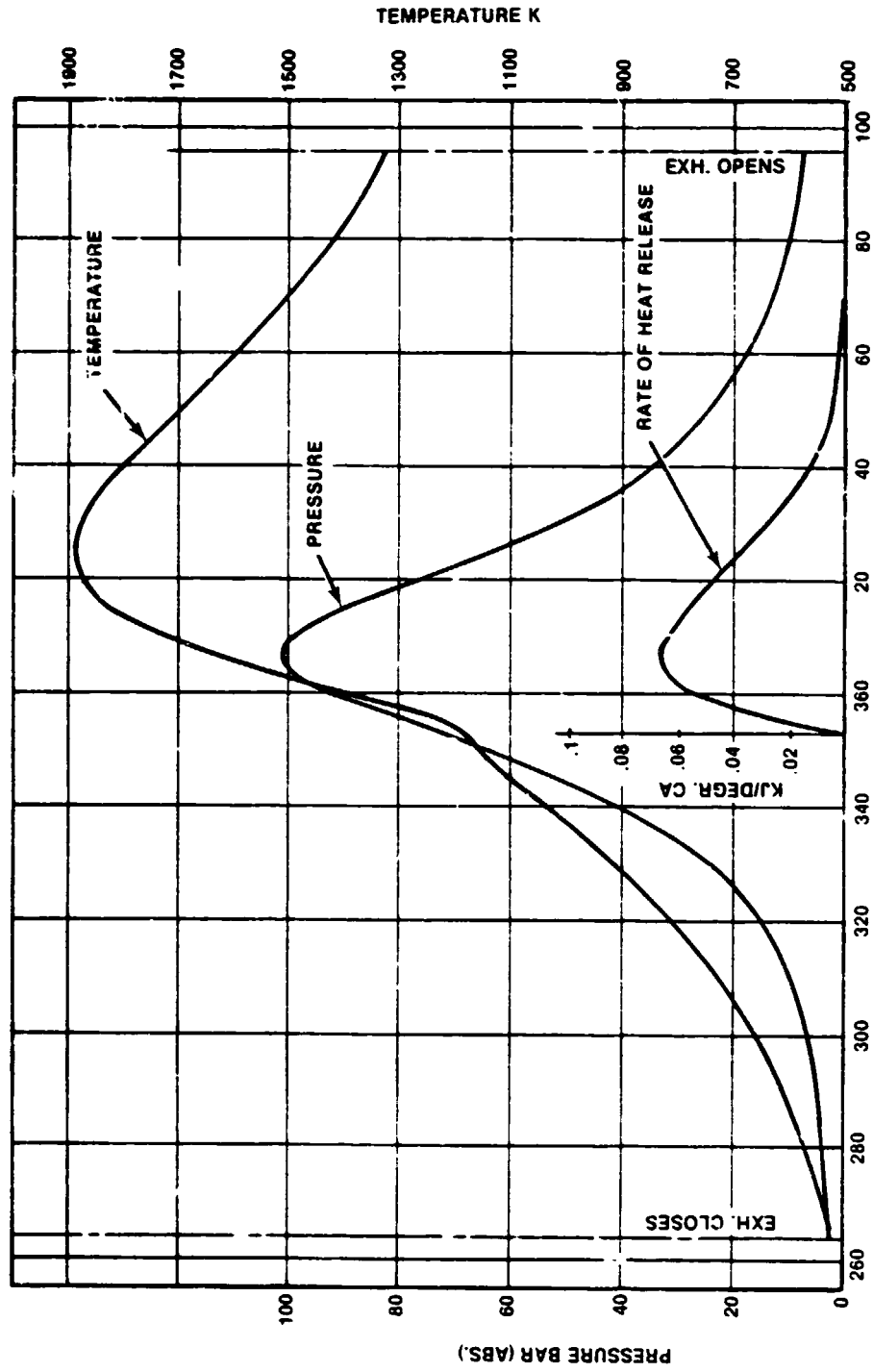

Figure 3.2-7. High Pressure Diagram for Full Power Cruise

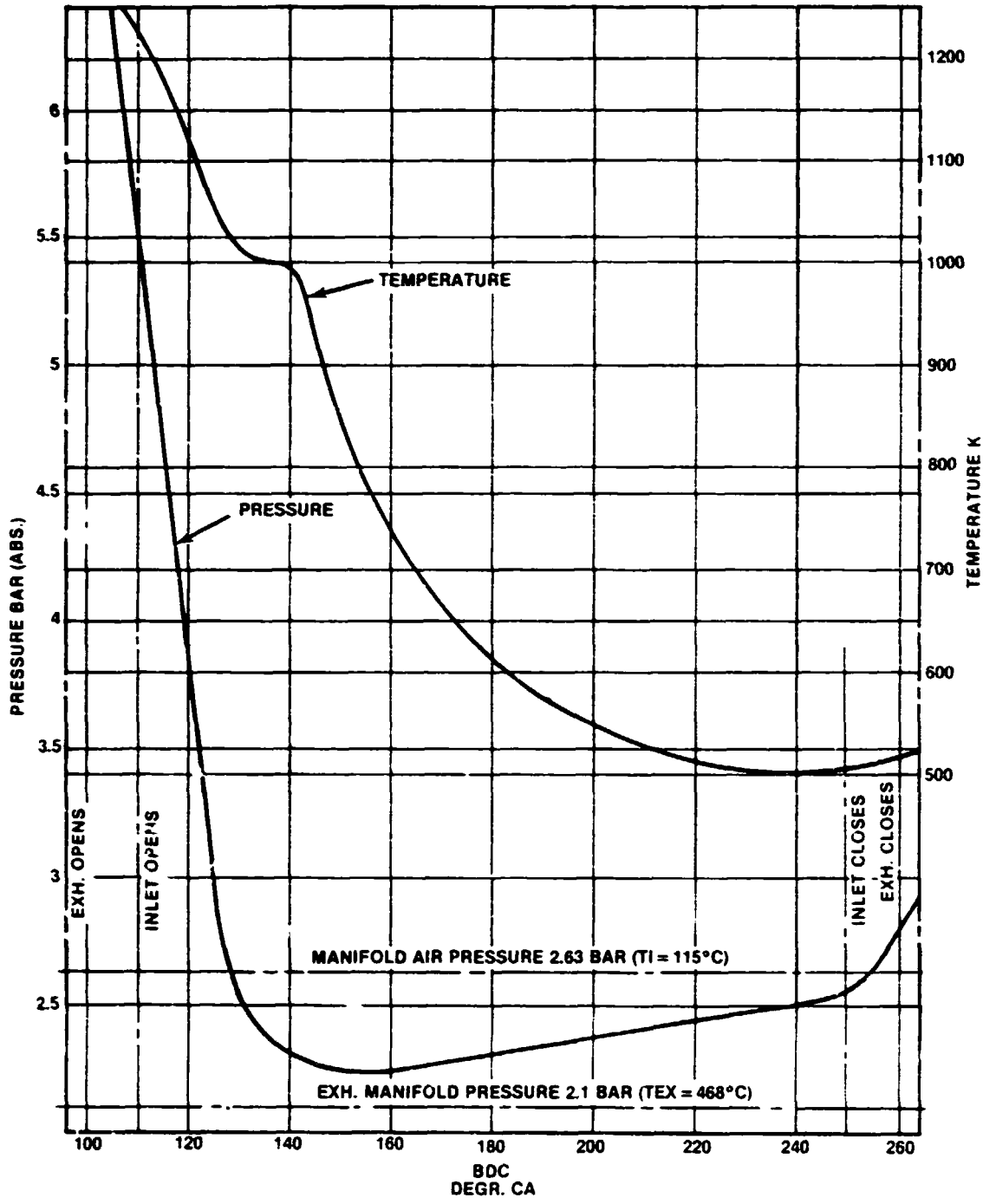

Figure 3.2-8. Low Pressure Diagram for Full Power Cruise

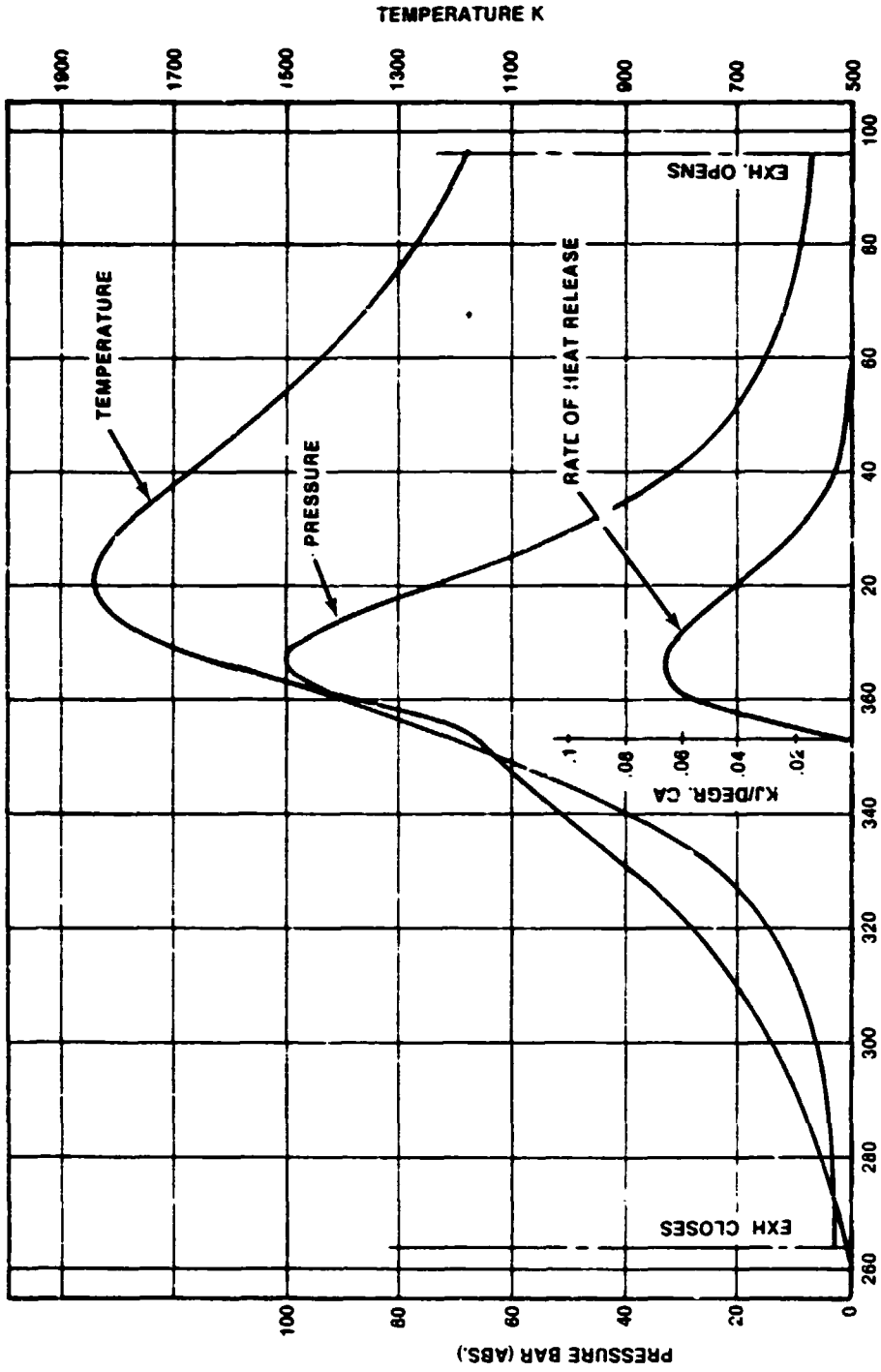

Figure 3.2-9. High Pressure Diagram for Economy Cruise Power

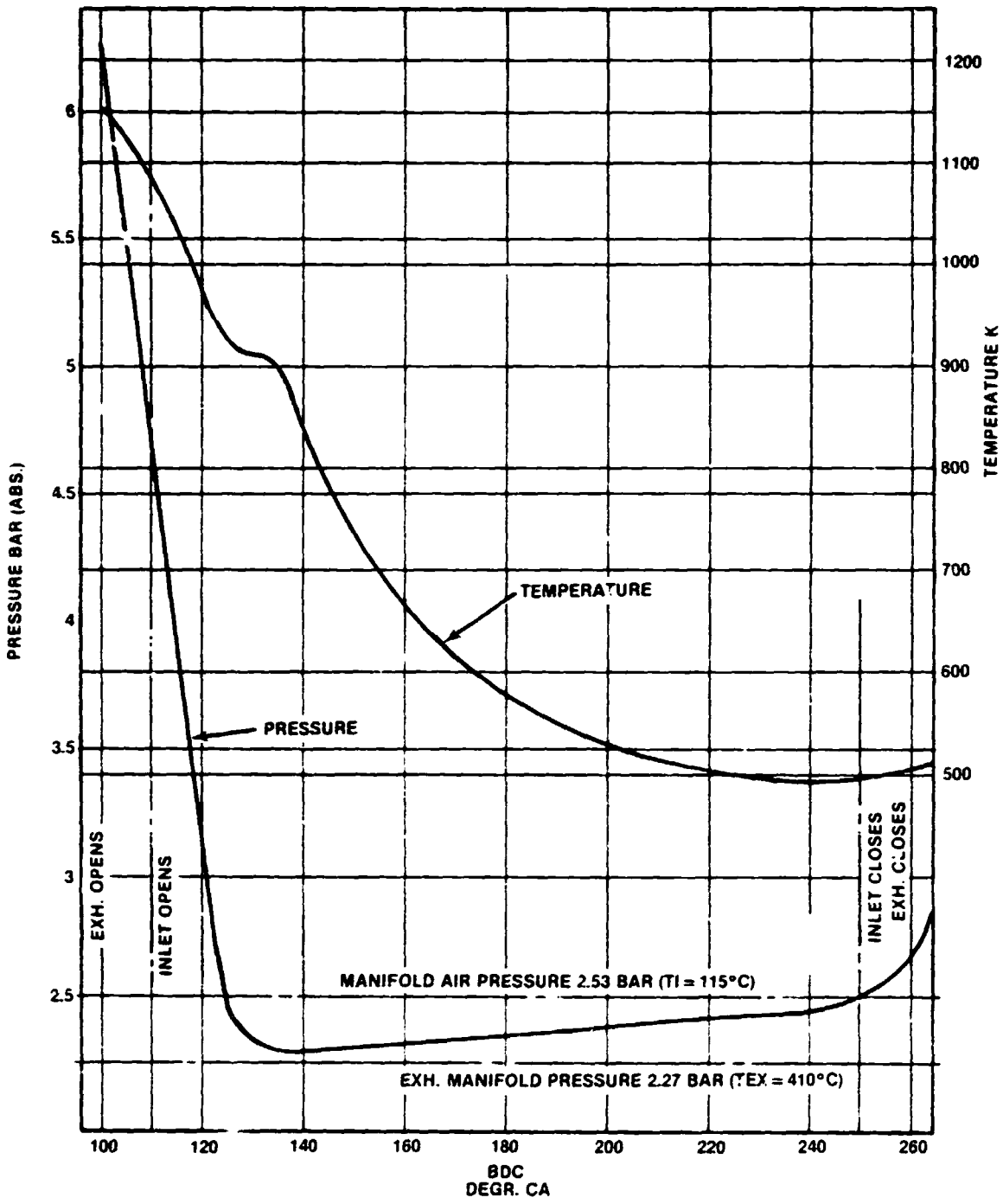

Figure 3.2-10. Low Pressure Diagram for Economy Cruise Power

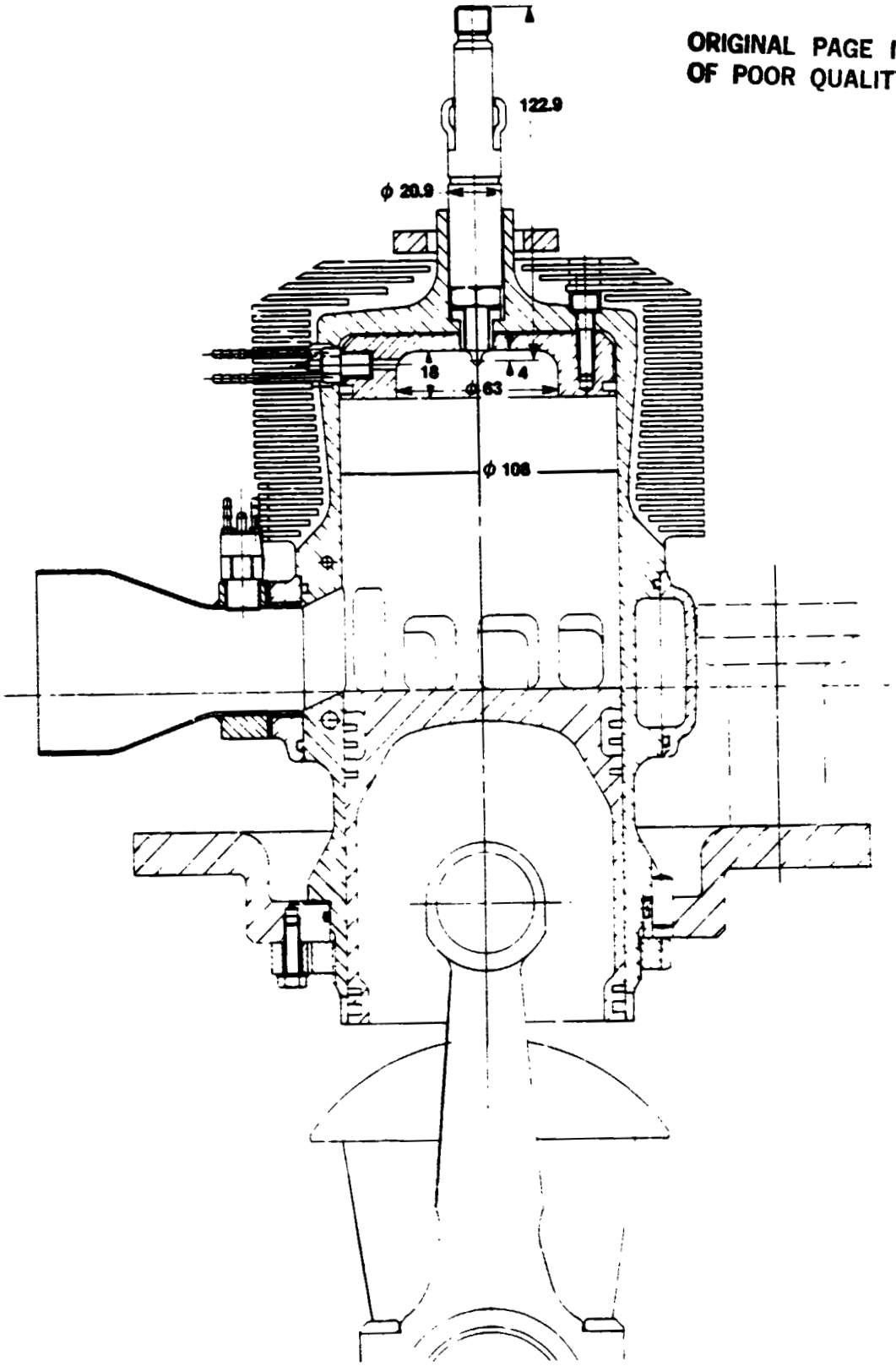

Figure 3.2-11. First Generation Single Cylinder Test Engine (SCTE)

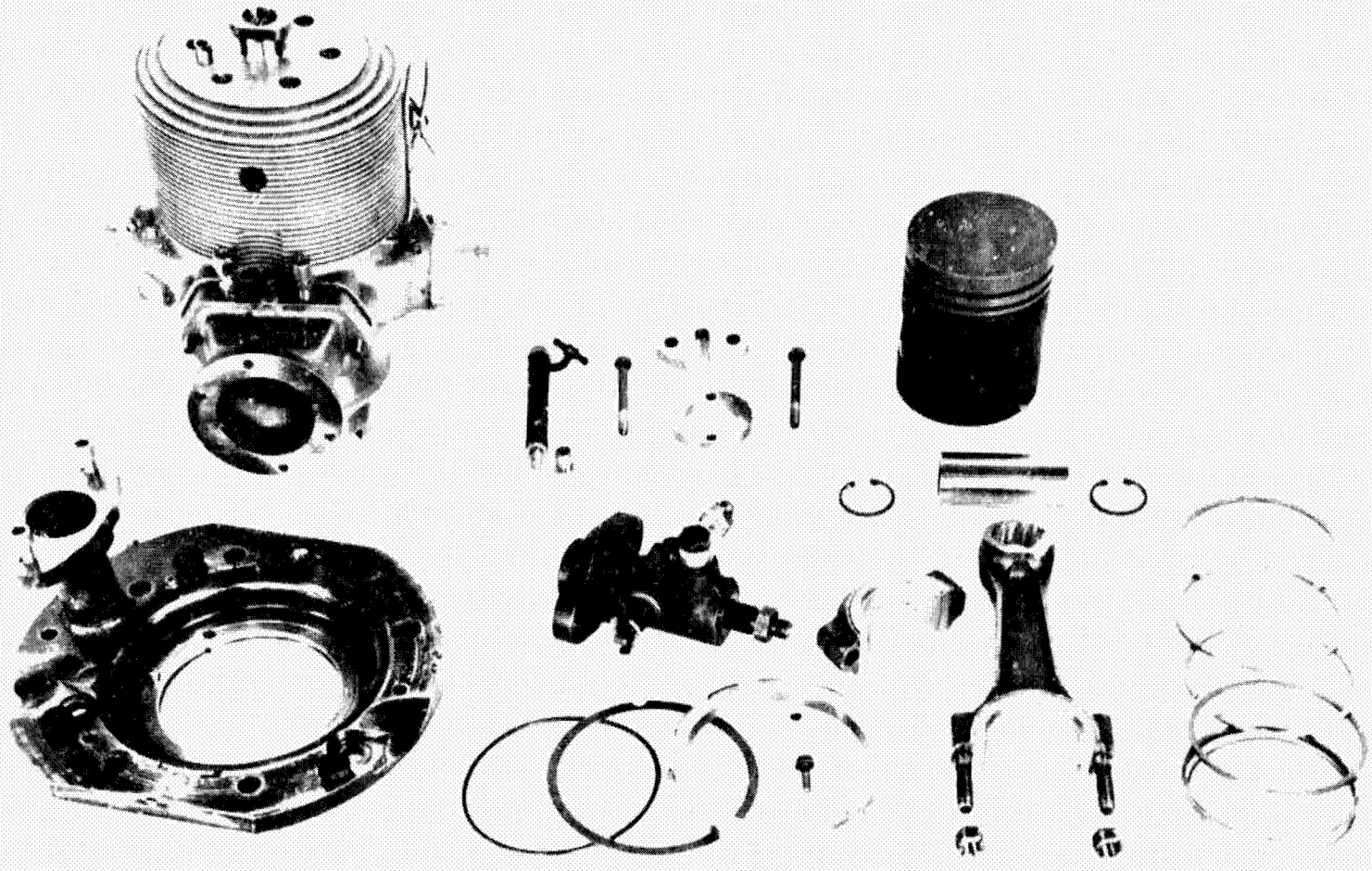

Figure 3.2-12. Layout of SCTE Cylinder Components

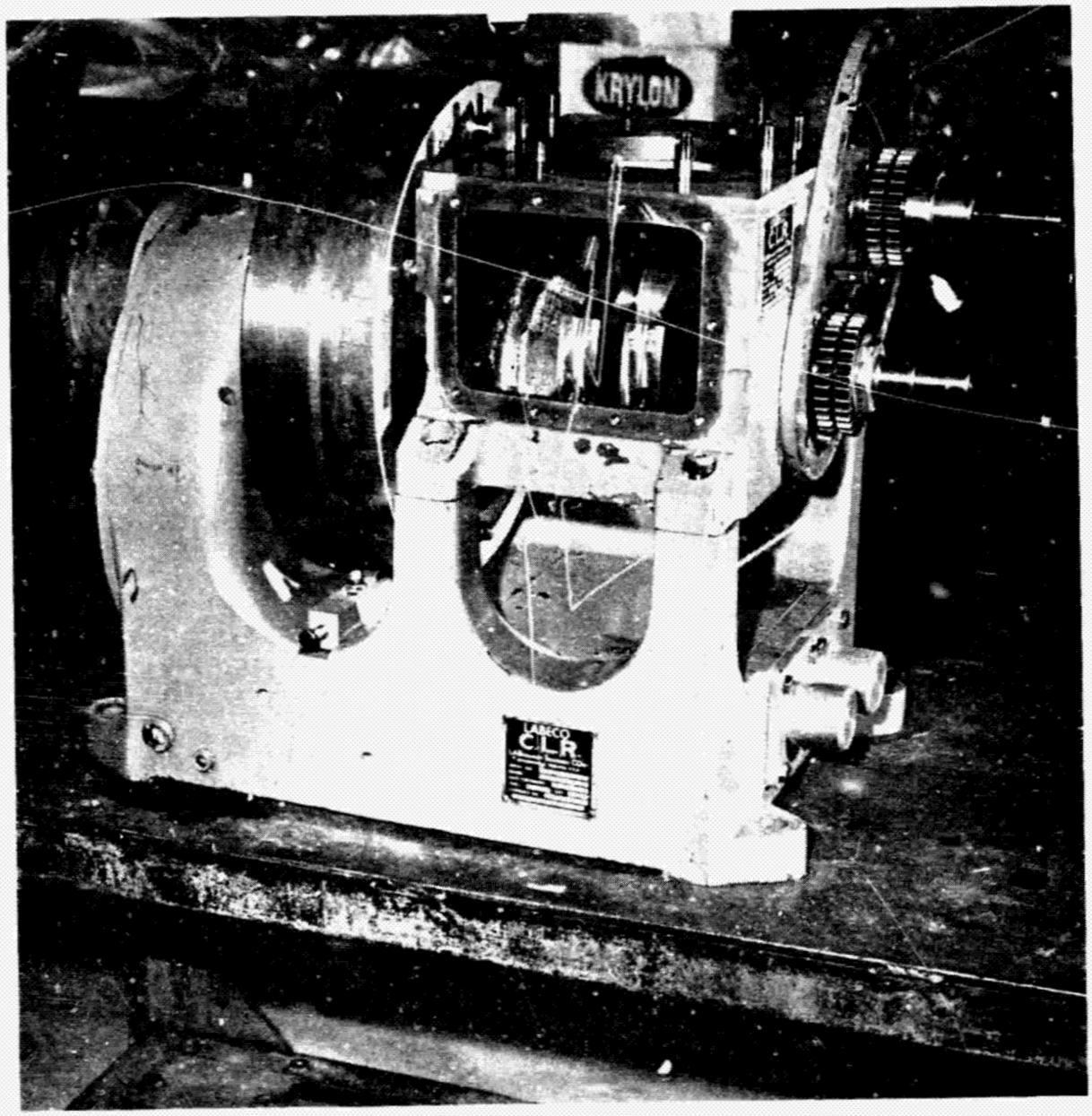

Figure 3-2.13. LABECO SCTE Test Base

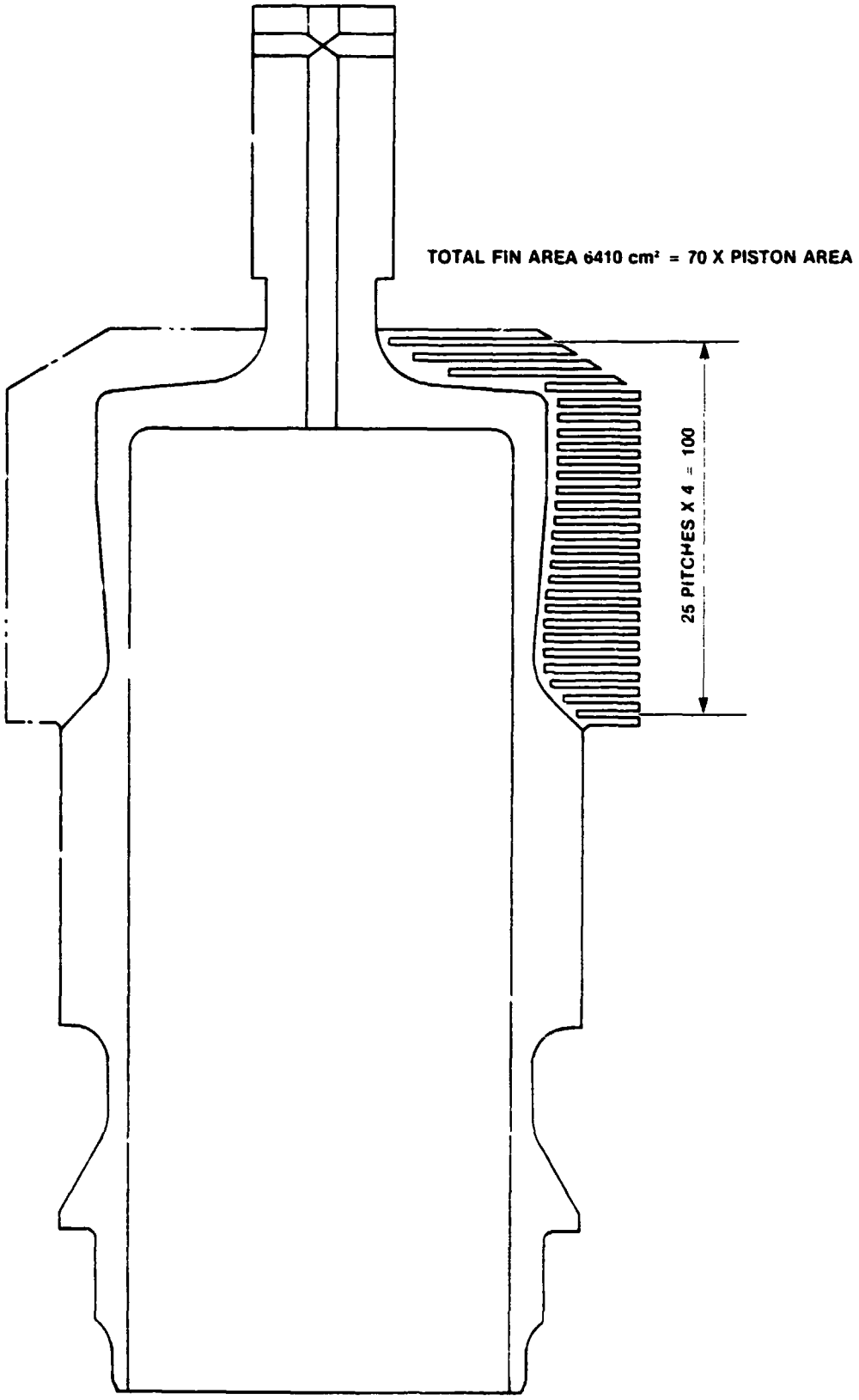

Figure 3-2.14. Cylinder

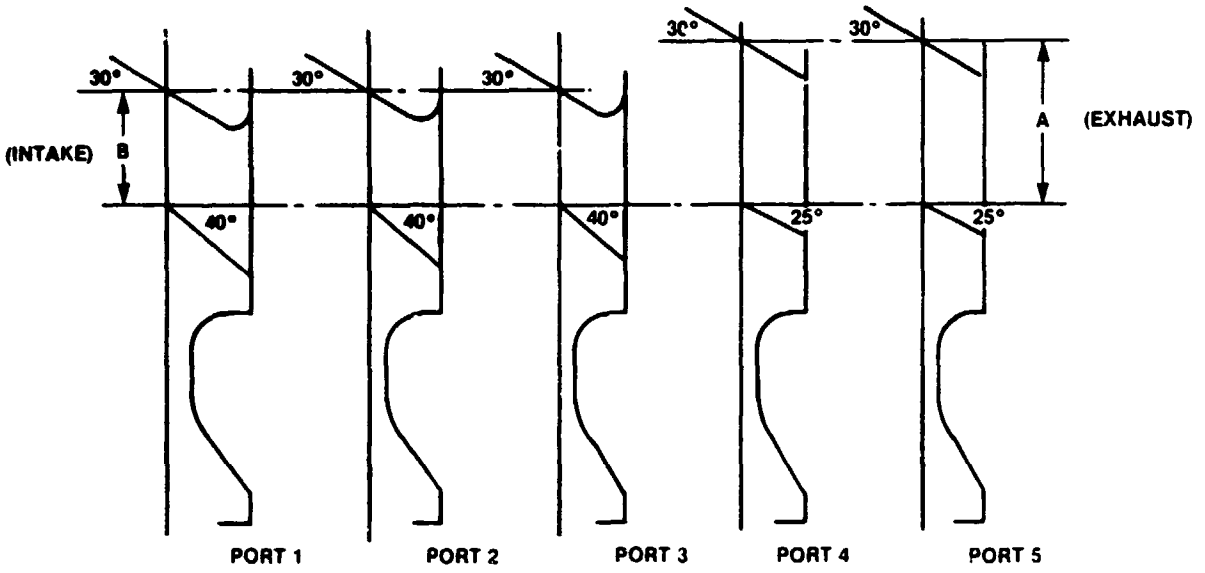

CYL. NO.	A	B
1	41	29
2	35	26
3	43	31

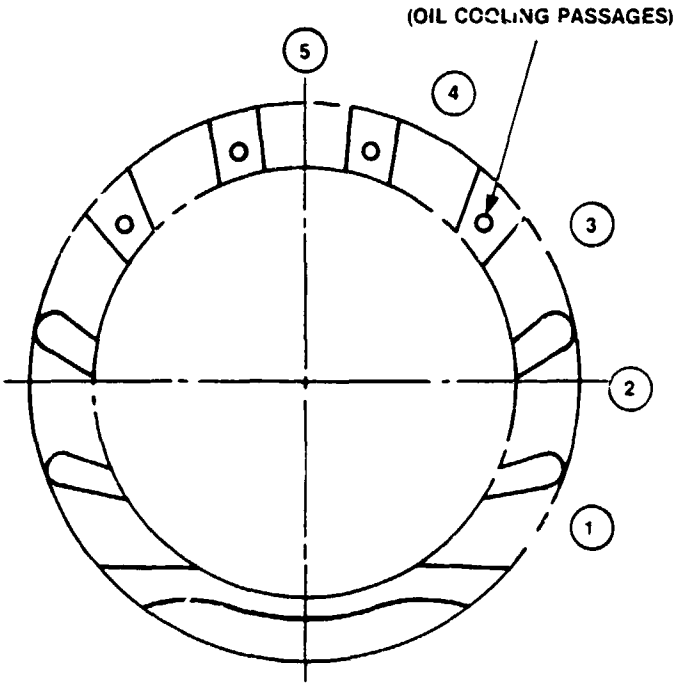

Figure 3.2-15. Cylinder Porting Arrangement

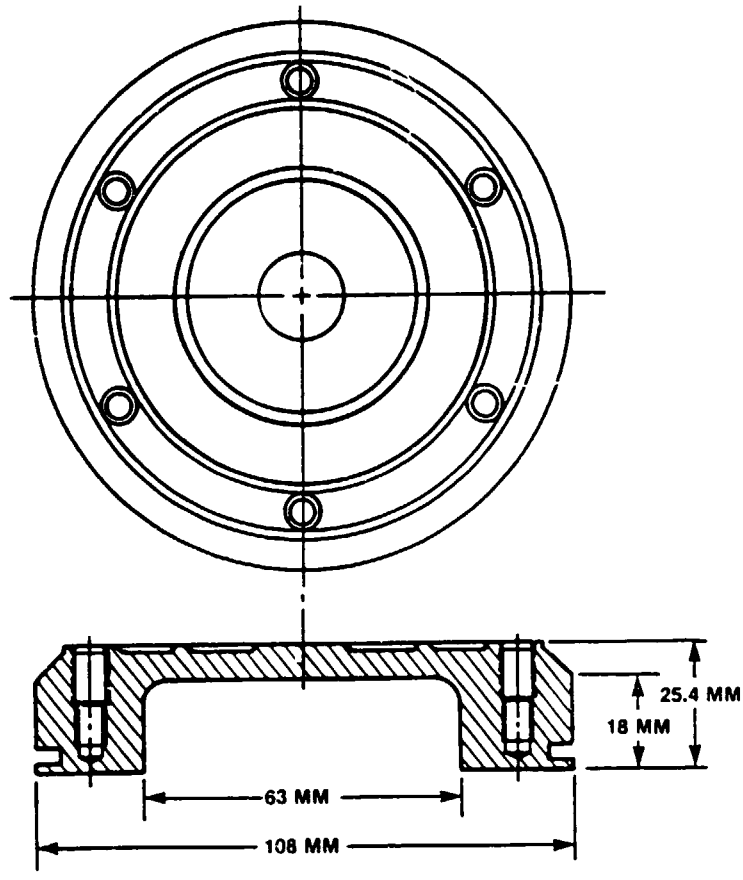

Figure 3.2-16. Combustion Bowl Insert

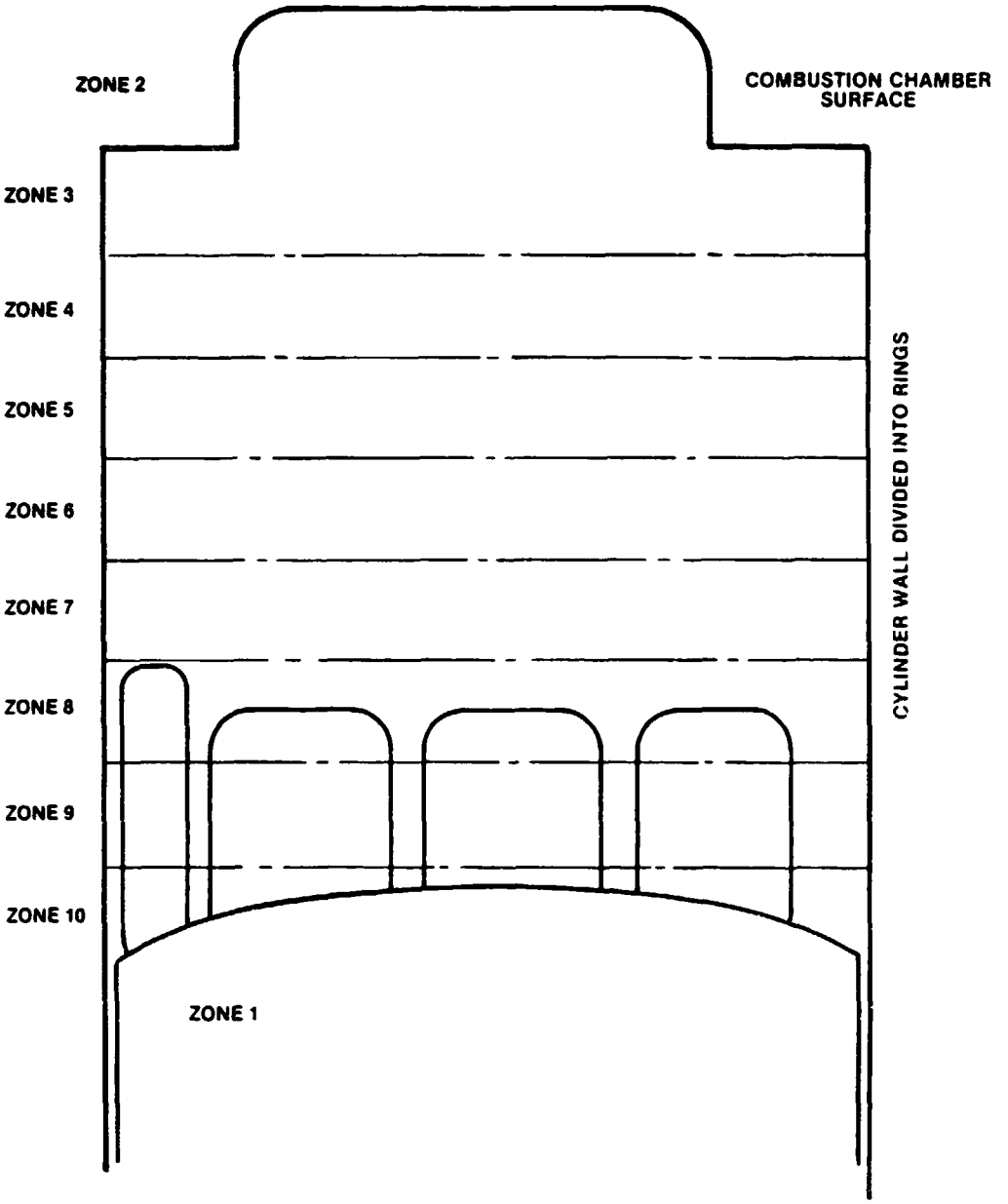

Figure 3.3-1. Temperature Zones Used for Thermal Model

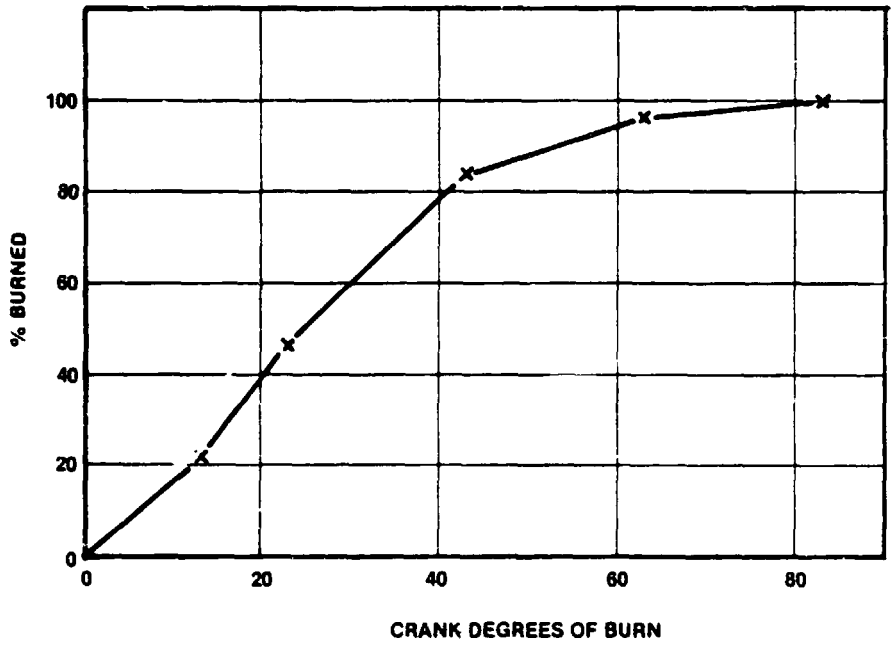

Figure 3.3-2. Heat Release Curve Assumed in Initial Cycle Analysis
Aircraft Diesel – 3500 RPM

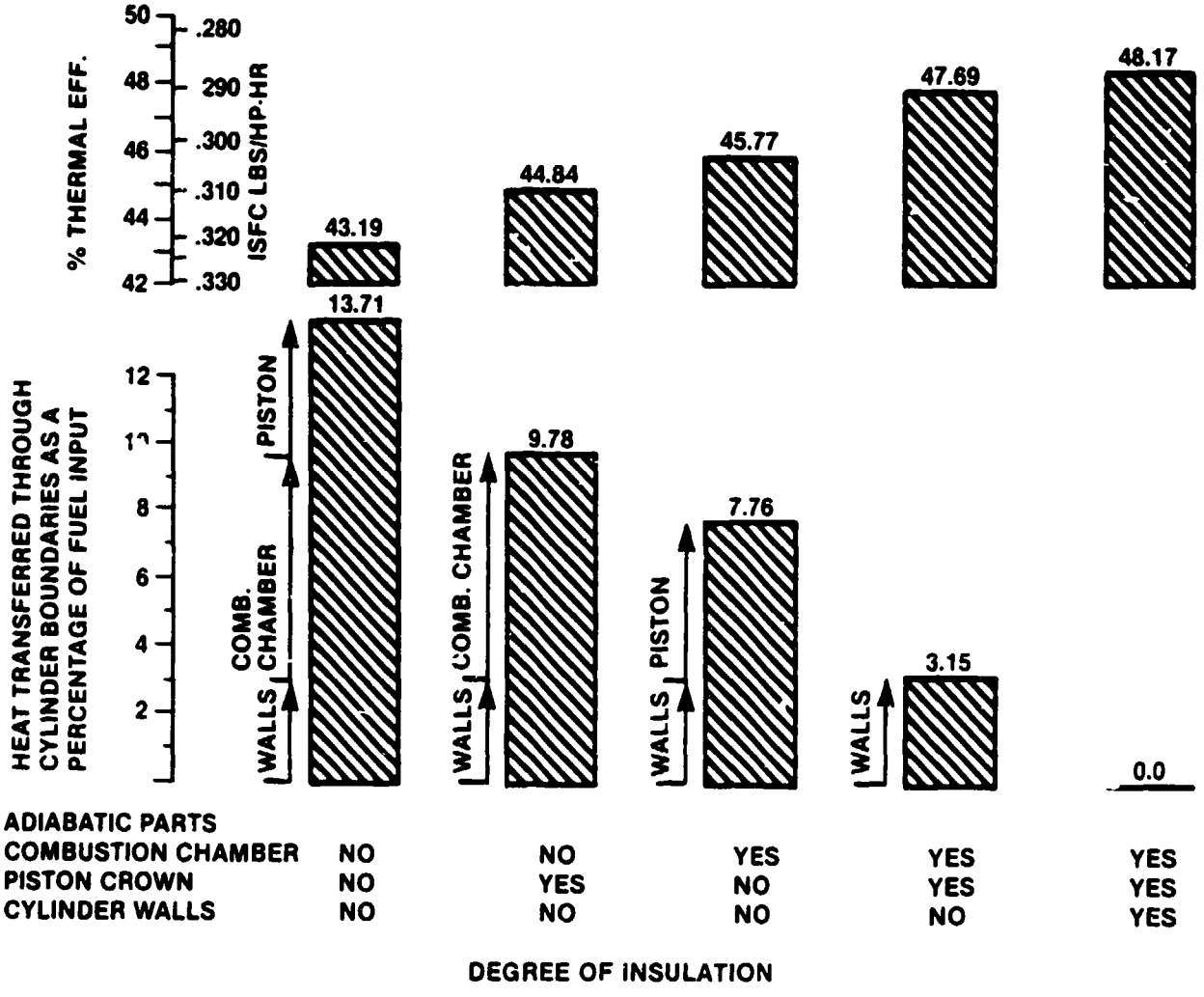

Figure 3.3-3. Computer Predicted Effect of Component Insulation at Power Cruise

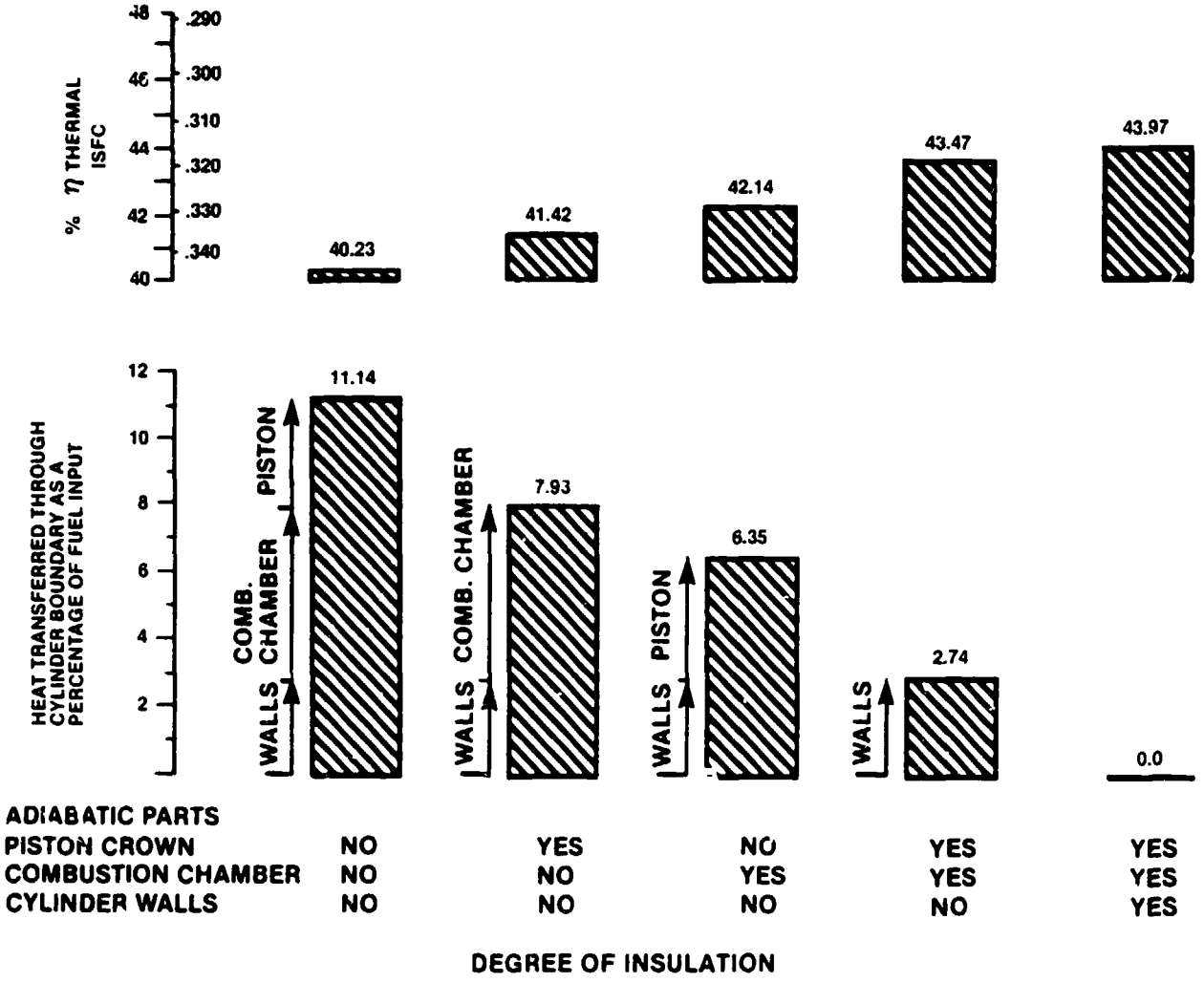

Figure 3.3-4. Computer Predicted Effects of Engine Insulation — Takeoff Power

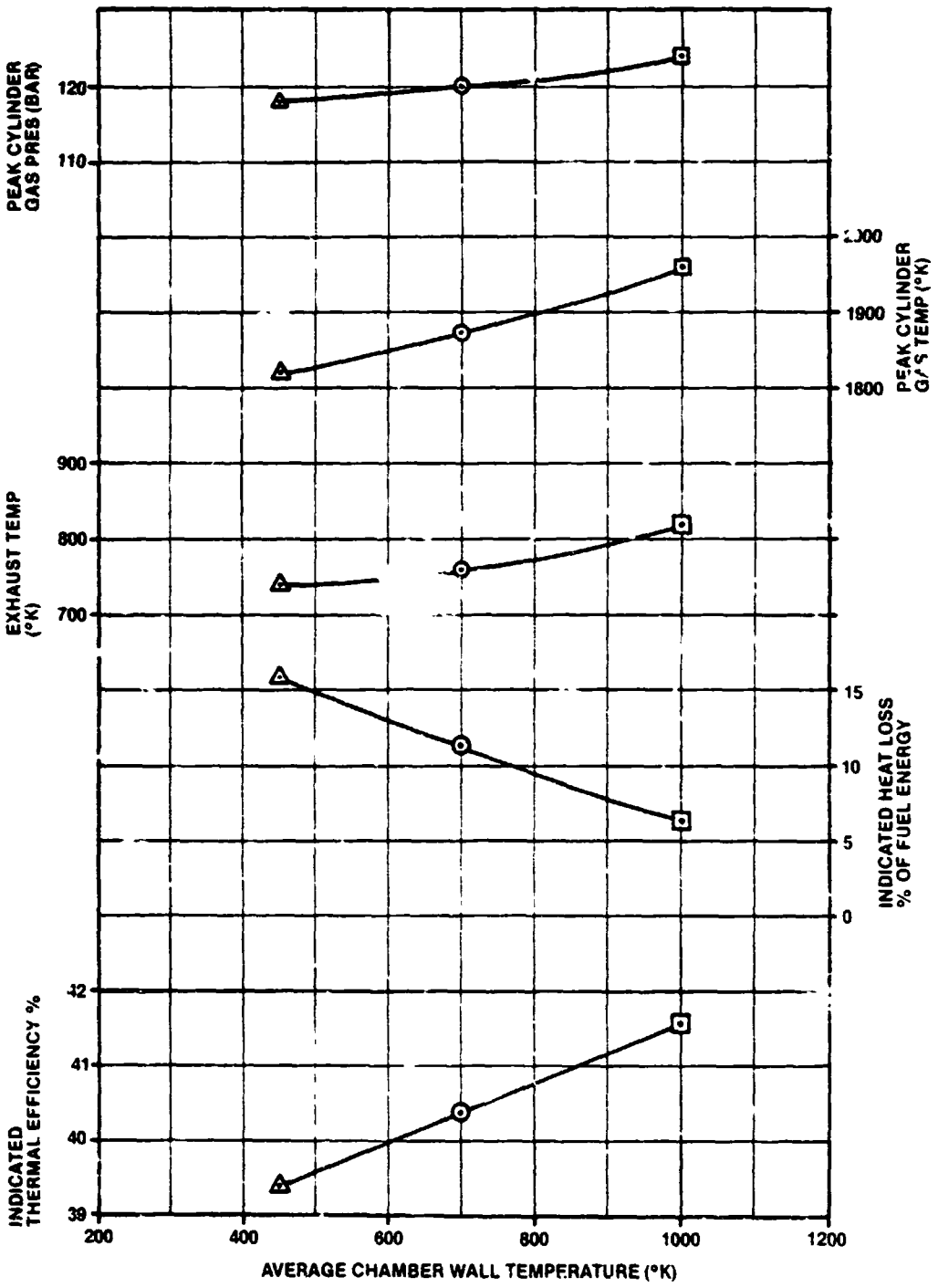

Figure 3.3-5. Computer Predicted Engine Performance Versus Average Chamber Wall Temperature

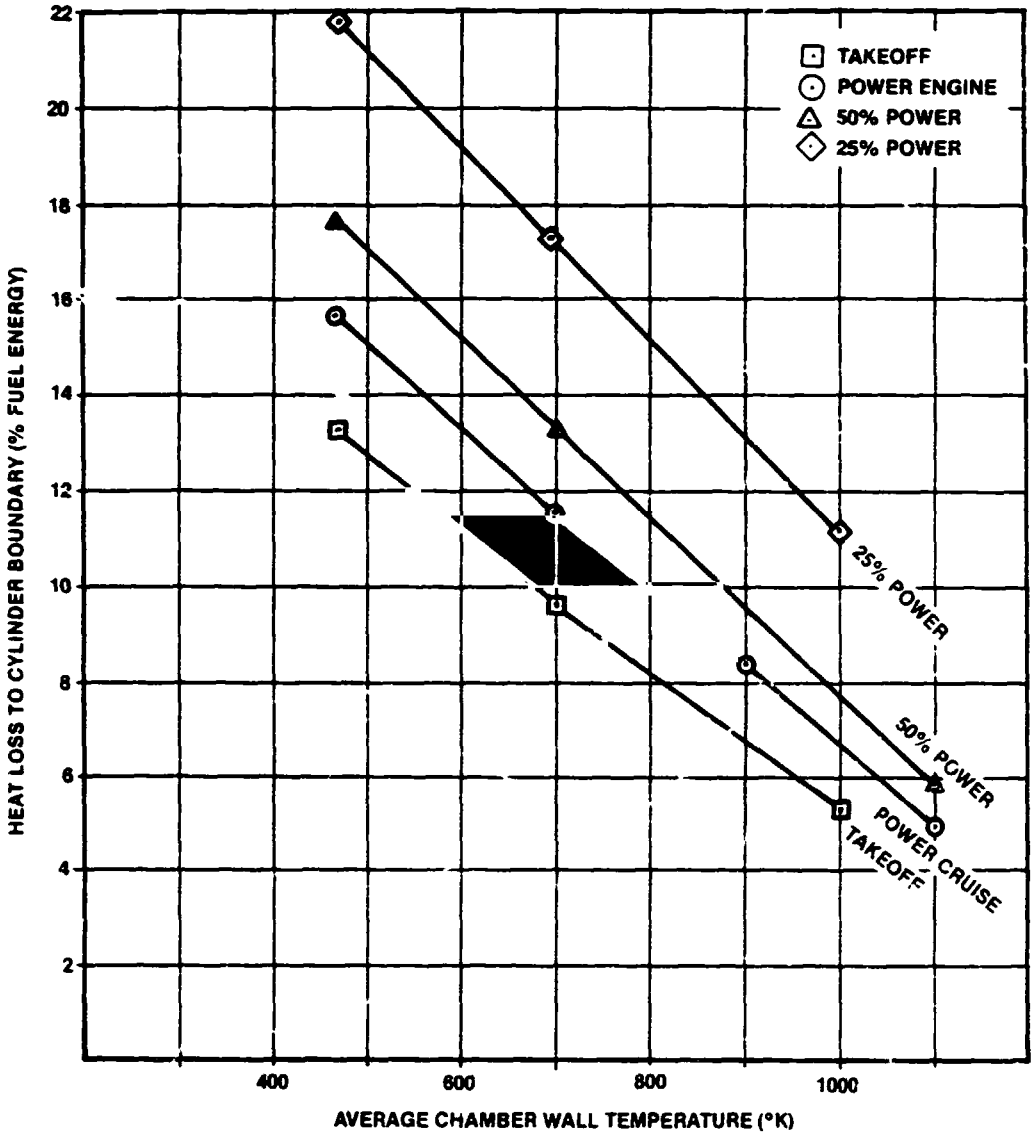

Figure 3.3-6. Heat Rejection as a Function of Average Chamber Wall Temperature for Four Load Points at 3500 RPM

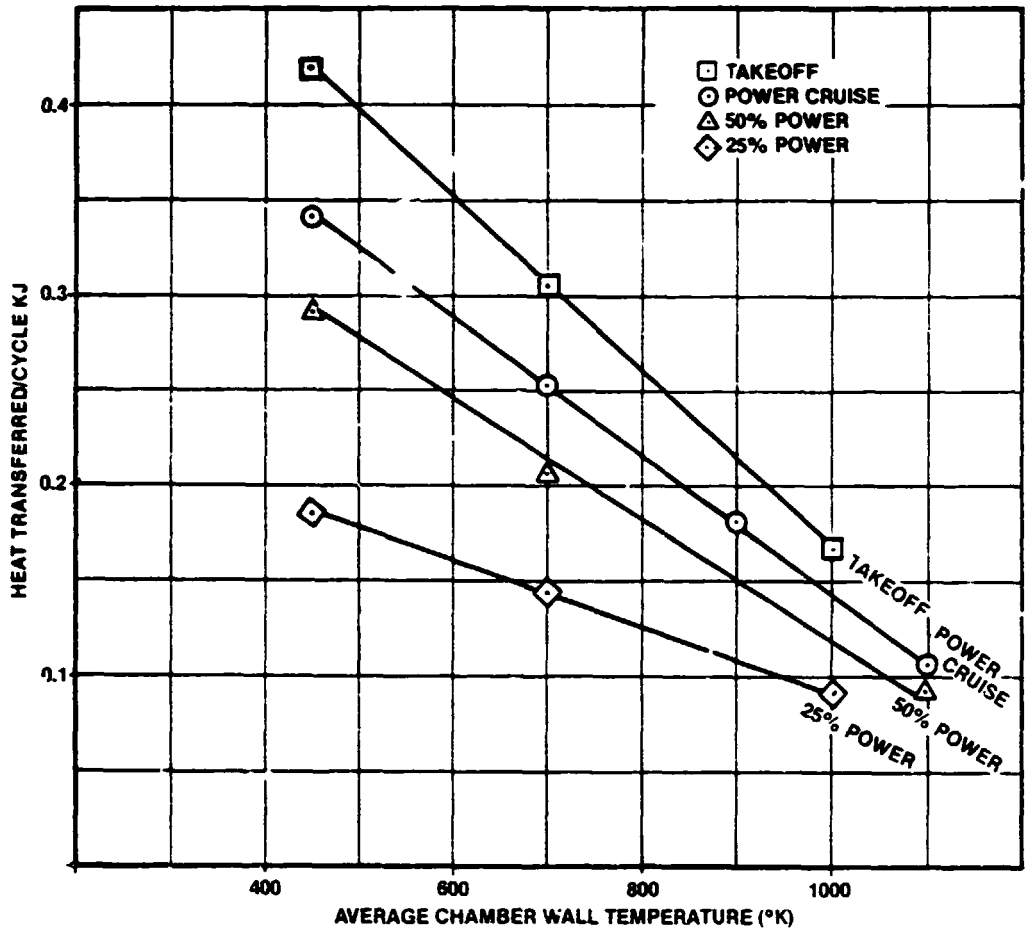

Figure 3.3-7. Absolute Heat Rejection as a Function of Average Chamber Wall Temperature at Four Load Points at 3500 RPM

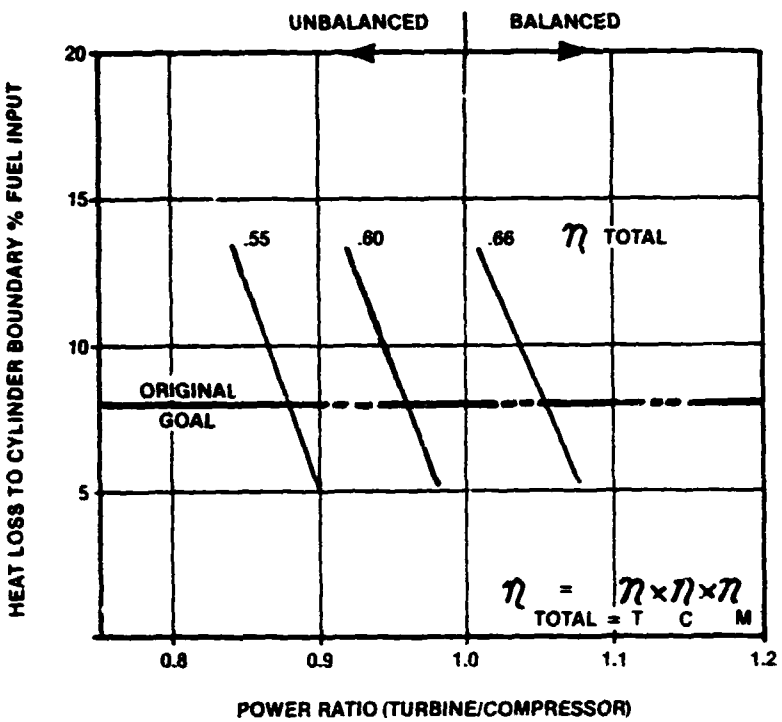

Figure 3.3-8. Computer Predicted Turbocharger Power Balance Comparison Versus Heat Loss 3500 RPM Takeoff Power at Sea Level

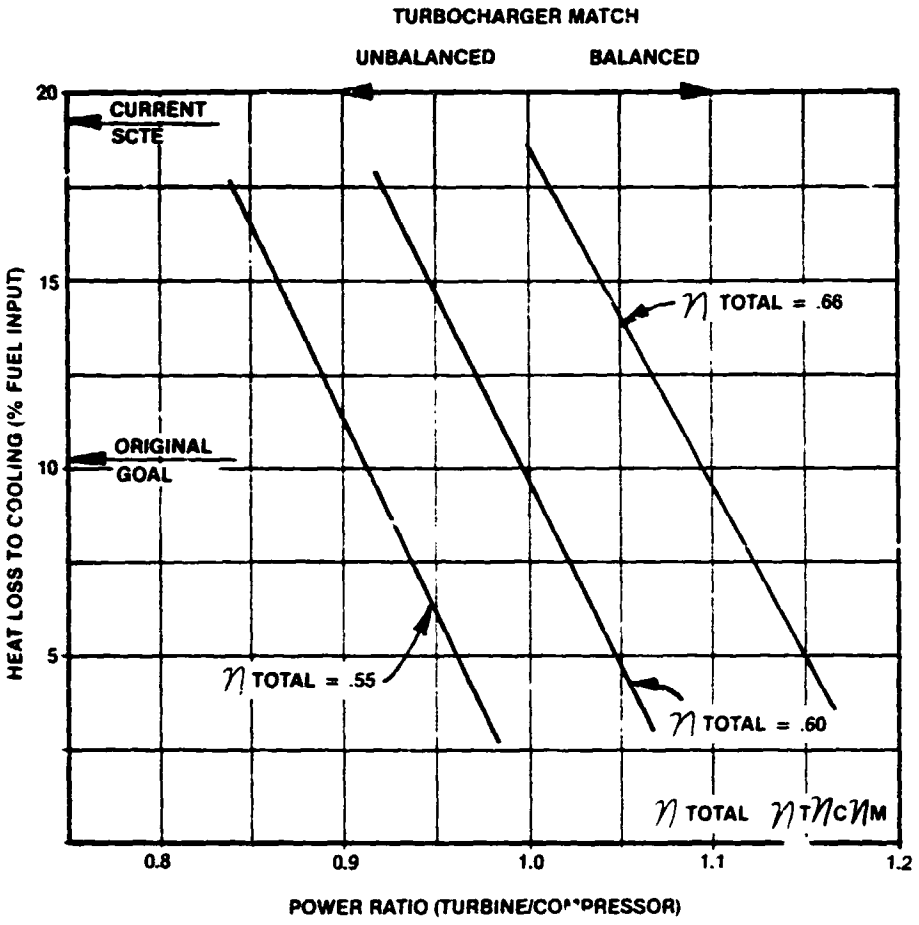

Figure 3.3-9. Computer Predicted Turbocharger Power Balance Comparison Versus Heat Loss at Power Cruise at 7800 Meters Altitude

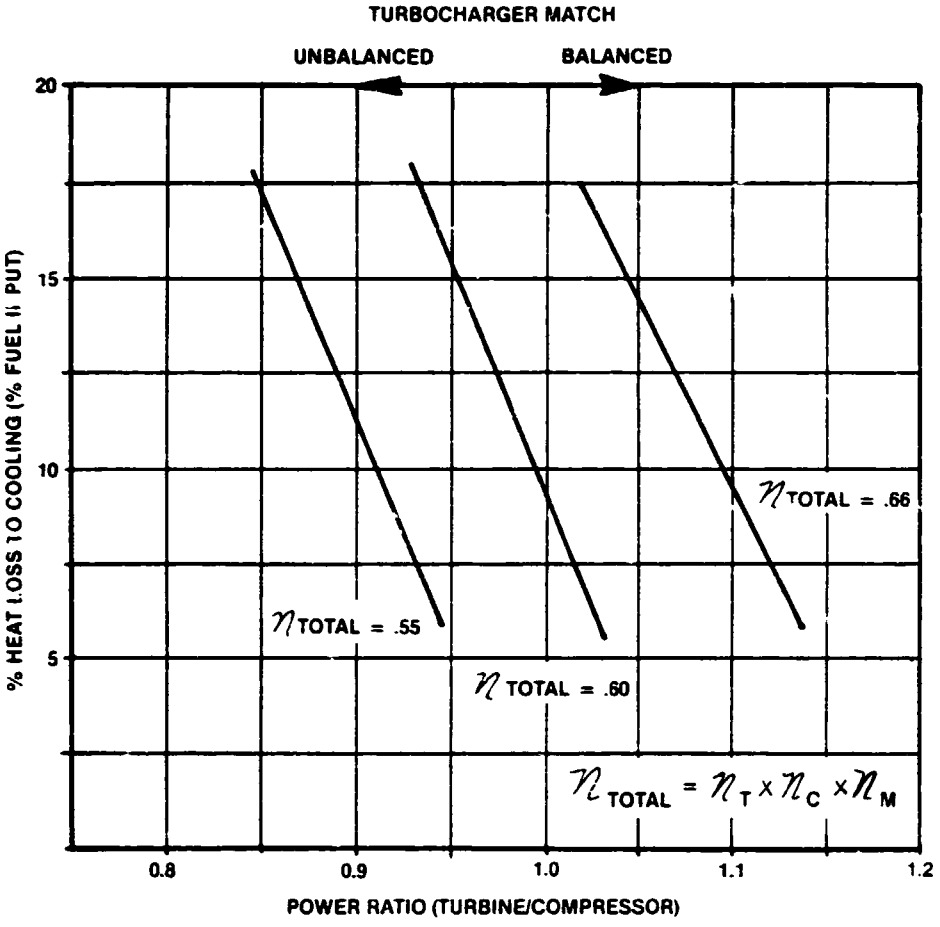

Figure 3.3-10. Computer Predicted Turbocharger Power Balance Comparison Versus Heat Loss at 50% Power at 7800 Meters Altitude

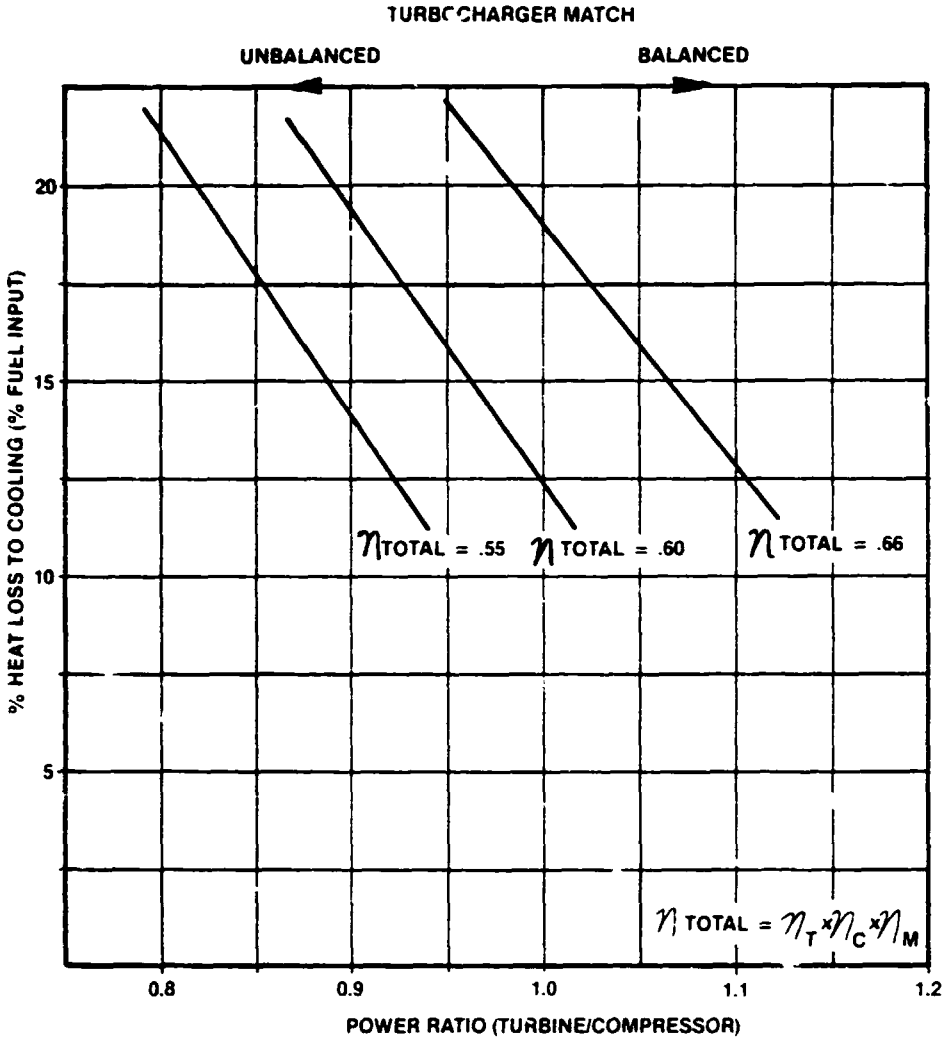

Figure 3.3-11. Computer Predicted Turbocharger Power Balance Comparison Versus Heat Loss at 25% Power at 7800 Meters Altitude

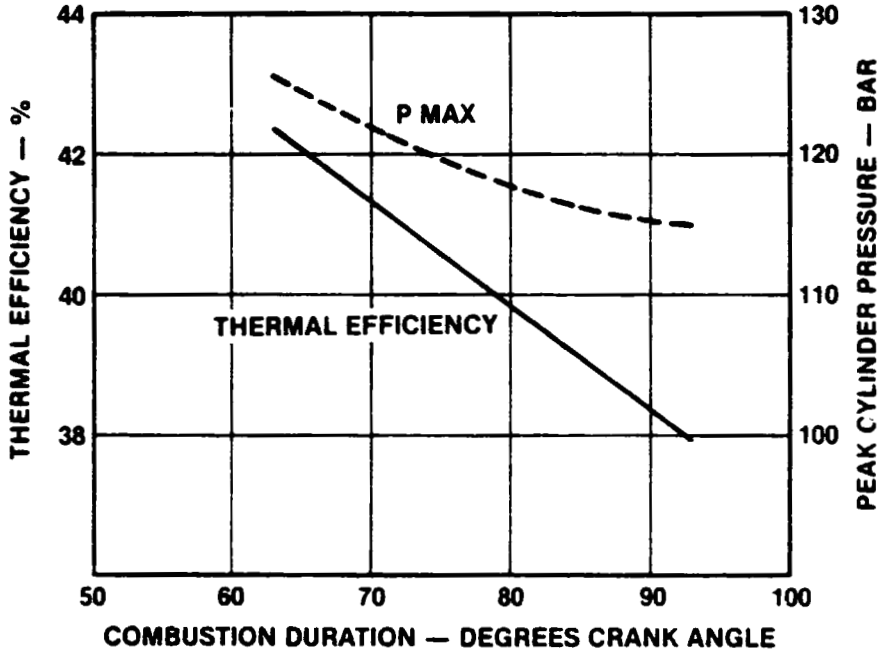

Figure 3.3-12. Computer Predicted Effect of Combustion Duration on Thermal Efficiency and Peak Cylinder Pressure 3500 RPM Takeoff Power

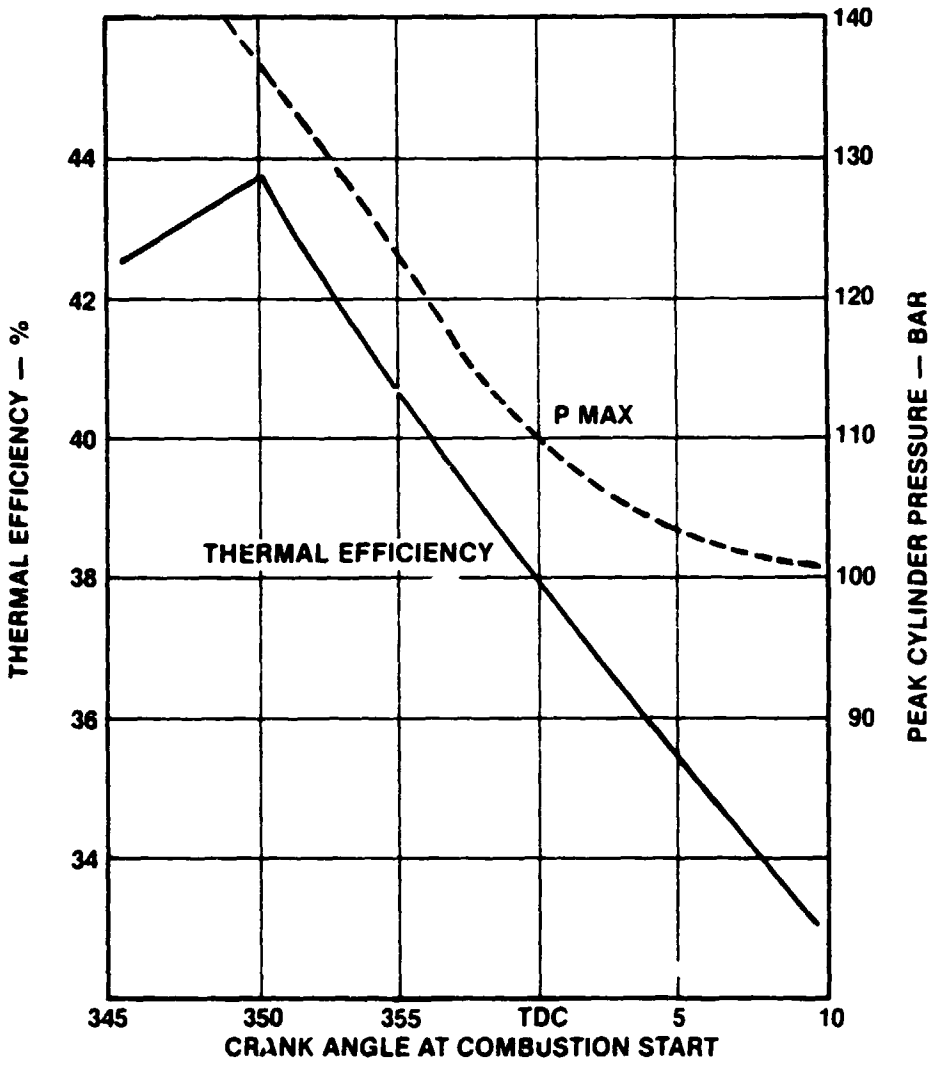

Figure 3.3-13. Computer Predicted Effect of Combustion Timing on Thermal Efficiency and Peak Cylinder Pressure 3500 RPM Takeoff Power

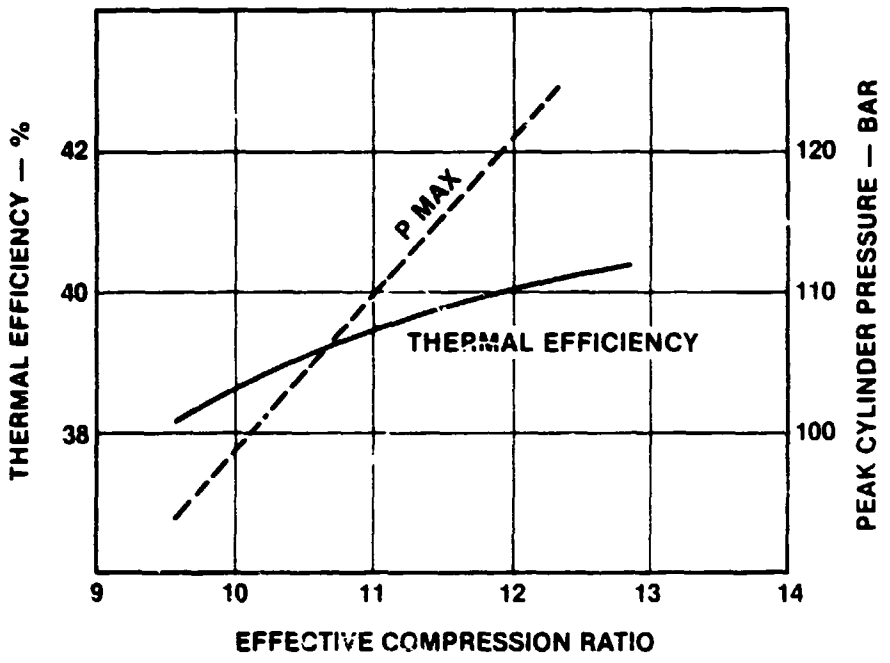

Figure 3.3-14. Computer Predicted Effect of Effective Compression Ratio on Thermal Efficiency and Peak Cylinder Pressure 3500 RPM Takeoff Power

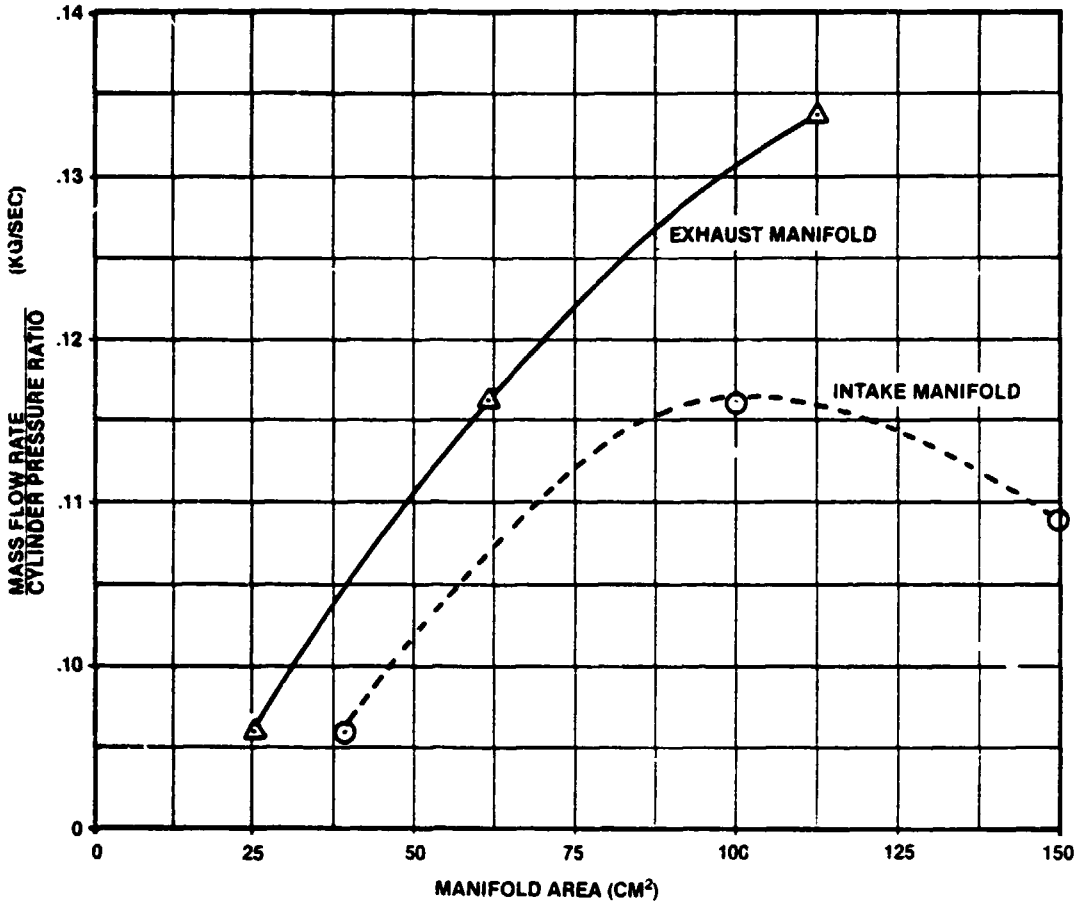

Figure 3.3-15. Mass Flow Rate/Cylinder Pressure Ratio Versus Manifold Area

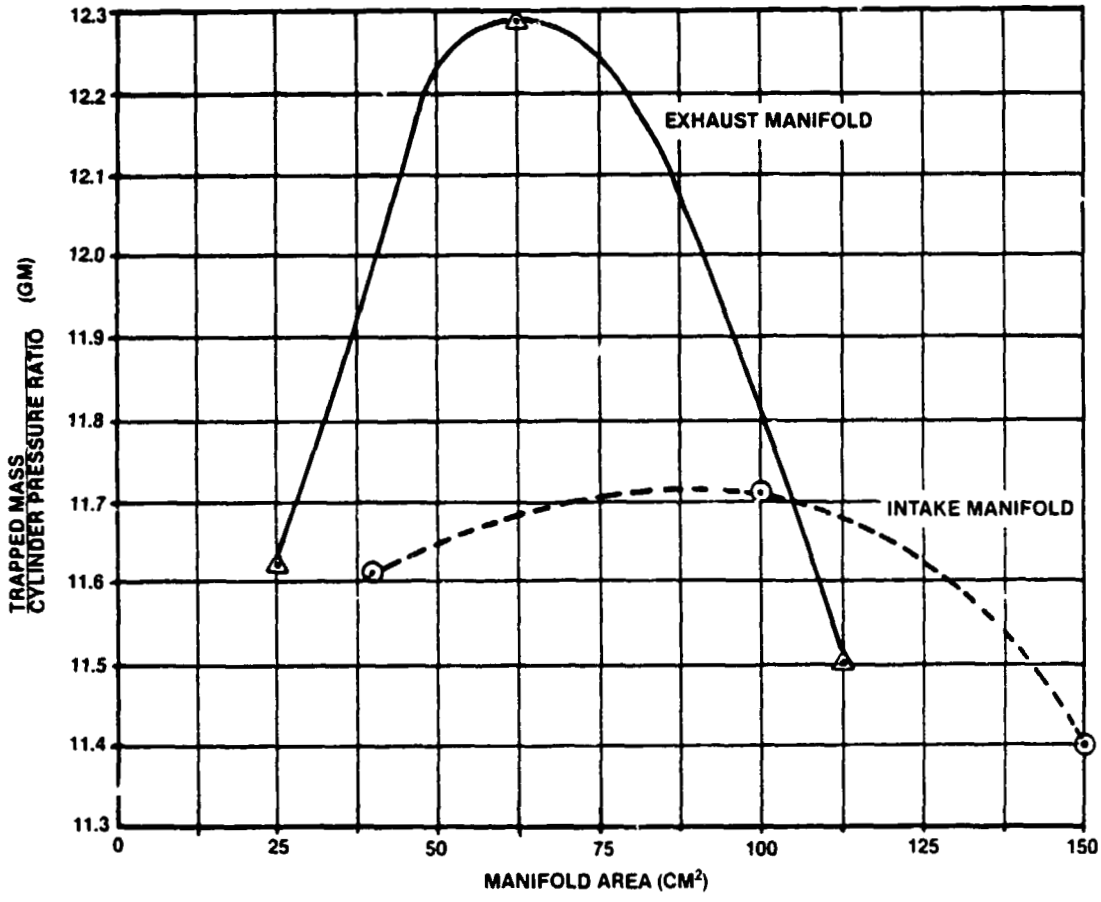

Figure 3.3-16. Trapped Mass/Cylinder Pressure Ratio Versus Manifold Area

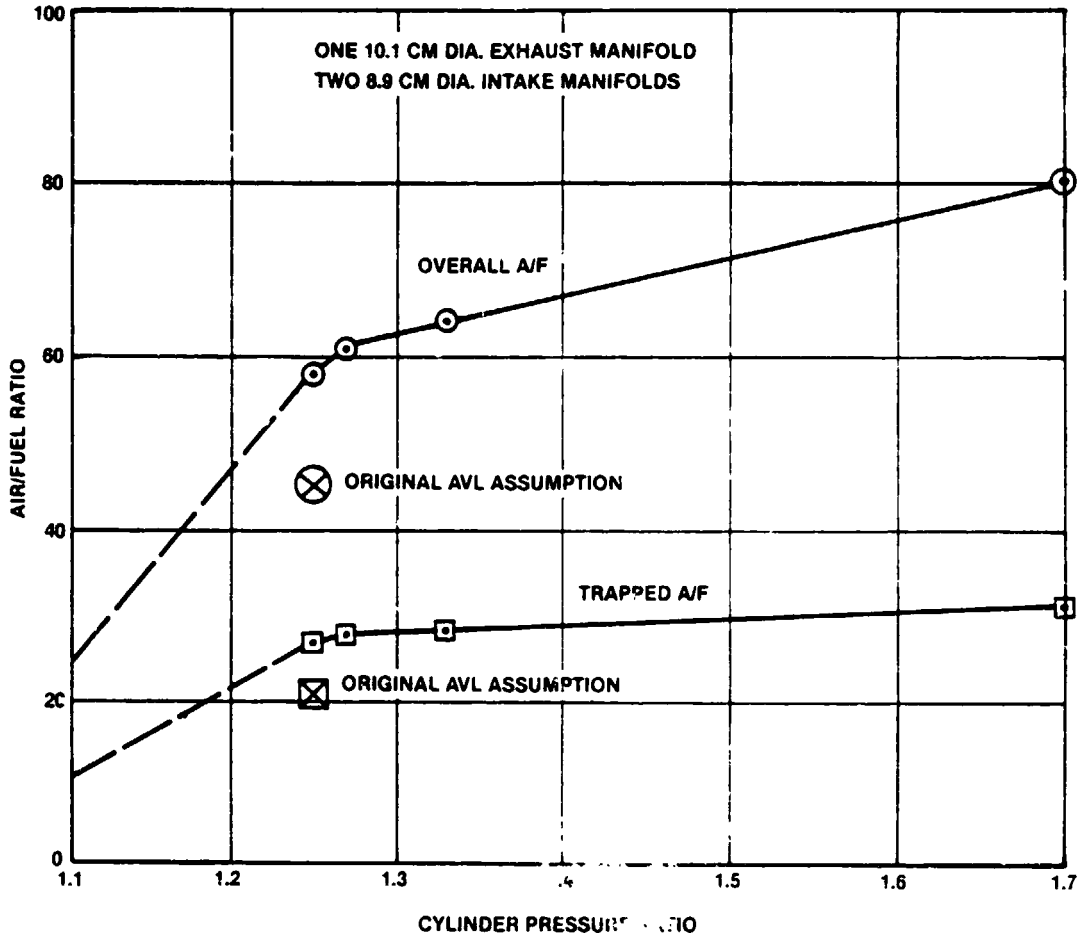

Figure 3.3-17. Air/Fuel Ratio Versus Cylinder Pressure Ratio for the Optimized Manifolding Configuration

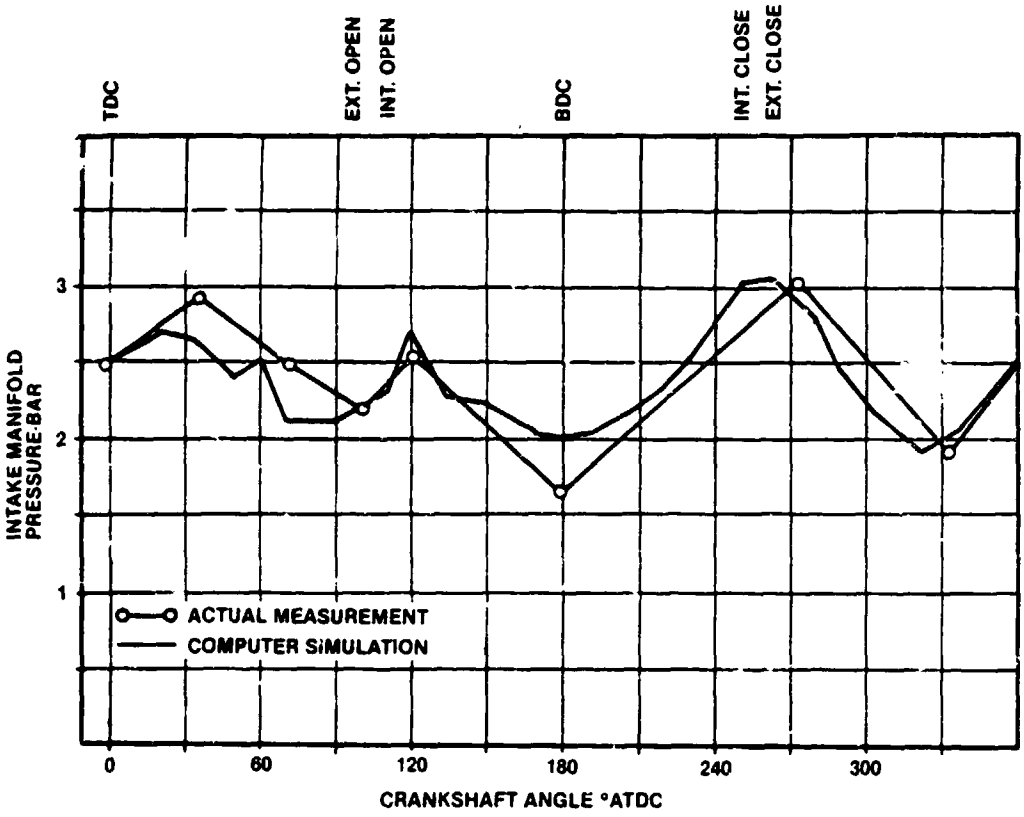

Figure 3.3-18. Experimental Versus Predicted Inlet Manifold Pressure at Pressure Transducer Location

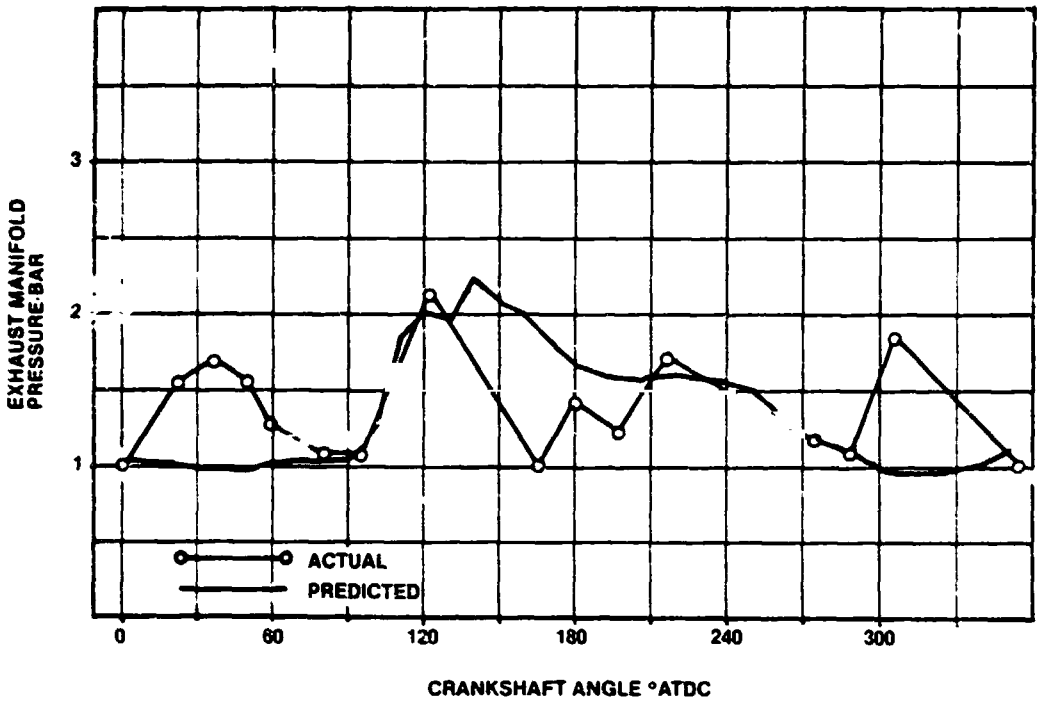

Figure 3.3-19. Experimental Versus Predicted Exhaust Manifold Pressure at Pressure Transducer Location

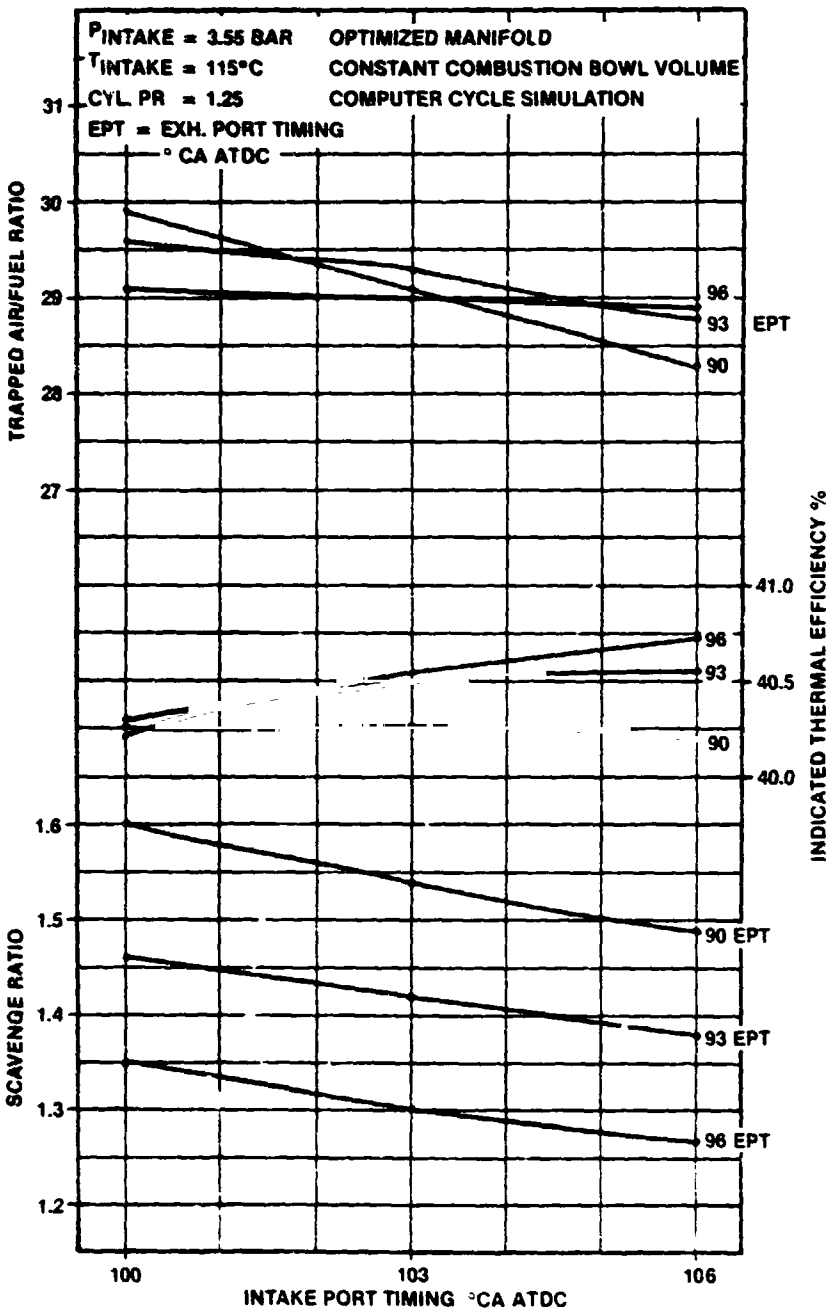

Figure 3.3-20. Port Timing Optimization at Takeoff Power Condition

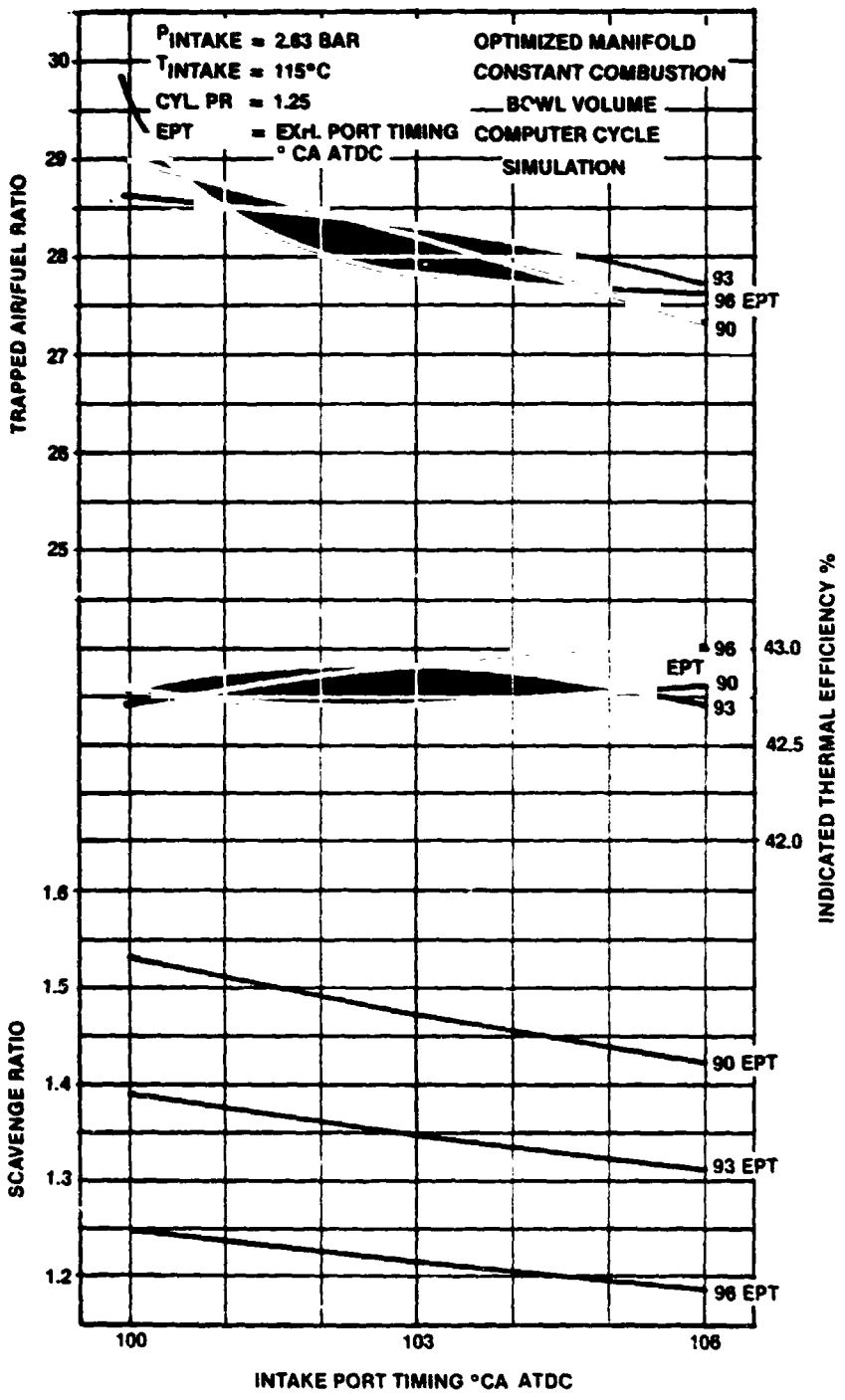

Figure 3.3-21. Port Timing Optimization at Power Cruise Condition

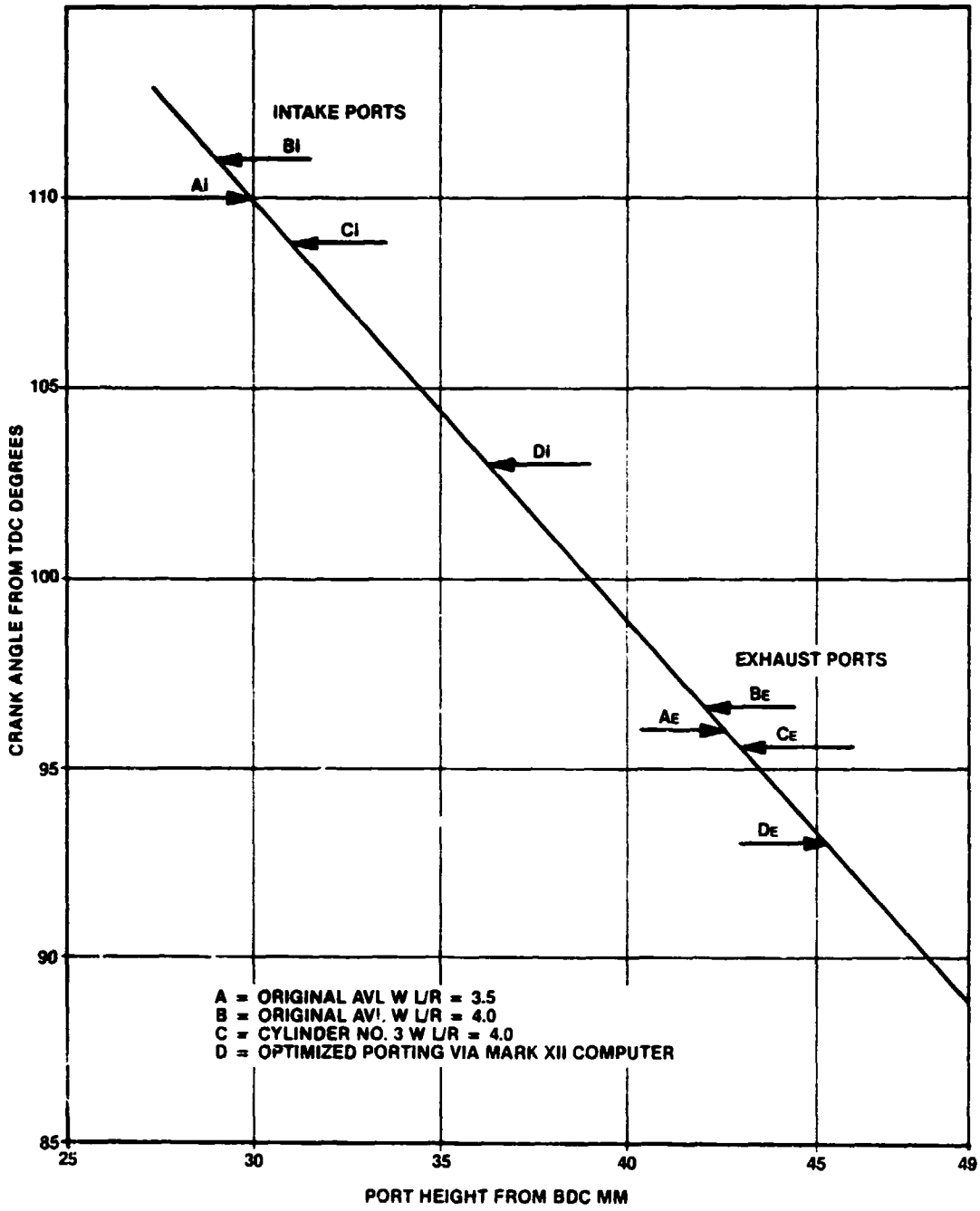

Figure 3.3-22. Port Timing Versus ° CA

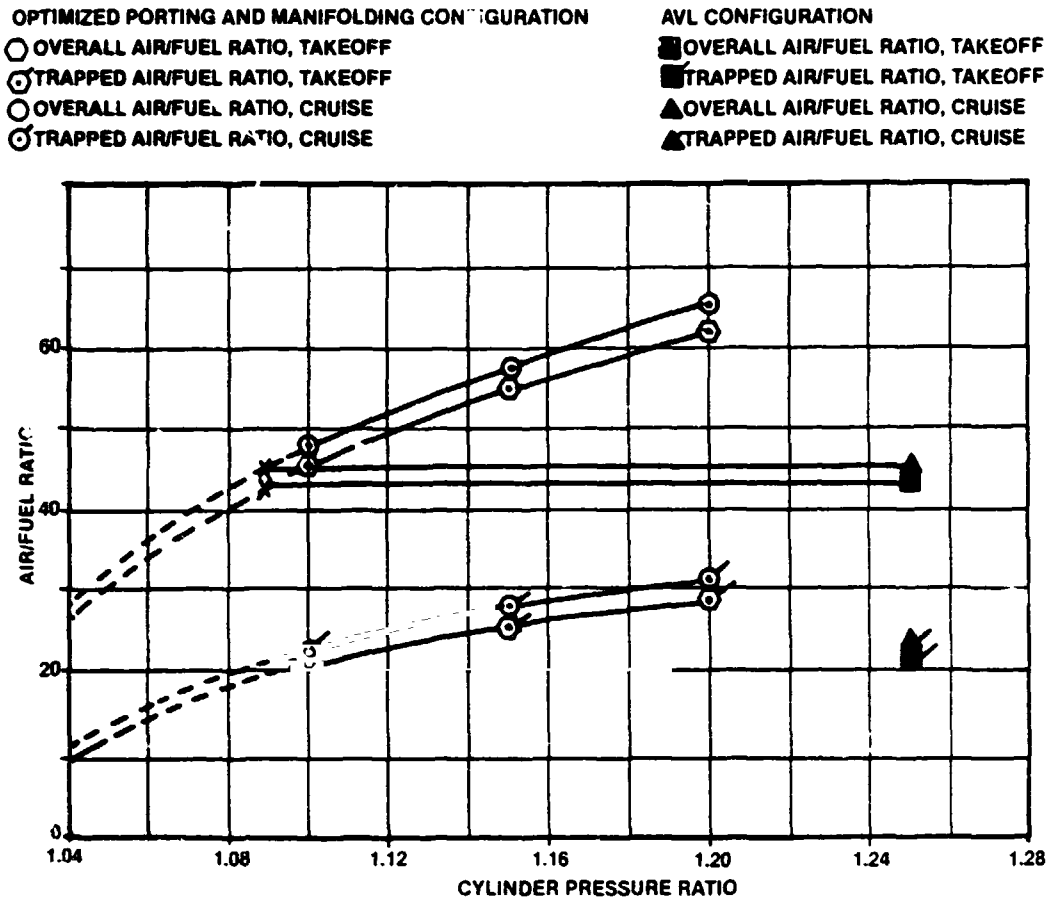

Figure 3.3-23. Air/Fuel Ratio Versus Cylinder Pressure Ratio for the Optimized Porting and Manifolding Configuration

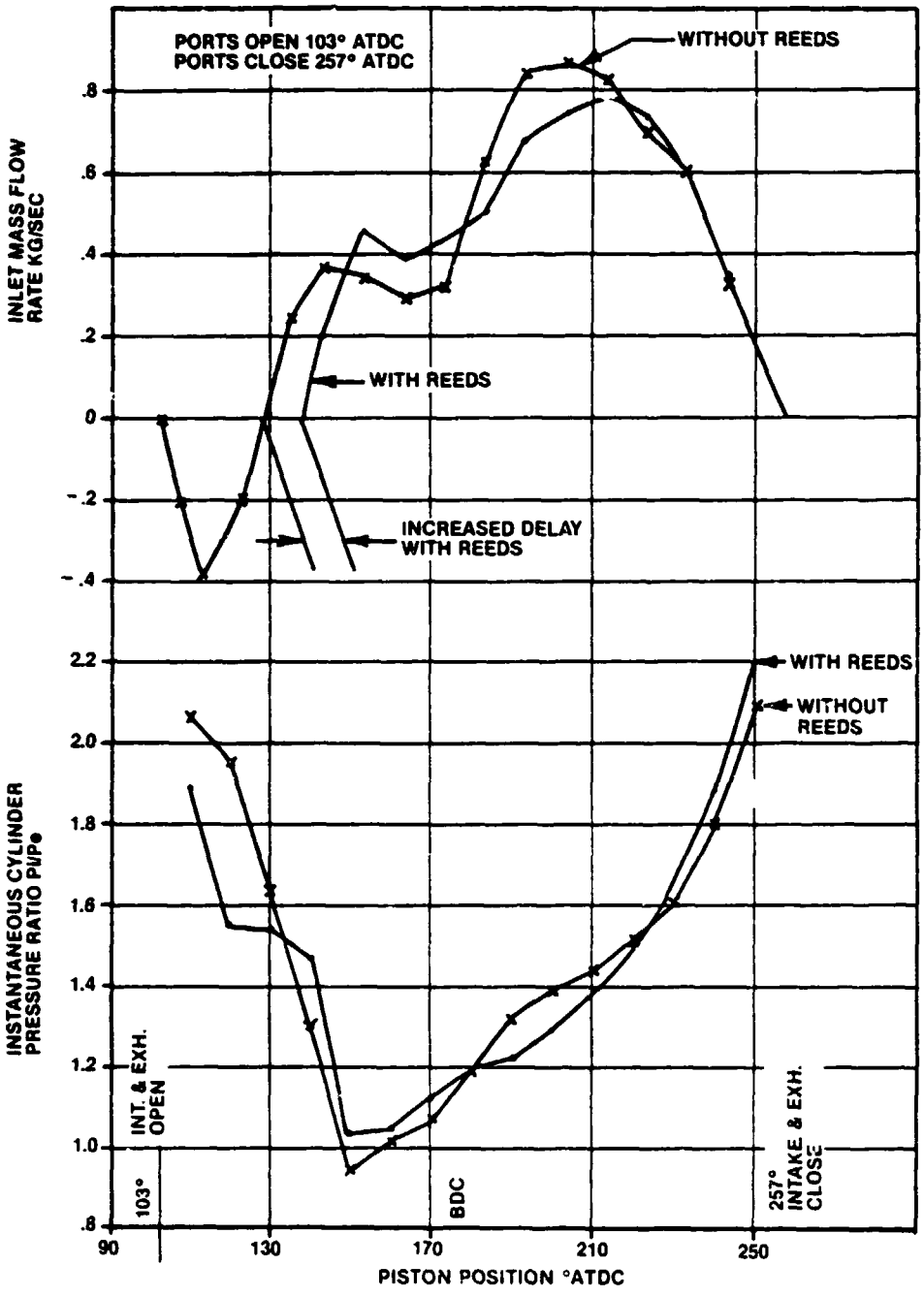

Figure 3.3-24. Effect of Reed Valves on Cylinder Airflow at Takeoff Power (Same Timing for Intake and Exhaust Ports)

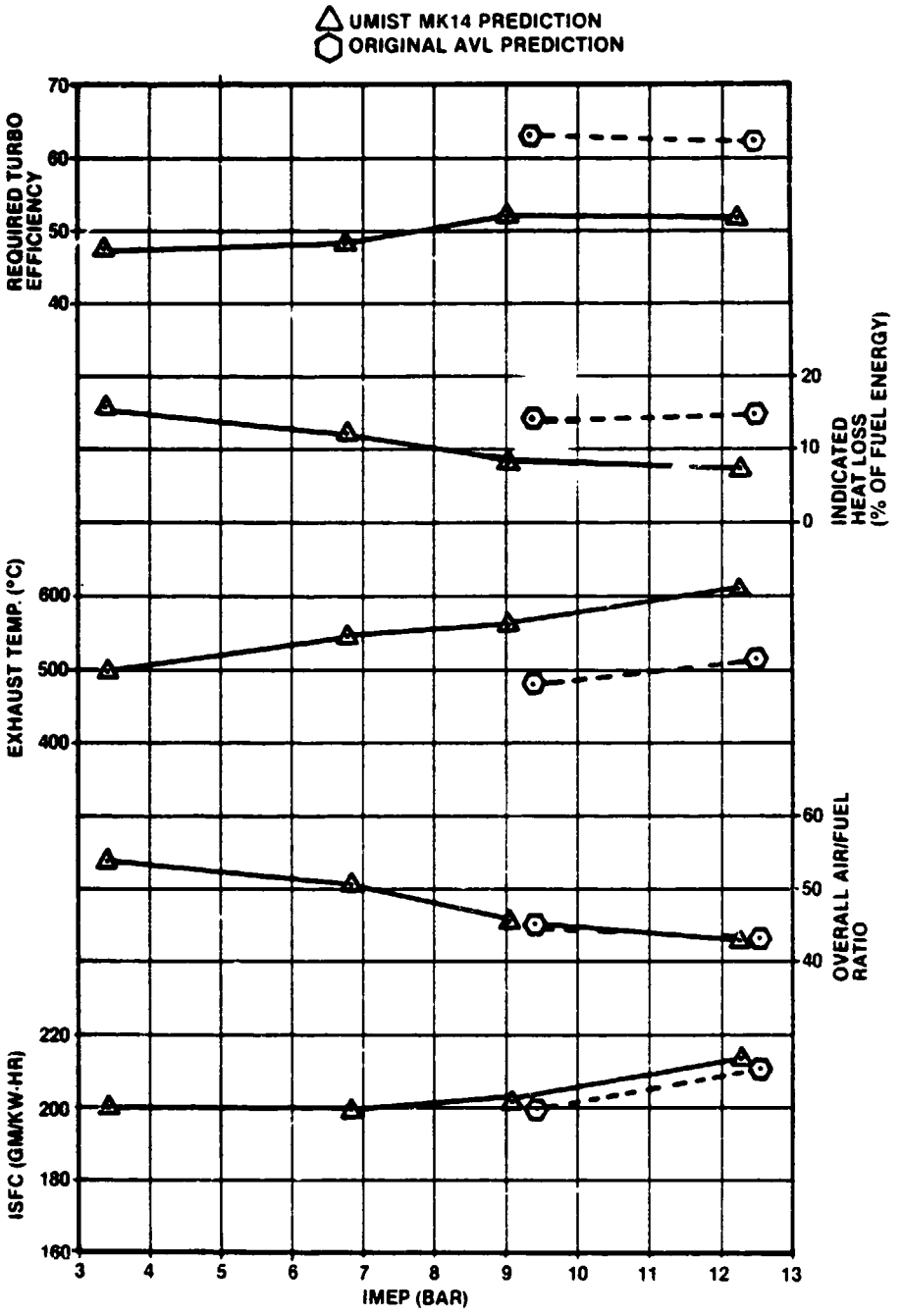

Figure 3.3-25. Predicted Performance for Optimized Configuration

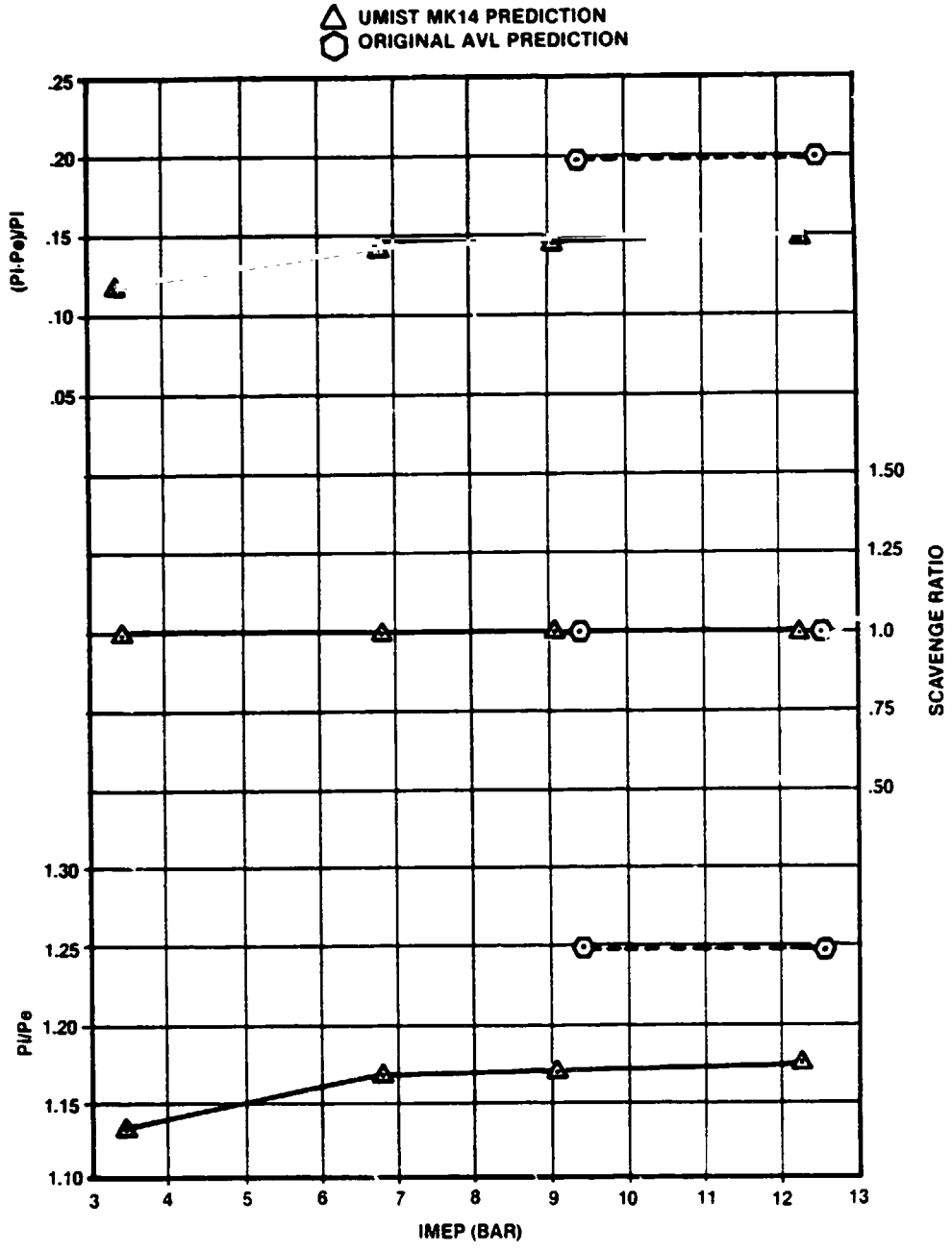

Figure 3.3 25. Predicted Performance for Optimized Configuration (Continued)

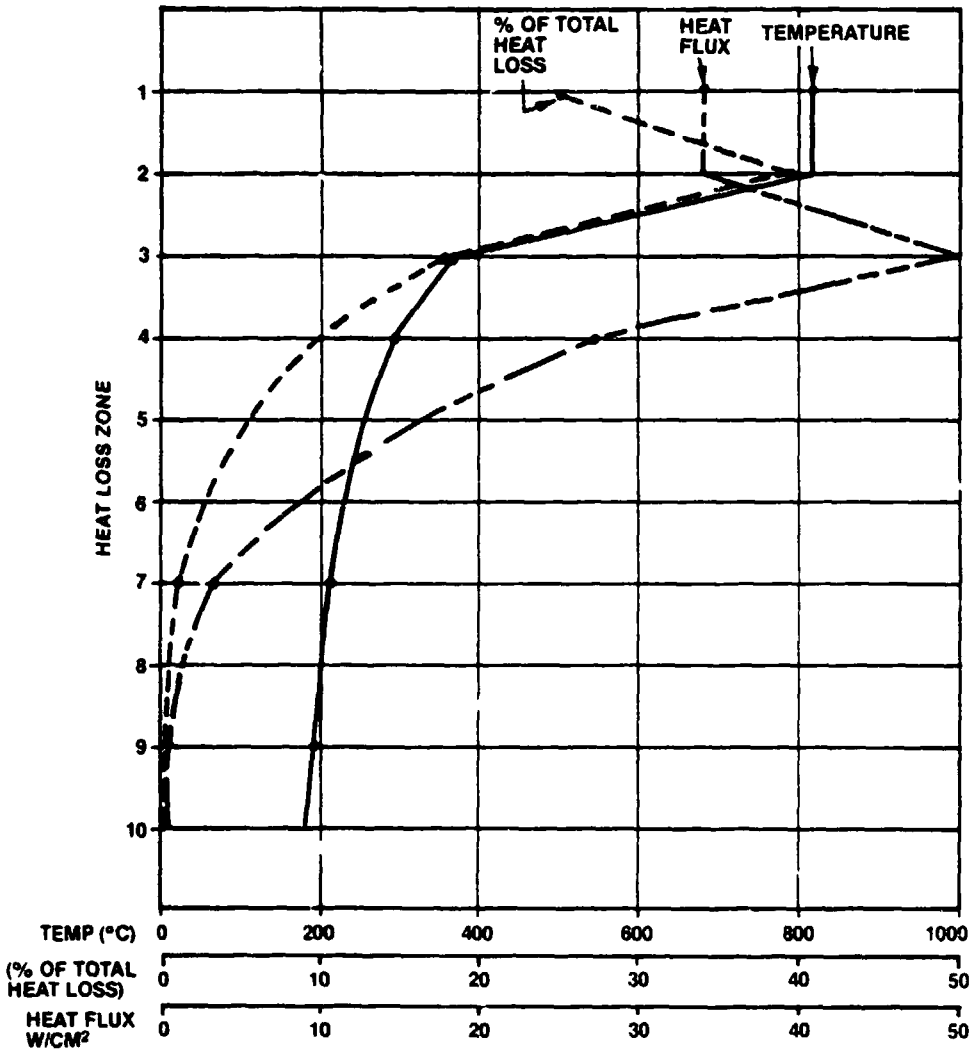

Figure 3.3-26. Temperature Inputs and Predicted Heat Loss Through Cylinder Zones at Takeoff Power

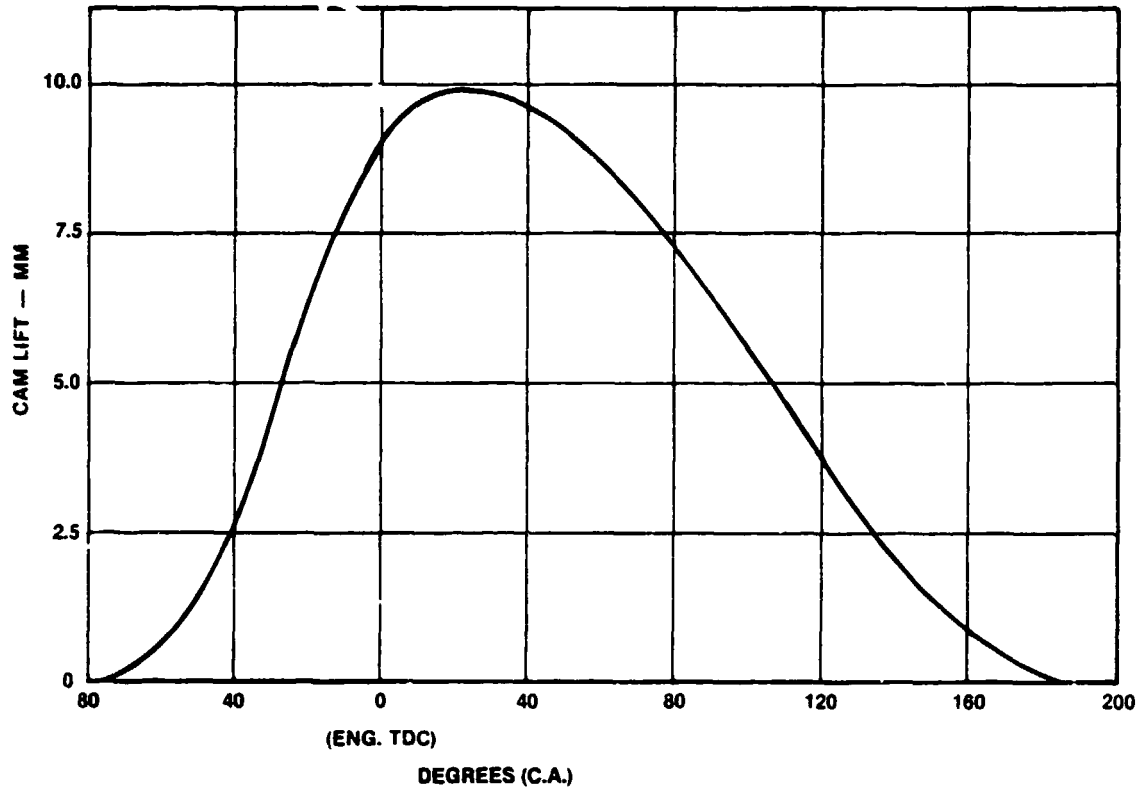

Figure 3.4-1. Fuel Injection Camshaft Profile

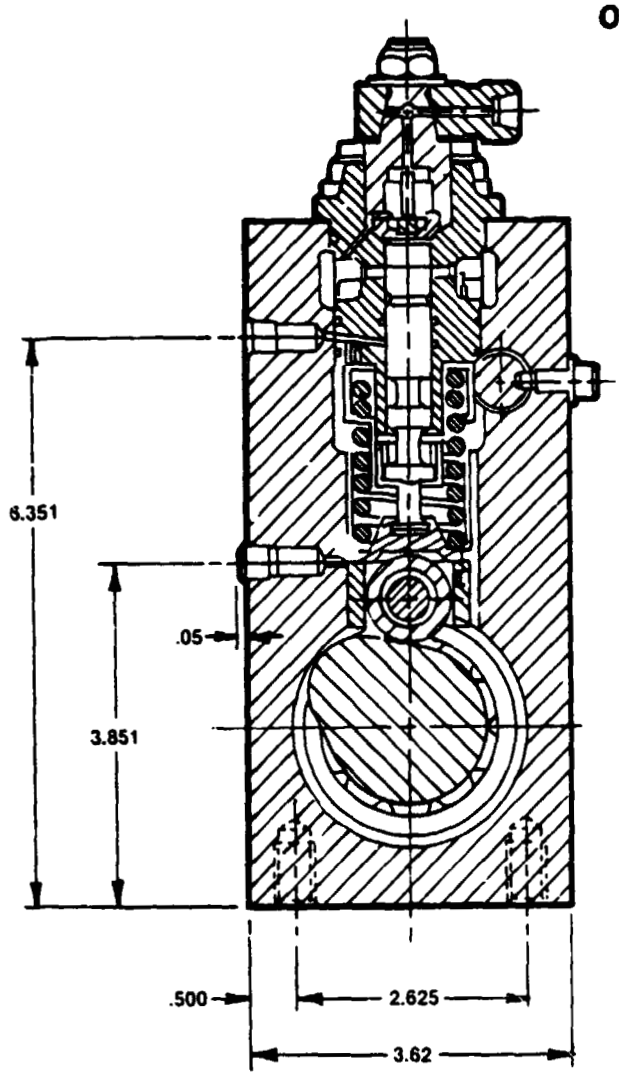

Figure 3.4-2. CAE-X Pump Cross Section

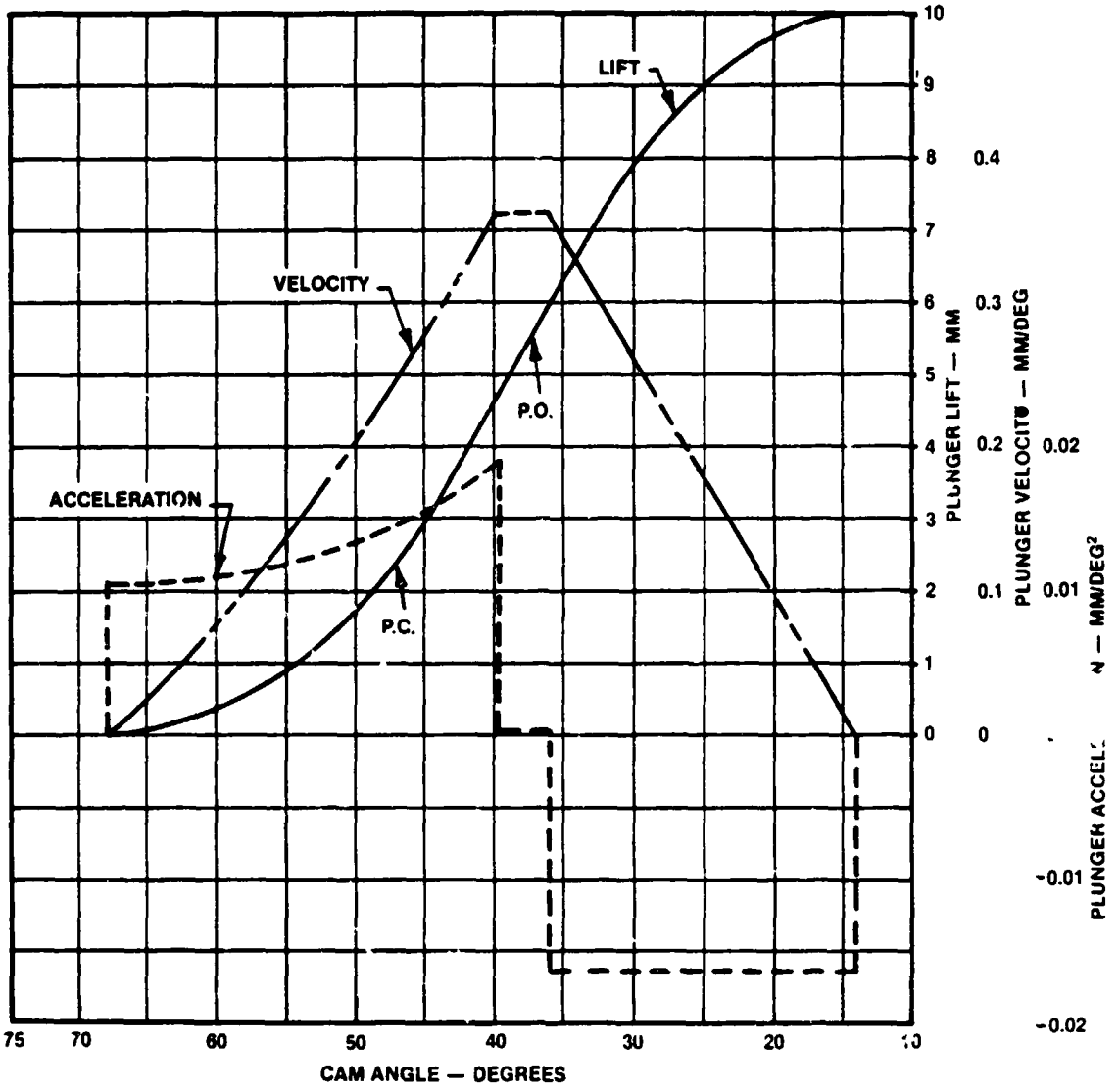

Figure 3.4-3. Camshaft Profile, Velocity, and Acceleration for AVCR-1360 Type Cam

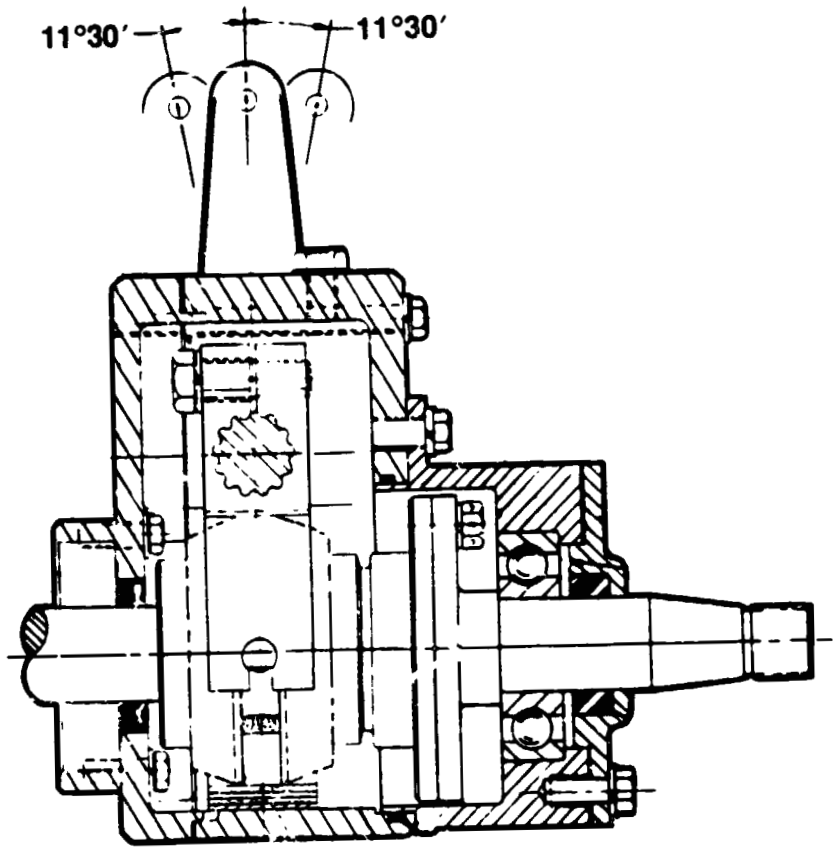

Figure 3.4-4. Advance Mechanism for CAE-X Pump (SCTE-Configuration)

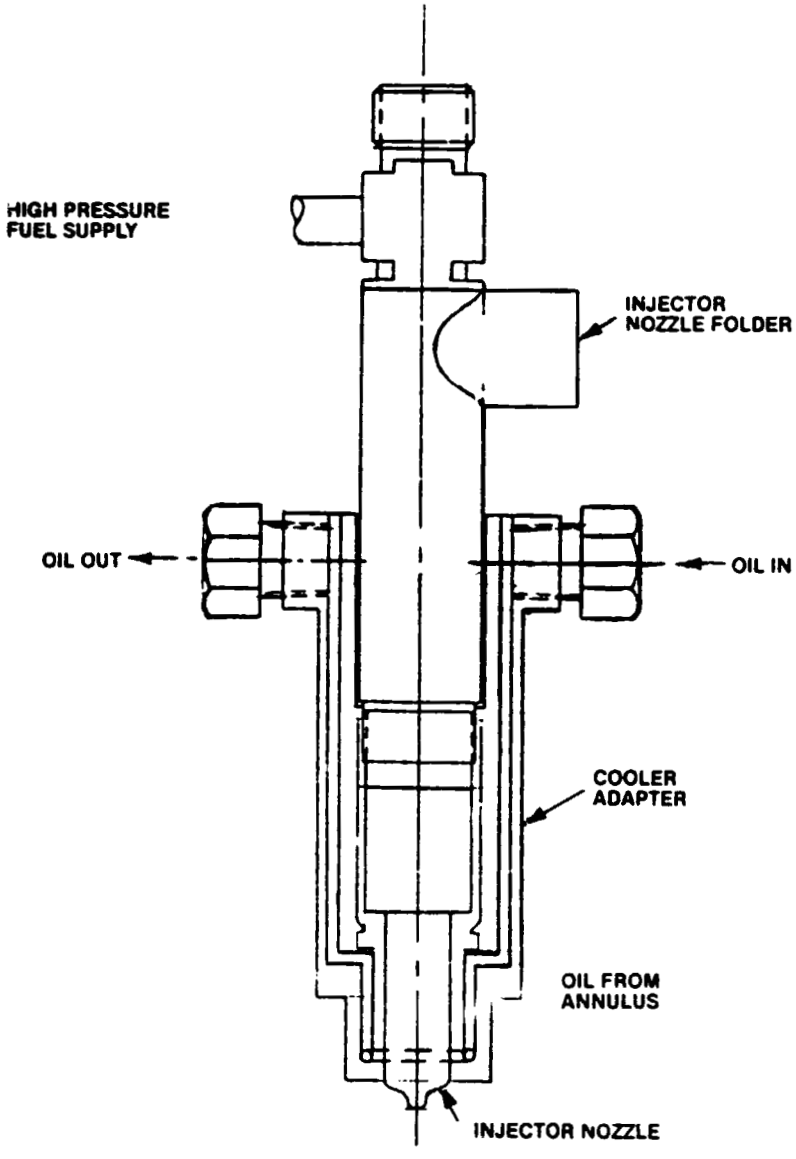

Figure 3.4-5. Cooled Injection Nozzle Holder and Adapter

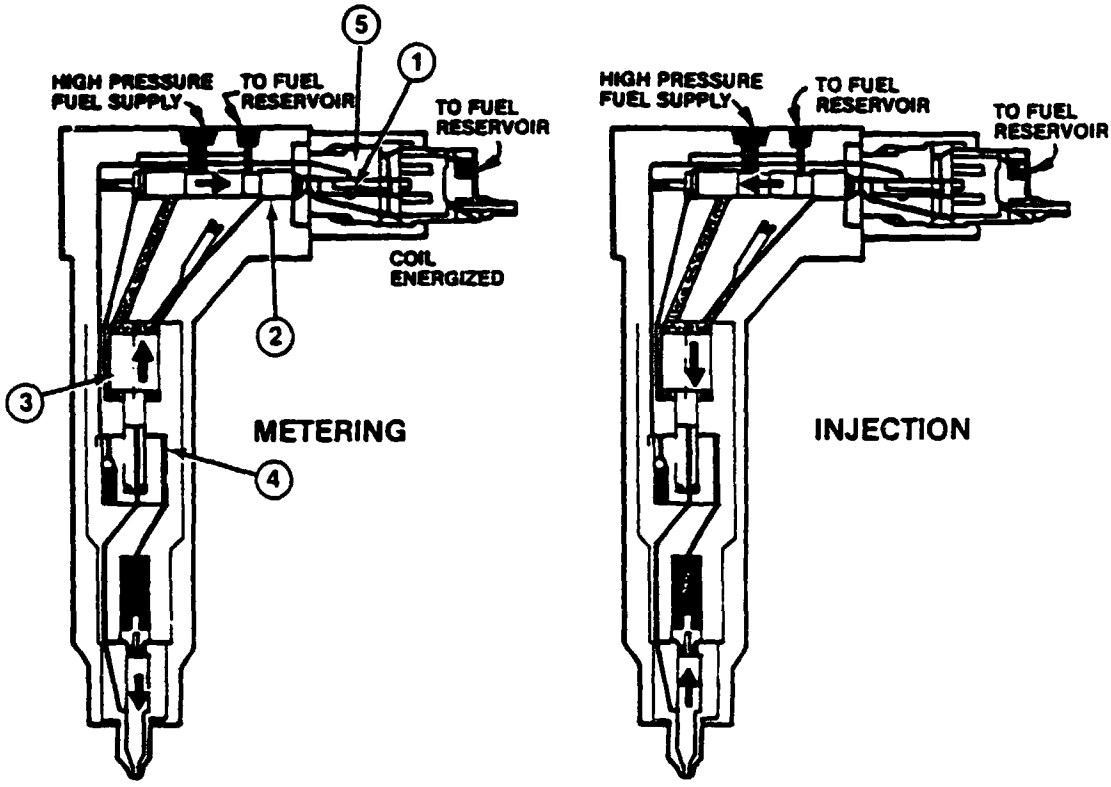

Figure 3.4-6. Bendix DCX-3-28 Injector

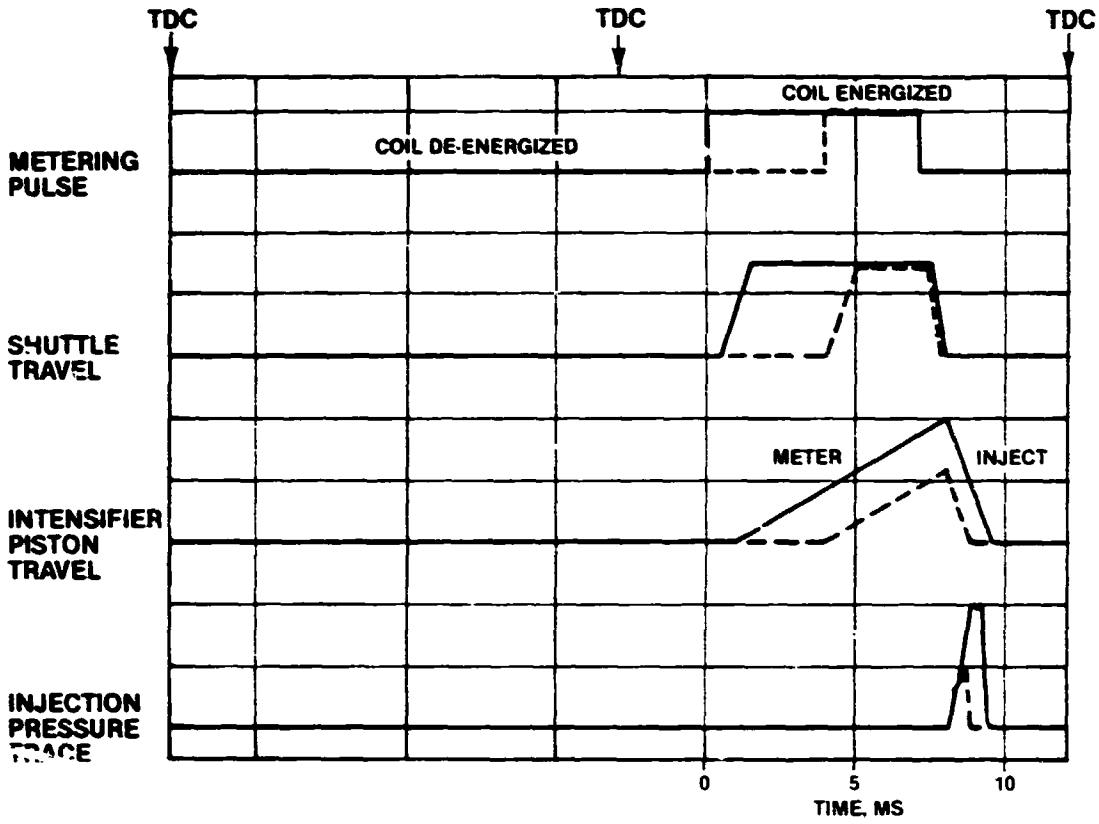

Figure 3.4-7. Fuel Injection Events with a Bendix DCX-3-28 Injector

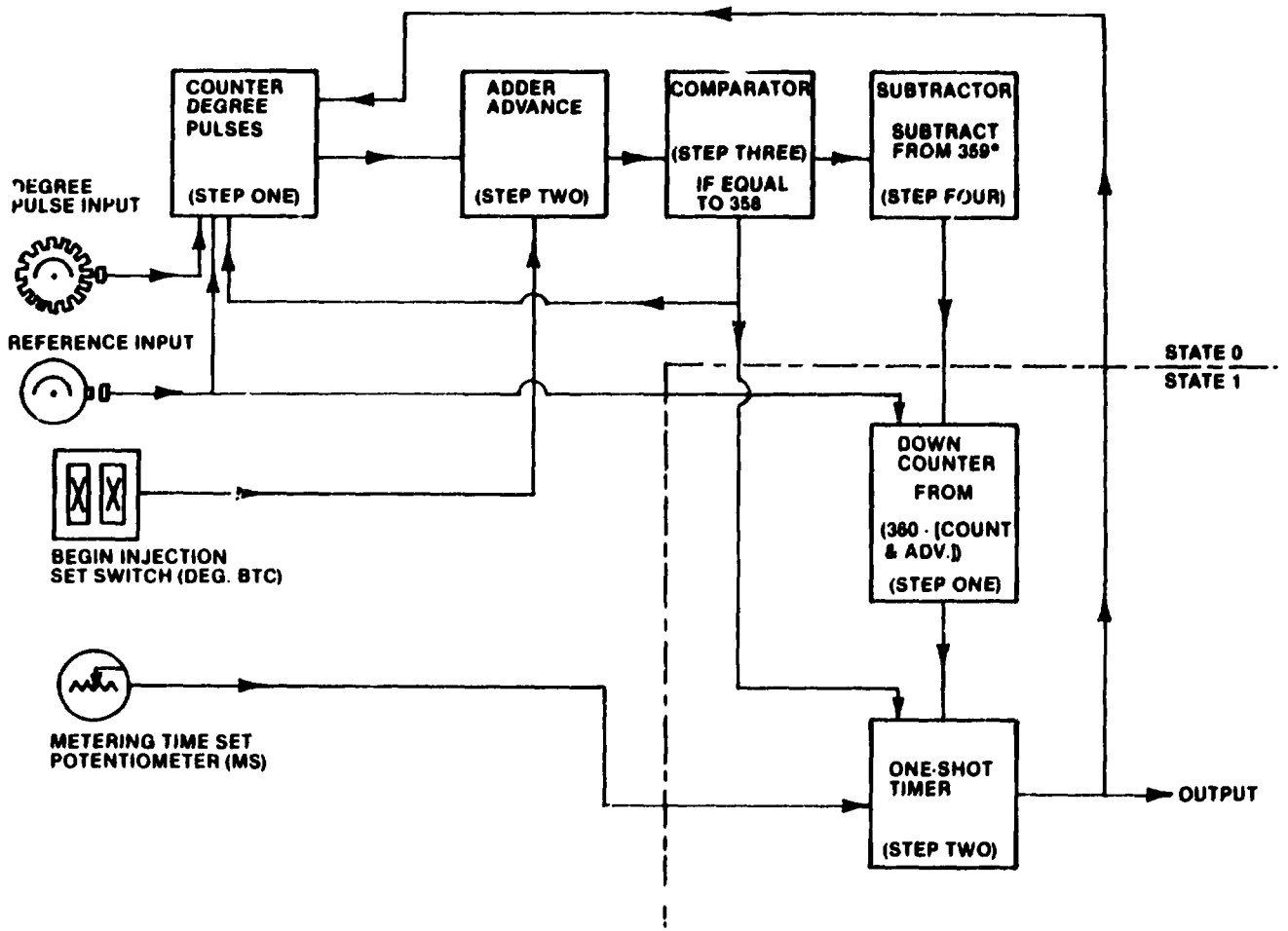

Figure 3.4-8. Fuel Injection Controller Block Diagram for Bendix DCX-3-28 System

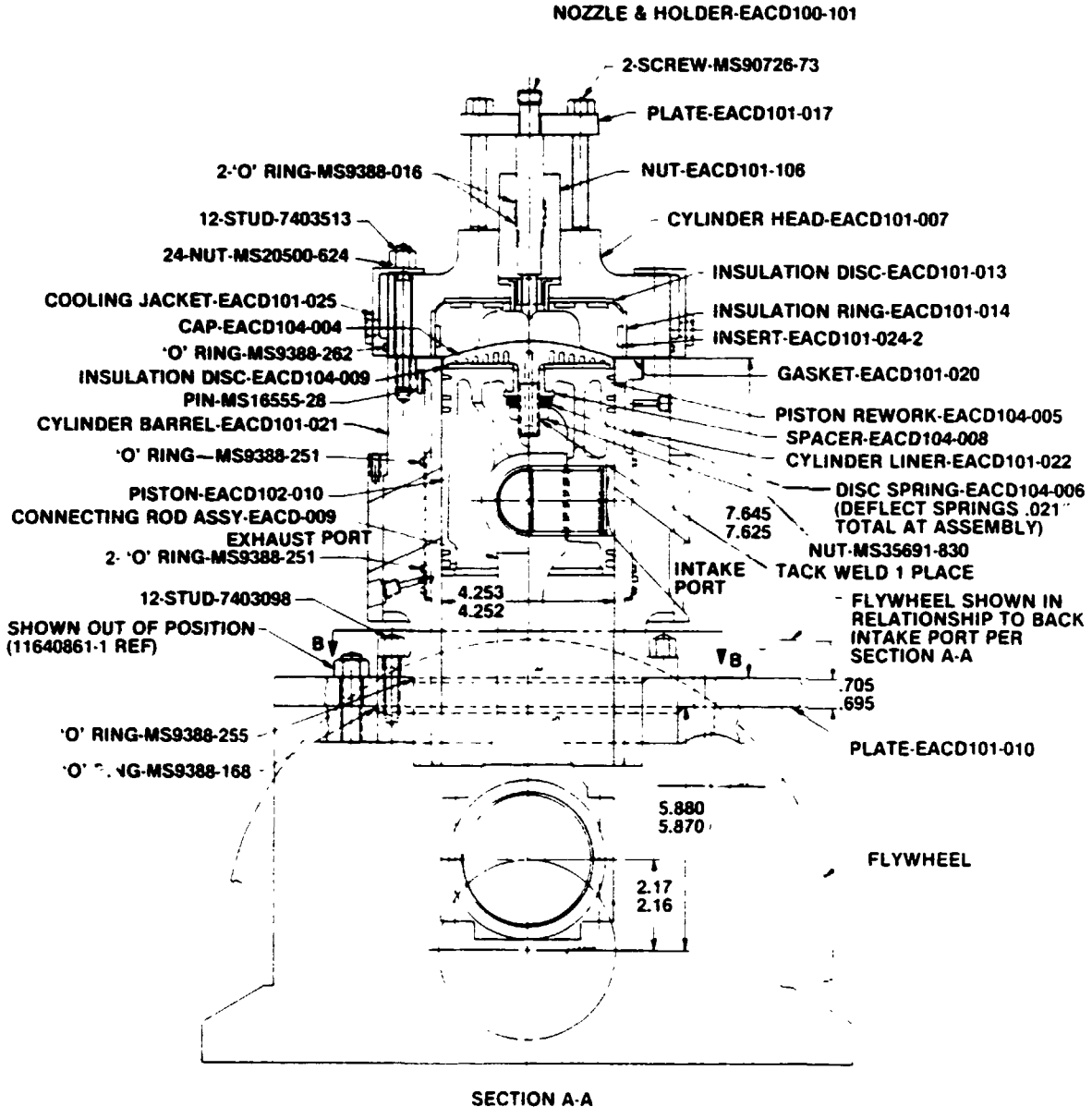

Figure 3.6-1. Second Generation Single Cylinder Test Engine — Cooled Configuration

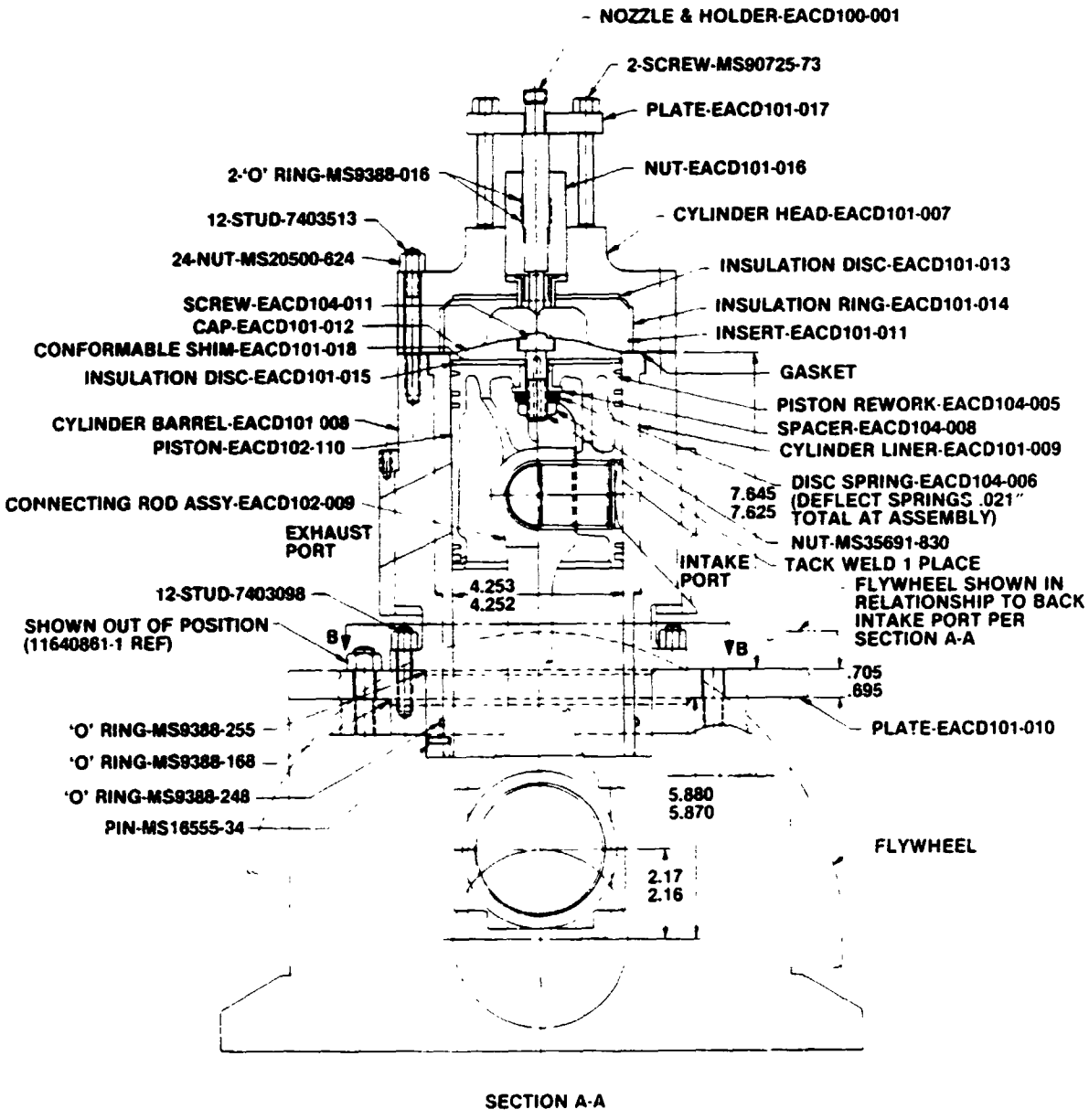

Figure 3.6-2. Second Generation Single Cylinder Test Engine — Insulated Configuration